JAGIELLONIAN UNIVERSITY IN KRAKOW

UNIVERSITÉ DE STRASBOURG

Thèse

présentée pour obtenir le grade de

Docteur de l'Université de Strasbourg et Docteur de l'Université Jagellonne de Cracovie

SPECIALITE : Physique du solide
Ecole Dosctorale UdS 182 – Physique et chimie physique

par

Mr Andrzej Biborski

Chemical Ordering Kinetics and Thermal Vacancy Thermodynamics in B2 Binary Intermetallics: Simulation Study

-

Cinétiques d'ordre chimique et thermodynamique des lacunes thermiques dans les intermétalliques binaires B2 : une étude par simulation

soutenue le 17 septembre à l'Institut de Physique de l'Université Jagellonne de Cracovie
devant le jury :

Professor Graeme MURCH, Newcastle University, Australia	**Rapporteur externe n'assistant pas à la soutenance**
Professor Krzysztof J. KURZYDLOWSKI, Warsaw University, Poland	**Rapporteur externe**
Professeur ALOUANI Mébarek, Université de Strasbourg, France	**Examinateur**
Professor Krzysztof J. Rosciszewski, Krakow Jagellonian University, Poland	**Examinateur**
Professor Rafal Kozubski, Institute of Physics, Krakow Jagellonian University, Poland	**Directeur de thèse**
Dr Véronique Pierron-Bohnes, DR au CNRS, IPCMS CNRS-UdS, Département Magnétisme et Objets Nanostructurés, Strasbourg, France	**Directrice de thèse**

Cinétiques d'ordre chimique et thermodynamique des lacunes

dans des alliages intermétalliques B2: étude par simulation

Andrzej Biborski

Directeurs de thèse: R. Kozubski (UJ, Krakow) et V. Pierron-Bohnes (IPCMS, Strasbourg)

Résumé

Les intermétalliques qui présentent la structure ordonnée B2 ont des propriétés physiques intéressantes dans le développement de nouveaux matériaux. C'est l'une des raisons pour lesquelles de nombreuses études, tant expérimentales que théoriques, leur ont été consacrées pendant la dernière décennie. D'autre part, les phénomènes observés dans les phases B2 sont intéressants d'un point de vue théorique du fait qu'une concentration de lacunes anormalement élevée est observée dans les alliages bien ordonnés. Les sauts atomiques élémentaires qui permettent la mise en ordre dans ces intermétalliques ont lieu par un mécanisme lacunaire. Etonnamment, les résultats expérimentaux dans la phase ordonnée B2-NiAl – un système où la concentration de lacunes est relativement élevée – montrent des vitesses de mise en ordre bien plus basses que dans les systèmes à basse concentration de lacunes (comme Ni_3Al-$L1_2$).

Ce phénomène a été souvent expliqué en invoquant la présence de 'défauts triples' où les lacunes sont piégées sur le sous-réseau Ni par des antisites de Ni sur le sous-réseau Al. Effectivement, statistiquement, on dénombre deux lacunes par antisite de Ni dans ce système.

Le but général de cette thèse est de mettre au point une méthodologie de simulations par une méthode de type Monte-Carlo pour simuler les cinétiques de transformation structurale dans les intermétalliques B2 à haute concentration de lacunes. Pour ce faire, il a été nécessaire de développer et appliquer un modèle thermodynamique qui permette de déterminer la concentration des lacunes – la dépendance en température de la concentration de lacunes ne pouvant plus être négligée. La concentration d'équilibre des lacunes a été étudiée dans le cadre d'un modèle de décomposition d'un gaz de réseau, testé au préalable dans l'approximation de Bragg-Williams et résolu par des simulations Monte-Carlo dans l'ensemble semi-grand canonique sur un gaz de réseau ternaire (A+B+lacunes). Les valeurs d'équilibre de la concentration des lacunes thermiques ont été ensuite utilisées dans les simulations Monte-Carlo des cinétiques de mise en ordre, effectuées avec la méthode des temps de résidence avec des barrières énergétiques (énergies de col) évaluées grâce à des calculs de statique moléculaire (dynamique moléculaire

trempée). Les simulations Monte-Carlo étaient basées sur un Hamiltonien de type Ising avec des interactions de paires choisies pour reproduire la formation de triples défauts.

1. Concentration des lacunes à l'équilibre dans un modèle de décomposition sur un gaz de réseau

La motivation expérimentale de cette étude est de décrire les systèmes comme l'intermétallique NiAl-B2 dont les cinétiques de modification de l'ordre sont très lentes et qui présentent un comportement de type 'triples défauts'. Ce comportement est associé à l'existence d'une forte concentration de lacunes thermiques corrélée avec un fort degré d'ordre. L'idée à la base de ces simulations des concentrations de lacunes thermiques à l'équilibre est issue du concept proposé par Schapink [1]. Ce modèle considère la possibilité de décomposer un gaz de réseau A – B – V (V = lacune) en deux phases à l'équilibre, l'une riche en lacunes, l'autre pauvre en lacunes. Pour cela, les lacunes sont traitées comme un troisième composant de l'alliage. La phase pauvre en lacunes a été interprétée comme le cristal $A_{1-\delta}B_{\delta}$ avec une concentration de lacunes à l'équilibre, la phase riche en lacune comme le gaz en équilibre avec l'alliage. Même si différentes procédures de détermination de la concentration des lacunes d'équilibre (par exemple l'approche annulant le potentiel chimique des lacunes) sont connues, le modèle de décomposition du gaz de réseau s'est montré très efficace combiné avec les méthodes de type Monte-Carlo. Cela nous a permis d'étudier les phénomènes d'ordre chimique dans les systèmes avec triples défauts dans le cadre de simulation Monte-Carlo de manière consistante.

Le modèle a été résolu dans un premier temps dans une approximation de type Bragg-Williams en supposant des interactions de paires limitées aux premiers voisins. Cette limitation a permis une analyse complète du modèle en variant les paramètres d'interactions de paires sur une large gamme afin de sélectionner les valeurs qui font apparaitre le comportement à triples défauts. Une extension du modèle à des paires plus lointaines est possible mais ne devrait pas apporter des résultats substantiellement nouveaux dans le domaine qui nous intéresse. Ce point a déjà été mentionné par Breuer et al [2] qui ont utilisé une méthode basée sur une approximation de Bragg-Williams pour déterminer les concentrations de lacunes d'équilibre dans le système NiAl B2. Ils ont déterminé les interactions de paires jusqu'aux deuxièmes voisins en ajustant les valeurs expérimentales des enthalpies et des activités. Ils ont conclu que les énergies d'interactions de paires correspondant aux seconds voisins pouvaient être négligées dans le cadre du modèle considéré. D'autre part, d'autres auteurs ont montré [3] des écarts notables entre les résultats

expérimentaux et les résultats de simulations Monte-Carlo pour la mise en ordre atomique dans les systèmes binaires B2 réalisés avec des interactions de paires de premiers et seconds voisins, mais avec des nombres fixés de lacunes, indépendants de la température. Il semble donc que les problèmes de ces modélisations antérieures étaient plus dus au fait qu'ils aient ignoré la thermodynamique des lacunes plutôt qu'à la porté limitée des interactions de paires.

Pour l'analyse de la distribution des défauts sur les deux sous-réseaux et de la dépendance en température, nous avons défini des indicateurs qui nous ont permis de mettre en évidence la présence de triples défauts (basés sur les rapports entre les concentrations de lacunes et d'antisites). Ils nous ont permis de sélectionner les interactions de paires qui reproduisaient le comportement avec triples défauts. Les systèmes identifiés comme contenant des triples défauts montraient l'existence de lacunes de constitution sur le sous-réseau riche en atomes B (atomes minoritaires – en accord avec les définitions données par Wasilewski [4]), dans la limite des très basses températures.

Le modèle de décomposition du gaz de réseau a montré que le potentiel chimique des lacunes tend vers 0 à basse température, ce qui veut dire que pour $T \rightarrow 0$ cette approche converge vers le formalisme standard [5] basé sur une simple minimisation du potentiel thermodynamique du cristal par rapport au nombre de lacunes et qui relie la valeur d'équilibre de la concentration de lacunes à un potentiel chimique nul des lacunes.

Les interactions de paires qui favorisaient les triples défauts ont été par la suite appliquées à des simulations Monte-Carlo dans l'ensemble semi-grand canonique. Dans ces simulations, nous avons comparé les potentiels chimiques, étudié l'hystérésis de la séparation de phase et fait des intégrations thermodynamiques. Il faut mentionner que les méthodes proposées ici pour obtenir les concentrations d'équilibre des lacunes par des simulations Monte-Carlo dans l'ensemble semi-grand canonique est une approche nouvelle, à notre connaissance. Cette étude a permis de déterminer les concentrations de lacunes à l'équilibre sur une large gamme de température dans les alliages binaires AB de type B2, mais aussi d'analyser les configurations en termes de paramètres d'ordre à courte et à longue distance. Les résultats sont en bon accord qualitatif avec la solution Bragg-Williams. La phase riche en atomes, interprétée comme le cristal avec une concentration de lacunes en équilibre a montré un comportement clair de type triples défauts ce qui se manifestait par l'existence d'une plateau de valeur ½ sur la courbe du rapport entre lacunes et antisites de type A (atome majoritaire) sur sous-réseau B et par la présence de lacunes de constitution pour $\delta > ½$.

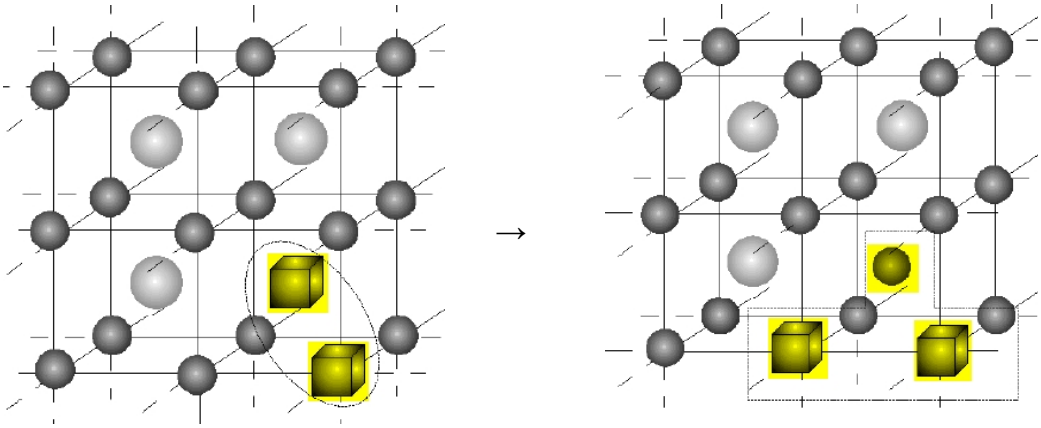

Figure 1 : Formation d'un défaut triple dans la phase ordonnée AB (gros atomes : B=Al sous réseau α, petits atomes A=Ni sous-réseau β) à partir de deux lacunes voisines sur les deux sous-réseaux.

De plus, les simulations ont permis d'examiner les corrélations dans la distribution spatiale dans les cas présentant des triples défauts par l'analyse des paramètres d'ordre à courte distance. Nous avons trouvé que les lacunes sur le sous réseau A et les antisites sur le sous réseau B n'étaient pas groupés sous la forme de complexes de défauts triples (voir figure 1), alors qu'un tel effet pouvait être attendu puisque l'interaction lacune-A a été supposé répulsif.

Cependant, le traitement présenté est limité au modèle de type Ising, généralement utilisé dans ce domaine [2,6], le développement récent de méthodes de calcul « ab initio » ont permis d'obtenir des résultats directement « ab initio » [7]. Des approches hybrides consistant à évaluer les interactions de paires « ab initio » ont aussi été proposées [8].

Dans le premier cas [7], la méthode de variation des amas (CVM) a été développée pour un système considéré comme une solution solide régulière. Les énergies d'interaction de paires sont généralement considérées comme indépendantes de la température et de la concentration de défauts, mais les énergies de formation des défauts, à partir d'une configuration particulière, peut en dépendre. Même si la méthode d'expansion des amas a été élaborée comme le lien naturel entre la méthode CVM et les calculs énergétiques ab-initio [9], les systèmes qui ont été décrits par cette méthode sont encore fort rares. Pour l'instant, les énergies de formation des défauts calculées ab-initio ont été le plus souvent effectués dans une approche de type Wagner_Schotky [7,10] avec l'énergie du système supposée linéaire avec la concentration de défauts. Ces énergies, même si elles sont déduites de considérations physiques valides, correspondent le plus souvent à une limité basse température et sont des paramètres considérés comme constants.

Alors que l'application directe de méthodes énergétiques ab-initio dans des simulations Monte-Carlo est encore dans ce domaine un challenge impossible, si on prend en compte les puissances

de calculs accessibles, les potentiels quasi-phénoménologiques à n corps (comme en EAM – embedded atom method) peuvent être appliqués dans le cadre de ces simulations. Des simulations Monte-Carlo dans l'ensemble semi-grand canonique basées sur des potentiels EAM ont été menées dans différents contextes[i] [11], en particulier pour les alliages B2 NiAl [12].

Evidemment, le modèle de décomposition du gaz de réseau (en deux phases l'une riche, l'autre pauvre en lacunes), en considérant les lacunes comme un troisième constituant, ne doit pas être considéré comme une description d'une décomposition, mais plutôt comme une méthode de calcul qui permet d'obtenir la concentration de lacunes à l'équilibre dans le cadre d'une traitement sur réseau rigide qui peut s'appliquer directement à des simulations Monte-Carlo. Même si l'utilisation de potentiels réalistes peut sembler quelque peu artificielle dans le modèle présenté, l'application des potentiels de type EAM peut être considéré comme un « petit pas vers la réalité »[ii].

Les potentiels EAM élaborés pour NiAl B2 [13] on été appliqués pour les calculs de statique moléculaire et adoptés aussi pour les simulations Monte-Carlo dans l'ensemble semi-grand canonique. Les simplifications faites ont été de considérer un réseau rigide où seuls les degrés de liberté de configuration sont considérés, mais aussi la boite de simulation a été limitée à 10x10x10 cellules cubiques avec le paramètre de réseau fixe a_0= 2.859 Å. La procédure de simulation Monte-Carlo dans l'ensemble semi-grand canonique a été faite pour la température de 1500 K. Nous avons trouvé que le système Ni-Al-V (V = lacune) montre une tendance à la décomposition en deux phases riche et pauvre en lacunes (voir figure 2), cependant la phase riche en lacunes apparait comme pratiquement pure en lacunes. La concentration de lacunes d'équilibre dans la phase $Ni_{0.5}Al_{0.5}$-V a été trouvée proche de la limite de résolution : $c_V \approx 10^{-3}$, nous n'avons observé que peu de lacunes dans un échantillon à proximité de la limite de séparation de phase qui apparait comme une discontinuité dans le plan : $c_V\{\Delta\mu_{Ni\text{-}V}, \Delta\mu_{Al\text{-}V}\}$ (dans le cycle d'hystérésis pendant les simulations en mode pas à pas).

Schaefer et al [14] ont mesuré une concentration de lacunes de 7.10^{-4} par dilatométrie à une température de 955 K (deux fois plus faible que la température de fusion). Breuer et al [2] rapporte les valeurs obtenues par Zobel dans sa thèse (Berlin 1994) sur un large domaine en température dont on déduit une concentration de 5.10^{-3} à 1500 K. Ces résultats sont en très bons accord avec les valeurs que j'ai obtenues dans le modèle présenté[iii].

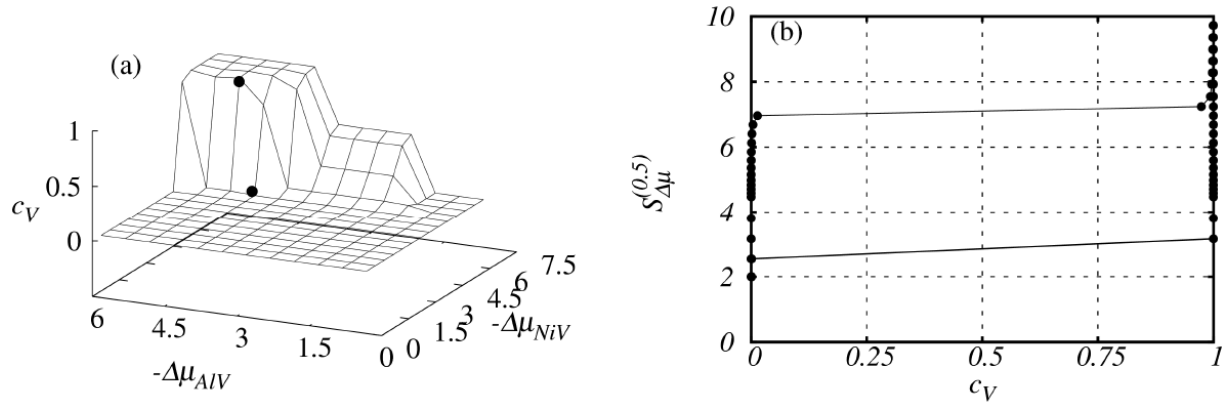

Figure 2 : (a) La facette qui induit la séparation de phase, trouvée dans les simulations Monte-Carlo dans l'ensemble semi-grand canonique avec les potentiels EAM dans l'espace de la concentration de lacunes et des potentiels chimiques relatifs (en eV). Les cercles correspondent approximativement à la phase $Ni_{0.5}Al_{0.5}$-V (point du bas) en équilibre avec une phase pratiquement pure en lacunes. (b) Cycle d'hystérésis obtenu dans les simulations dans un mode 'pas à pas' pour la stoechiométrie B2 NiAl.

Un point remarquable de nos résultats est que nous avons obtenu un rapport stable de 0.5 pour la concentration des lacunes sur le sous-réseau A ($c_V^{(\alpha)}$) divisée par celle des antisites A sur le sous-réseau de B ($c_A^{(\beta)}$) alors que les valeurs des deux grandeurs fluctuaient fortement et que le nombre de ces défauts premiers voisins restait faible (10^{-2}), montrant le caractère statistique de ces défauts triples. Ce résultat n'est pas trivial puisque contrairement au cas du modèle d'Ising où l'interaction entre lacune et atomes A est répulsive et où la formation des défauts triples séparés spatialement est favorisée par l'énergie de configuration, l'énergie de formation à température nulle d'un triple défaut premier voisin dans NiAl traité en EAM est significativement plus faible que l'énergie de formation d'un triple défaut spatialement séparé (statistiquement). Des résultats préliminaires de calculs ab-initio ont prédit une énergie plus basse pour des défauts spatialement séparés dans NiAl B2 stoechiométrique [15] ; un effet semblable a été reporté dans FeAl B2 pour des calculs de statique moléculaire [16].

2. Cinétiques « ordre-ordre » et énergies de col

Les concentrations de lacunes thermiques d'équilibre obtenues par les simulations Monte-Carlo dans l'ensemble semi-grand canonique basées sur des interactions de paires qui favorisaient le comportement avec triple défauts ont été appliquées à des simulations de dynamiques en Monte-Carlo dans l'ensemble canonique effectuées par la méthode du temps de résidence. La configuration initiale du système a été générée en introduisant le nombre d'équilibre de lacunes

de manière aléatoire sur un réseau B2 parfaitement ordonné. La validité de cette simplification est justifiée par le fait que l'équilibrage de la concentration des lacunes est environ deux fois plus rapide que les transformations « ordre-ordre » [17].

Les simulations des cinétiques de mise en désordre en Monte-Carlo demandent d'évaluer les énergies de col. Ces énergies, qui dépendent de la nature de l'atome qui saute, ont été évaluées dans des cas simples et fixées ensuite en prenant en compte des relations quantitatives entre les valeurs obtenues en statique moléculaire basée sur les potentiels EAM développés dans le système NiAl B2 [13]. Mentionnons que les études des sauts atomiques reportés pendant les dix dernières années dans NiAl B2 [12,18] correspondaient essentiellement à des chemins de self-diffusion (séquence de sauts) qui maintenaient des configurations initiale et finale identiques du point de vue de l'état d'ordre à longue distance. Dans notre travail, les configurations étudiées et les chemins considérés ne conservent pas le degré d'ordre à longue distance puisque nous considérons des phénomènes de mise en désordre. Il a été problématique d'étudier l'énergie de col pour les sauts de l'aluminium, du fait de la difficulté de trouver un minimum d'énergie potentielle pour un antisite d'Al lorsqu'il est proche voisin d'une lacune dans NiAl B2. Cet effet avait déjà été signalé [12,19] sous la forme d'un manque de stabilité de certaines configurations dans les calculs de statique moléculaire. Cependant, dans ce travail, nous avons trouvé que si l'atome d'Al saute dans une lacune du réseau de Ni voisine d'un Ni en antisite (sur le réseau Al), un minimum local peu profond apparait sur la courbe du profil énergétique, minimum qui ne peut être atteint qu'au prix du saut d'une barrière énergétique significativement plus haute que toutes les barrières correspondant aux différents sauts possibles pour les atomes de Ni. Ceci nous a amené à conclure qu'une petite concentration d'antisite d'Al est possible dans NiAl B2 stoechiométrique si des triples défauts existent préalablement (probablement à haute température).

Il me faut insister sur le fait que même si les énergies au maximum des cols des sauts de A et B sont fixés, l'énergie de col effective des différents sauts (différence d'énergie entre la valeur moyenne des énergies des positions initiale et finale et le maximum du col) évolue au cours de la relaxation puisque sa valeur dépend des positions initiales et finales. De ce fait, la configuration influence la dynamique de l'évolution du système. L'utilisation de l'algorithme de temps de résidence nous a permis d'éviter la faible efficacité (faible taux d'acceptation des sauts en Monte-Carlo) attendue dans un algorithme de Glauber. Cependant, le temps de calcul nécessaire a été toutefois très long du fait du faible nombre de lacunes introduites dans le système. En conséquence, les courbes de relaxation à basse température n'étaient pas saturées. Les études

détaillées concernent les cinétiques « ordre-ordre » dans l'alliage binaire AB ordonné B2 à T/T_C = 0.37 (cas typique avec triples défauts) et à T/T_C = 0.53.

Le premier stade, extrêmement rapide, de l'évolution du système avec des lacunes initialement distribuées au hasard sur les sites de l'alliage B2 parfaitement ordonné est la génération de triples défauts, ce qui se traduit par la génération d'antisites d'atomes A sur le sous-réseau β des atomes B et la migration de presque toutes les lacunes sur le sous-réseau α des atomes A. La force motrice élevée de ce processus vient du fait qu'alors que la création de tout antisite augmente l'énergie de configuration d'un système AB sans lacunes, la situation s'inverse en présence de lacunes : la configuration avec un triple défaut a une énergie plus basse qu'une configuration sans antisite avec une lacune sur chacun des sous-réseaux.

La forte contribution de la force motrice dans le stade initial de la relaxation a pu être mieux comprise grâce à l'analyse de la surface de la fonctionnelle énergie libre $f(\eta_A, \eta_V)|_{T,\delta,c_V}$ obtenue dans l'approximation de Bragg-Williams (Figure 3). La configuration de départ implique que l'évolution du système est au départ dominée par le processus responsable de la mise en ordre des lacunes jusqu'à ce que la configuration correspondant aux triples défauts soit approchée (aire la plus foncée sur la figure). Ce processus immédiat (formations des défauts triples) est suivi d'un processus plus lent, qui consiste essentiellement en la formation d'antisites d'atomes A sur le sous-réseau β, même si à T/T_C = 0.53 la création d'antisites d'atomes B sur le sous-réseau α commence à devenir probable. L'analyse des paramètres d'ordre à longue et à courte distance et l'étude de la statistique des sauts atomiques et de leurs barrières énergétiques nous a permis de

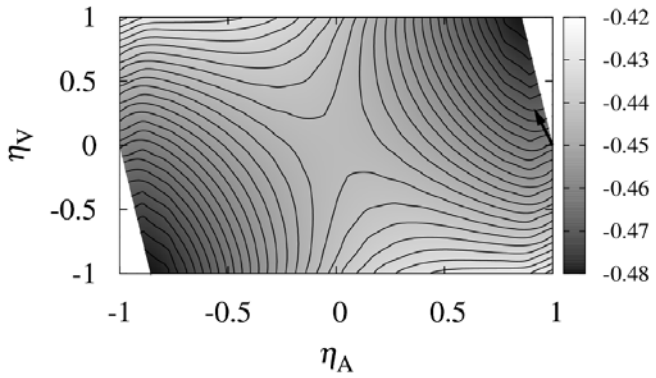

Figure 3 : Fonctionnelle d'énergie libre obtenue dans l'approximation Bragg-Williams à T/T_C = 0.53, à la stoechiométrie et avec une concentration de lacunes à l'équilibre de 0.067. η_A est la différence de concentration normalisée entre les deux sous-réseaux (paramètre d'ordre à longue distance). η_V est de façon équivalente la différence de concentration de lacunes entre les deux sous-réseau normalisée au nombre totale de lacunes. La flèche indique la direction de la force de rappel au point (η_A, η_V) = (1,0) qui correspond au point de configuration initiale de la simulation Monte-Carlo cinétique. Les valeurs des échelles de gris correspondent à des eV. Les triangles blancs en haut à droite et en bas à gauche correspondent aux limites dues aux contraintes en concentration.

conclure que l'évolution lente du système était causée par l'inefficacité des sauts effectués. De plus, il est apparu que cette inefficacité avait pour origine la compétition entre la tendance énergétique qui favorise les sauts des atomes A du sous-réseau α vers le sous-réseau β et la formation concomitante de lacunes sur le sous-réseau α qui favorise statistiquement le saut inverse.

Les remarques finales sont centrées sur la comparaison avec les cinétiques d'ordre chimique dans les systèmes $L1_2$ A_3B (le système modèle de Ni_3Al $L1_2$) décrites par Oramus et al [20]. Il est intéressant de considérer le paramètre d'efficacité de la mise en désordre défini dans cet article :

$$E^{dis}_{A:\alpha\to\beta}(\%) \equiv \frac{f_{A:\alpha\to\beta} - f_{A:\beta\to\alpha}}{f_{A:\alpha\to\beta}} \times 100\%$$

et de comparer son évolution dans les phases ordonnées B2 et $L1_2$.

Le paramètre $E^{dis}_{A:\alpha\to\beta}$ considéré comme une fonction du paramètre d'ordre à longue distance η_A est montré sur la figure 4.

Un dernier commentaire à propos du but principal de cette étude, l'explication des vitesses de relaxation de l'ordre extrêmement lentes observées expérimentalement dans l'intermétallique $Ni_{0.505}Al_{0.495}$ [20]

On voit clairement qu'alors que dans le cas de la phase A_3B ordonnée $L1_2$ le paramètre $E^{dis}_{A:\alpha\to\beta}$ montrait un comportement de type relaxation en parallèle avec celui du paramètre d'ordre et tend asymptotiquement vers 0, dans le cas du système AB ordonné B2 avec des défauts triples, $E^{dis}_{A:\alpha\to\beta}$ est proche de 0 pendant tout la stade lent de la relaxation de l'ordre après une chute abrupte dès les premiers instants (Figure 3a). Même si il faut garder en mémoire que les courbes montrées sur les deux figures 3 ont été obtenues par des algorithmes différents, à des températures différentes et avec des modèles énergétiques différents, cette analyse comparative

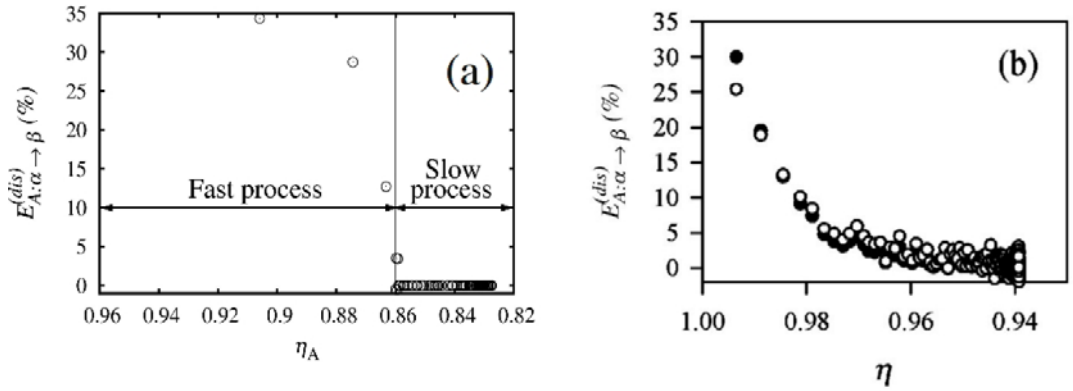

Figure 4 : Paramètre d'efficacité de mise en désordre en fonction du degré d'ordre à longue distance : (a) système AB de phase B2 (ce travail) $T/T_C = 0.53$, (b) système A_3B de phase $L1_2$ [20] $T_{init}/T_C = 0.52$ et $T_{final}/T_C = 0.78$.

très approximative des cinétiques « ordre-ordre » dans les phases ordonnées $L1_2$ et B2 suggèrent une efficacité très faible de la mise en désordre atomique dans le dernier cas.

Un dernier commentaire portera sur le but initial de ce travail : expliquer les résultats expérimentaux qui montraient une vitesse extrêmement lente de relaxation de l'ordre dans l'intermétallique $Ni_{50.5}Al_{49.5}$ [17]. Nous pouvons avancer deux raisons pour lesquelles seul le stade lent de la simulation a pu être observé expérimentalement :

- Le stade rapide de la simulation est dû à la distribution initialement au hasard de la distribution des lacunes qui se rééquilibre très rapidement, il n'existe probablement pas dans les systèmes réels
- Les expériences ont été effectuées en utilisant une méthode de résistométrie « in situ » où l'inertie thermique de l'équipement rend impossible la détection d'un stade initial très rapide.

On peut ainsi conclure que les raisons atomistiques trouvées par nos simulations pour la vitesse lente du stade final de la relaxation de l'ordre dans les systèmes B2 avec triples défauts permettent d'expliquer les résultats expérimentaux.

[1] F.W. Schapink, "Thermodynamics of vacancies in binary alloys", Philos. Mag. 12 (1965), p. 1055; F.W. Schapink, "The distribution of vacancies in ordered alloys of CsCl-type", Scr Metal 3 (1969), p. 113.
[2] J. Breuer, F. Sommer and E.J. Mittemeijer, "Thermodynamics of B2 intermetallic compounds with triple defects: a Bragg-Williams model for (Ni,Co)Al", Metall Mater. Trans. A 32 (2001), p. 2157 ; J. Breuer, F. Sommer and E.J. Mittemeijer, "Thermodynamics of constitutional and thermal point defects in B2 Ni1-xAlx", Philos. Mag. A 82 (2002), p. 479.
[3] P. Oramus, M. Kozlowski, R. Kozubski, V. Pierron-Bohnes, M.C. Cadeville and W. Pfeiler, "Dynamics of atomic ordering in intermetallics", Mater. Sci. Eng. A 365 (2004), p. 165.
[4] R.J. Wasilewski, "Structure defects in CsCl intermetallic compound", J. Phys. Chem. Solids 29 (1968), p. 39.
[5] Mats Hillert, "Phase Equilibria, Phase Diagram and Phase Transformations - Their Thermodynamic Basis", Cambridge University Press (2008), p. 78, p. 462
[6] M.P. Gururajan and T.A. Abinandanan, "Effect of interaction energies on the vacancy behaviour in B2 ordered intermetallics", Mater. Sci. Eng. A 329_331 (2002), p. 388
[7] C.L. Fu, Y.-Y. Ye, M.H. Yoo and K.M. Ho, "Equilibrium point defects in intermetallics with B2 structure: NiAl and FeAl", Phys. Rev. B 48 (1993), p. 6712; J. Mayer and M. Fähnle, "On the meaning of effective formation energies, entropies and volumes for atomic defects in ordered compounds", Acta. Mater. 45 (1997), p. 2207; M. Fähnle, J. Mayer and B. Meyer, "Theory of atomic defects and diffusion in ordered compounds, and application to B2-FeAl", Intermetallics 7 (1999), p. 315; B. Meyer and M. Fähnle, "Atomic defects in the ordered compound B2-NiAl: a combination of ab initio electron theory and statistical mechanics", Phys. Rev. B 59 (1999), p. 6072; P.A. Korzhavyj, A.V. Ruban, A.Y. Lozovoi, Yu. Kh. Vekilov, I.A. Abrikosov and B. Johansson, "Constitutional and thermal point defects in B2 NiAl", Phys. Rev. B 61 (2000)
[8] R. Krachler and H. Ipser, "Triple defect complexes in the B2 intermetallic compound NiAl", Phys Rev B 70 (2004), p. 054113 ; Y.L. Hao, Y. Song, R. Yang, Y.Y. Cui, D. Li and M. Niinomi, "Concentration of point defects in binary NiAl" , Philos. Mag. Lett. 83 (2003), p. 375 ; P. Oramus, A. Biborski, R. Kozubski, K. Parlinski and P.T. Jochym, "Superstructure stability and site preferences in b-NiAl doped with Fe, Co, and Cr Monte Carlo simulation", Arch Metall Mater 52 (2007), 33

[9] S. Müller, W. Wolf and R. Podloucky In: W. Pfeiler, Editor, "Alloy physics. A comprehensive reference", Wiley-VCH, Weinheim (2007), 612
[10] M. Hagen and M.W. Finnis, "Point defects and chemical potentials in ordered alloys", Philos. Mag. A 77 (1998), 447
[11] J. J. Hoyt , J. W. Garvin , E. B. Webb III and Mark Asta, "An embedded atom method interatomic potential for the Cu_Pb system", Modelling Simul. Mater. Sci. Eng. 11 (2003) 287; Ivailo Atanasov, Marc Hou, "Equilibrium ordering properties of Au_Pd alloys and nanoalloys ", Surface Science 603 (2009) 2639
[12] A. Y. Lozovoi, Y. Mishin, "Point defects in NiAl: The effect of lattice vibrations », Phys. Rev. B 68, 184113 (2003)
[13] Y. Mishin, M. J. Mehl and D. A. Papaconstantopoulos, "Embedded-atom potential for B2-NiAl ", Phys. Rev. B 65 (2002)
[14] H.-E. Schaefer, K. Frenner, R. Wurschum, "High-temperature atomic defect properties and diusion processes in intermetallic compounds",Intermetallics 7 (1999) 277
[15] R. Sot ICM Warsaw, private communication
[16] R.N. Nogueira and C.G. Schön, "Embedded atom study of the interaction between point defect in iron aluminides: Triple Defects", Intermetallics 13 (2005) 1245
[17] R. Kozubski, D. Kmiec, E. Partyka and M. Danielewski, "Order-order kinetics in $Ni_{50.5}Al_{49:5}$ single crystal", Intermetallics 11 (2003), 897 ; H.-E. Schaefer, K. Frenner and R. Würschum, "Time-differential length measurements for thermal defect investigations: intermetallic B2-FeAl and B2-NiAl compounds, a case study", Phys. Rev. Lett. 82 (1999), 949
[18] K. A. Marino, E. A. Carter, "First-principles characterization of Ni diffusion kinetics in β-NiAl", Phys. Rev. B 78, 184105 (2008)
[19] S. Divinski , Chr. Herzig ,"On the six-jump cycle mechanism of self-diffusion in NiAl », Intermetallics 8 (2000) 1357
[20] P. Oramus, R. Kozubski ,V. Pierron-Bohnes, M. C. Cadeville, W. Pfeiler, "Monte Carlo computer simulation of order-order kinetics in the $L1_2$ -ordered Ni_3Al binary system", Phys. Rev. B 63, 174109 (2001)

---

[i] Par exemple la coexistence de deux phases liquides, la stabilité de nanoparticules etc.

[ii] Le fait de négliger les degrés de liberté de type élastique, comme la relaxation des positions atomiques au voisinage des défauts ou la modification du volume total due à la dilatation thermique, peut être remis en question puisque le « bulk modulus » par exemple a été utilisé pour déterminer les potentiels EAM.

[iii] La valeur obtenue dans notre procédure d'intégration dans le potentiel semi-grand canonique est exactement : $c_V(1500\ K) = 7.5\ 10^{-3}$. Cependant, nous avons estimé la barre d'erreur à 30%, nous ne pouvons dons seulement discuter l'accord entre les ordres de grandeurs des valeurs obtenues.

Contents

List of Figures

List of Tables

Index of Symbols and Abbreviations

δ	stoichiometry parameter
$\Delta\mu_{pr}$	relative chemical potential
$\delta_{\mu\nu}$	Kronecker delta
ϵ	infinitesimal factor
η_p	long range order parameter related to constituent p
Γ, Γ_i	microstate
μ_p	chemical potential of constituent p
ν, μ	indeces labeling sub-lattices
Ω	phase space, also grand potential
ω	Semi Grand Canonical potential per lattice site
$\omega^{(i)}$	Semi Grand Canonical potential per particle in the phase i
ω_{ij}	frequency of successful atomic jump (TST)
$\overline{A}$	An average value of observable obtained by means of Monte Carlo method
σ	configuration of a system
σ_i	atomic cluster
$\tilde{\Omega}$	Semi Grand Canonical potential
$\triangle J_{X:\mu\rightarrow\nu}$	number of jumps performed by atom X within given time interval
Υ	Semi Grand Canonical partition function
$\vec{r_i}, \vec{v_i}, \vec{a}_i$	position, velocity and accelaration related to particle i
Ξ	Grand Canonical partition function
$\xi_{k:X^{(\nu)}-Y^{(\mu)}}, \xi_{X-Y}$	short range order correlation parameters
$\{\alpha_k\}$	set of variables defininig the point in a phase space

$\{\chi_p\}$	chemical composition parameter
a_0	lattice constant
a_{ij}	probability of sampling the transition between microstates per MC Time unit
B	bulk modulus
c_p	concentration of p-atoms in a system
$c_p^{(\mu)}$	concentration of p-atoms residing on μ sub-lattice
$E^{(s,j)}$	saddle point energy
E_0	cohesive energy
$E^{dis}_{A:\alpha\to\beta}$	efficiency of disordering related to A atoms
$f(\{\sigma_i\})$	free Hemholtz energy functional in per lattice site in terms of cluster variables
$f(H_N(\Gamma))$	density of probability distribution function
$F(\sigma)$	free Helmholtz energy functional
$f_{X:\alpha\leftrightarrow\beta}$	ratio between jump frequencies
$f_{X:\mu\to\nu}$	frequency of jump
H_N	Hamiltonian
$J_{X:\mu\to\nu}$	X atom jump
k_B	Boltzmann constant
N	total number of lattice sites
$N^{(\mu)}$	number of sub-lattice sites
$n^{(\mu)}$	number of sub-lattice sites per number of total lattice sites
N_{pq}	number of atomic pair pq
N_X	total number of atoms of kind X present in a system
$N_X^{(\nu)}$	number of atoms (vacancies) residing on sub-lattice ν
P	pressure
$P(\Gamma)$	probability of microstate sampling
p, q, r	indices of kind of constituents
R	electrical resistivity
r_{ij}	distance between two atoms/lattice sites
$R^{(i)}_{N_{V\times z}}, R^{(i)}_{N_T}$	cumulative function in Residence Time Algorithm

S	entropy
T_C	order-disorder temperature
$TDI, TDI_{ACT}, TDI_{ACT}^{(A)}$	triple defect indicators
V_{pq}	pair-wise interaction
W	ordering energy
w_{ij}	probability of transition between microstates
$W_{ij}(\Gamma_i \rightarrow \Gamma_j)$, W_{ij}	transition probability rate
$X^{(\nu)}$	atom of kind X residing on sub-lattice ν
$z_{\mu\nu}$	nearest neighbours co-ordination matrix
Z_N, $Z_{\{N_p\}}$	Canonical Ensemble partition function
B-W	Bragg-Williams
EAM	Embedded Atom Method
KMC	Kinetic Monte Carlo
MC	Monte Carlo
nn	nearest neigbour
nnn	next-nearest neighbour
RTA	Residence Time Algorithm
SGCE	Semi Grand Canonical Ensemble
SGCMC	Semi Grand Canonical Monte Carlo
TST	Transition State Theory

Acknowledgements

I especially thank Prof. Rafał Kozubski for providing me with great deal of assistance and for discussions which gave me an opportunity to improve my knowledge. His kindness, enthusiasm and passion always stimulated me in my scientific research. I also especially thank Dr Veronique Pierron-Bohnes for her scientific advises and friendliness. My stays in Strasbourg always helped me to look at investigated problems in the fresh perspective. I would like to thank sincerely Prof. Mebarek Alouani for precious discussions and advises. I also thank Mr. Łukasz Zosiak for his assistance in the field of computer science.

Streszczenie

Celem niniejszej pracy jest opracowanie modelu kinetyki porządkowania atomowego w związkach międzymetalicznych z nadstrukturą typu B2 metodami symulacji komputerowych opartych na technikach **Monte Carlo**.

Do grupy badanych związków metalicznych należą min. *NiAl*, *FeAl*, które ze względu na niską gęstość i wysoką odporność na działanie wysokich temperatur są kandydatami do zastosowań w nowoczesnej technologii materiałów konstrukcyjnych. Atrakcyjne właściwości wspomnianych układów związane są z uporządkowaniem atomowym dalekiego zasięgu, które powstaje w układzie na drodze migracji atomów odbywającej się za pośrednictwem wakancji. Eksperymentalnie stwierdzono, że w związku $NiAl$ zawierającym kilka rzędów wielkości więcej wakancji niż Ni_3Al proces porządkowania atomowego przebiega znacznie wolniej. Przeprowadzone badania miały na celu weryfikację hipotezy, iż przyczyną obserwowanego zjawiska jest **defekt potrójny** - w specyficzny sposób „pułapkujący" wakancje powstające w związku NiAl. W ramach studium nad przyczyną wspomnianego zjawiska opracowany został oparty na symulacjach Monte Carlo model procesu tworzenia defektów antystrukturalnych w układzie z nadstrukturą B2 wykazującym tendencję do tworzenia defektów potrójnych. Realizacja projektu przebiegała w dwóch etapach: **(i)** Opracowanie analitycznego i symulacyjnego modelu termodynamicznego do wyznaczania równowagowej koncentracji wakancji. **(ii)** Symulacja relaksacji „porządek-porządek" w układzie z nadstrukturą B2 metodami „Kinetic Monte Carlo" przy uwzględnieniu równowagowej koncentracji wakancji wyznaczanej metodami opracowanymi w etapie (i).

W ramach opracowanego modelu dwuskładnikowego związku międzymetalicznego AB opartego na nadstrukturze typu B2 przebadano naturę defektu potrójnego jak i jego wpływ na kinetykę przemian typu "porządek-porządek". Symulacyjne rozwiązanie modelu termodynamicznego tworzenia wakancji pozwoliło na przebadanie specyficznej korelacji tworzenia defektów punktowych - rozpoznano istnienie defektu potrójnego w wymodelowanym układzie. W ramach symulacji kinetyk typu "porządek-porządek" wykryto możliwą przyczynę zwolnienia procesów rozporządkowania (zarejstrowaną eksperymentalnie dla układu B2 *NiAl*) związaną z asymetrią tworzenia defektów punktowych w sieci krystalicznej (defekt potrójny). Tym samym cel pracy został osiągnięty.

Chapter 1

Introduction

Intermetallics compounds based on the B2 superstructure are systems known for their physical properties which are attractive for modern materials engineering. It is one of the reasons of intensive, both experimental and theoretical studies in the last decades. On the other hand, phenomena observed in B2 superstructure are interesting from the theoretical point of view. In many cases the origin of these effects should be considered on atomistic scale. Rapid development of computational power gives an opportunity to investigate those systems by means of simulation methods from very simplified analytical models to advanced and computationally complex techniques based on Monte-Carlo methods, Molecular Dynamic and Molecular Statics.

This work is a simulation study of chemical ordering in B2 superstructure based alloys. The main methodology applied is Monte-Carlo method though calculations in an analytical model based on the Bragg-Williams approximation and Molecular Static simulations were also performed. In the following sections not only B2 superstructure will be described but also experimental motivation of this study and the scheme of solution for the addressed problems will be given.

1.1 B2 superstructure. Chemical ordering.

Intermetallic compound systems are solid phases containing two or more metallic elements and stable within a limited concentrations range. Those based on B2 superstructure consist of two kinds of constituents A, B (e.g $NiAl$ with $A = Ni$ and $B = Al$; $FeAl$ with $A = Fe$ and $B = Al$) being distributed regularly in the body centered cubic (bcc) lattice. This regularity in atomic positions arrangement refers to the term *superstructure,* which means that system exhibits specific *chemical order.* In the case of B2 superstructure, perfectly ordered crystalline lattice may be divided into two interpenetrating simple cubic (sc) *sub-lattices* α, β being occupied only by one kind of element A or B respectively.

In practice no ideal crystals exist in finite but non zero temperatures and imperfections of the crystals exhibit as the presence of *defects* [1, 2]. The existence of defects assists the system increasing the entropy and contributes to attaining equilibrium in given external conditions (temperature,pressure, external field). Usually thermally activated defects are taken into consideration.

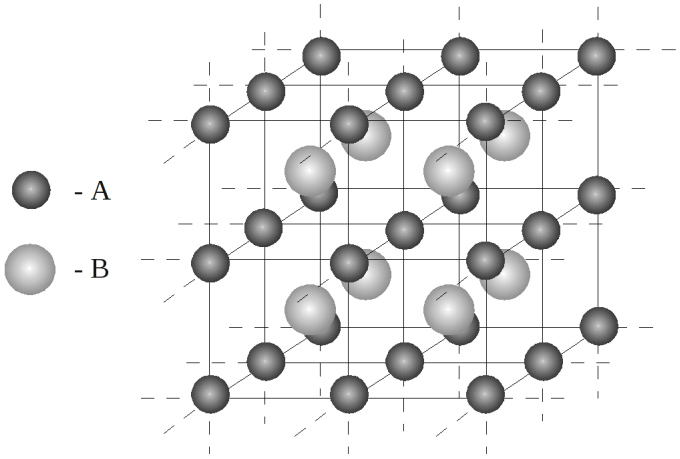

Figure 1.1: The part of the perfectly ordered B2 superstructure.

There are various possibilities of crystalline defects observed in experiments, such as: line defects (e.g. dislocations), planar defects (e.g. grain boundaries, stacking points) etc. In this study only particular kind of defect called *point defects* is investigated due to its direct association with chemical ordering phenomena.

Point defects perturb a chemical order of a superstructure, for example if A-atom occupies the site associated (in terms of ideal order of crystal) with B-atom sub-lattice the order of the system decreases. Such defect is called *anti-structural defect* or *antisite*. For clarity, the following notation for antisites (and other atoms residing on particular sub-lattice) will be used: $X^{(\nu)}$ where $X = A, B$ denotes the atomic constituent and $\nu = \alpha, \beta$ refers to the sub-lattice. Another, important kind of the point defect being of interest is *vacancy*. Vacancy (or Schottky defect) is an empty site in a crystalline lattice and will be denoted as $V^{(\nu)}$. The existence of the point defects induces perturbation of order of intermetallic by changing *a configuration* of atom distribution over the sub-lattices. This rearrangement of atomic configuration may be driven by vacancy migration mechanism in the intermetallic systems (see e.g. [3]). It means that atom being in the surrounding of a vacancy may force the energetic barrier and change its localization in the lattice performing the "jump" into the vacancy. The sequences of such events form *kinetic* processes leading to new, equilibrium configuration. These processes may be responsible for the variation of the chemical order, which is the case for B2 superstructure based intermetallics being of interest. In this work both equilibrium configuration and kinetic processes are investigated.

However, the order of the superstructure may be disturbed by point defects not being thermally activated but induced by the deviation in the chemical composition from *stoichiometry*. This kind of point defects is classified as *constitutional defects*[1]. Hence it is convenient to define stoichiometry deviation

[1]Some authors (see e.g. [2]) undermine validity of that terminology.

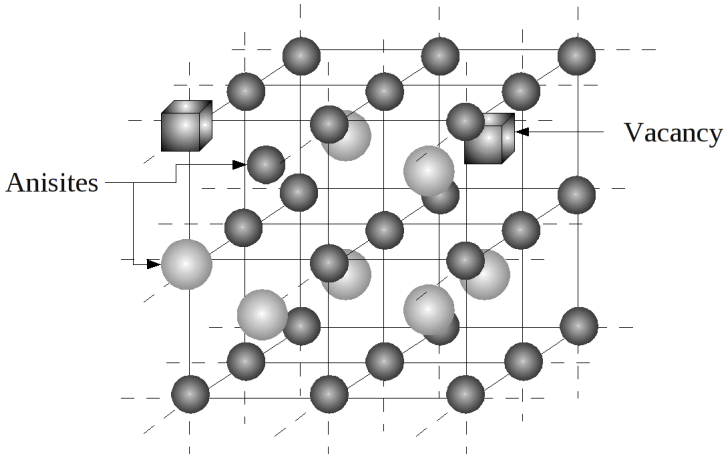

Figure 1.2: Point defects disturbing chemical order in B2 superstructure.

ratio by adding δ parameter in the chemical notation. In case of the B2 superstructure it is $A_{1-\delta}B_{\delta}$ where δ is defined by Eq.1.1.

$$\delta \equiv \frac{N_B}{N_A + N_B} \tag{1.1}$$

The quantities N_X in above equation are number of X atoms in a system. Therefore, according to definition of the perfectly ordered B2 superstructure, stoichiometry refers to $\delta = 0.5 \Longleftrightarrow N_A = N_B$.

The configuration altered by the defects is related to the variation of the macroscopic properties of the crystals such as: electrical resistivity, heat conductivity, hardness, magnetization etc. This fact gives an opportunity to study the chemical ordering phenomena by means of diverse indirect experimental techniques.

1.2 Experimental motivation for the study and triple defect

The intermetallics based on the B2 superstructure notably $NiAl$ and $FeAl$ are candidates for so called "super alloys" - materials exhibiting properties being suitable for the applications in extremal conditions - e.g. high temperatures through their mechanical strength, corrosion resistance, mutually accompanied by low density of material [4, 5]. Particularly high melting temperature of $NiAl$ B2 binary gives an opportunity to apply this material in gas turbine engines. These attractive features may be often better understood in the context of chemical order phenomena. Therefore, the investigations of the chemical ordering in B2 superstructure based intermetallics are not only interesting in framework of condensed matter physics itself but may also play an important role in the modern material science and engineering taking into account the importance of atomic kinetics processes in view of technological aspects.

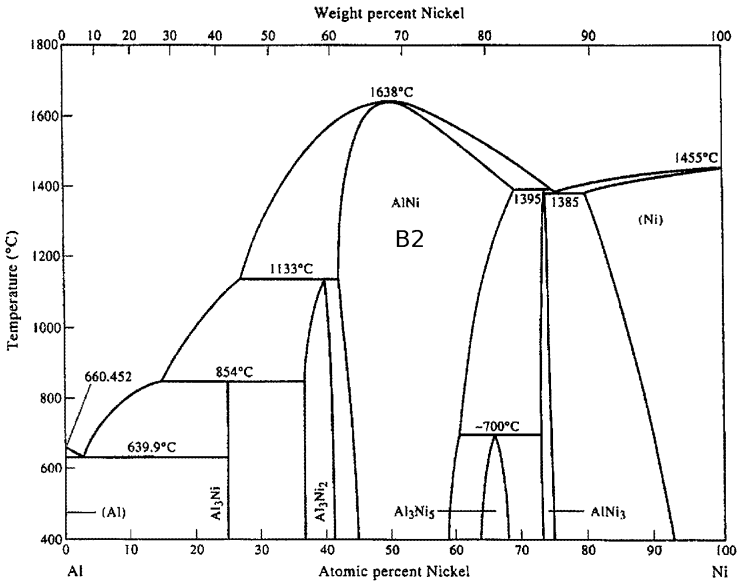

Figure 1.3: $Ni - Al$ system phase diagram [7].

This work is inspired by the experimental result on chemical ordering kinetics in nearly stoichiometric $B2 - NiAl$ intermetallic sample. Firstly let us shortly characterize this intermetallic:

The phase diagram for $Ni-Al$ system is shown in a Fig.1.3. The B2 ordered phase is the most stable one. Its melting temperature is the highest for the nearly stoichiometric phase and equals approximately 1911 $°K$ [2]. It must be mentioned that the range of the chemical composition referring to the existence of B2 $NiAl$ phase is quite wide and refers approximately to $\delta\epsilon(0.42, 0.55)$, which is not an ordinary feature for the typical intermetallic compound. For example, $L1_2$ Ni_3Al phase (based on the face centered cubic structure), being also deeply investigated due to its unusual yielding stress properties, is only "thin" area in a phase diagram space and one finds its chemical composition variation as typical for the intermetallic systems. No "order - disorder" transition temperature T_C of $B2$ $NiAl$ was found - it exhibits high chemical order up to the melting temperature. The lattice constant of nearly stoichiometric $B2$ $NiAl$ equals approximately 2.88 $\mathring{A}$ (linear thermal expansion coefficient in the temperature range of phase stability is less than $20 \times 10^{-6} K^{-1}$ see e.g. in [6]).

1.2.1 "Order - order" processes in B2 NiAl: resistometric experiments [8].

The change in the degree of an atomic order in the intermetallics caused by external conditions e.g. heating may be investigated by means of electrical

[2]The temperature in the figure is given in Celsius, however in the text Kelvin scale is used.

resistivity measurements. Typical procedure of this kind of experiment can be described by the following steps[3]:

1. A sample is equilibrated at a given temperature $T_i < T_C$ - such equilibration leads to a particular degree of chemical order of a sample[4].

2. The temperature T is increased/decreased to arbitrary chosen temperature $T_j < T_C$. Temperature dependence of the sample resistivity is monitored. The measurement is continued until $R(t)$ saturates to statistically constant value referring to a newly attained equilibrium.

3. The measurement is repeated: $T_j \rightarrow T_k < T_C$

The scheme of the procedure given above allows to investigate "order-order" processes by means of the $R(t)$ curves analysis. It must be noted that the resistivity variation is enforced by configurational and phonon factors [3]. In particular: an increase in the number of antisites results in an increase in electrical resistivity which justifies to study the ordering phenomena by means of the resistometry techniques.

Detailed analysis of $R(t)$ curves gives an opportunity to obtain time scale coefficients τ (relaxation times). In the experiment being of interest, $B2\ Ni_{0.505}Al_{0.495}$ single crystal was investigated. The set of measurements with increasing/decreasing temperatures (disordering/ordering) were performed and the deviation of resistivity $\triangle R(t)$ (Fig 1.4) were obtained.

The time scale coefficients τ for different temperatures were found after fitting functions to the experimental curves:

$$\frac{\triangle R}{R_{eq}} = \int P(\tau')e^{-\frac{t}{\tau'}}d\tau' \tag{1.2}$$

and evaluating:

$$\tau = \int_0^\infty P(\tau')\tau' d\tau' \tag{1.3}$$

Arrhenius type plots $ln\,(\tau(\beta))$ (where $\beta^{-1} = k_B T$) allowed to evaluate the activation energies of the ordering and disordering processes. Subsequently, the comparison of the results obtained for $L1_2\ Ni_3Al$ intermetallic evidenced that "order-order" relaxations for B2 superstructure proceeded remarkably slower than in the case of $L1_2$ (Fig.1.5). Precisely, the comparable values of the average relaxation times in B2 superstructure were observed at much higher temperatures than in Ni_3Al. Taking into account that (see sec.1.1) the change of antisite concentrations is due to sequences of atomic jumps into vacancy, the results cannot be understood intuitively, since vacancy concentration c_V in $B2\ NiAl$ was found much higher (app. $10^5 \sim 10^6$ times in the comparable temperatures) than in $L1_2\ Ni_3Al$ in the experiments reported by Schaefer et al. [9, 10].

[3]Given list includes fundamental ideas. At least two methods of measurements exists: "in situ" and REST. Interested reader is invited to study dedicated publications referred in the text.

[4]Note that in the case of B2 NiAl T_C may be regarded as melting temperature.

The possible explanation of the slow rate of "order-order" kinetics in the atomistic scale was given in Ref. [8]. It was inspired by the idea firstly given by Wasilewski [11] - the *triple defect* model of disordering for B2 based superstructures.

1.2.2 Nature of Triple Defect

Vacancy formation is assumed to be an event conserving the geometry of the lattice in the model. This assumption implies that vacancies have to be created/annihilated in pairs on both sub-lattices according to the fact that primitive cell of B2 superstructure consists of two atomic species. Hence, assuming the smallest increase/decrease in vacancy concentration, the pair of thermal ($T > 0$) vacancies are generated firstly (Fig.1.6b). Since vacancies are present, atom A or B may create antisite $A^{(\beta)}$ or $B^{(\alpha)}$ (Fig.1.6c and 1.6d respectively). Let us assume that atom $A^{(\alpha)}$ jumps into $V^{(\beta)}$ firstly (Fig.1.6c). It leads to the configuration in which both vacancies, visible on the picture are located on β sub-lattice. The disordering process may be continued by means of formation of an antisite of type $B^{(\alpha)}$(Fig.1.6d). Finally there are two vacancies on different sub-lattices, accompanied by the existence of two antisites. Let us present performed events in a form of chemical reactions:

$$\text{"0"} \overset{T>0}{\rightarrow} V^{(\alpha)} + V^{(\beta)} \rightarrow 2V^{(\alpha)} + A^{(\beta)} \rightarrow V^{(\alpha)} + V^{(\beta)} + A^{(\beta)} + B^{(\alpha)} \qquad (1.4)$$

The sequence described above may be repeated, progressing the disordering process, until equilibrium configuration is attained. Therefore, the number of antisites of both kinds produced by means of given mechanism should be

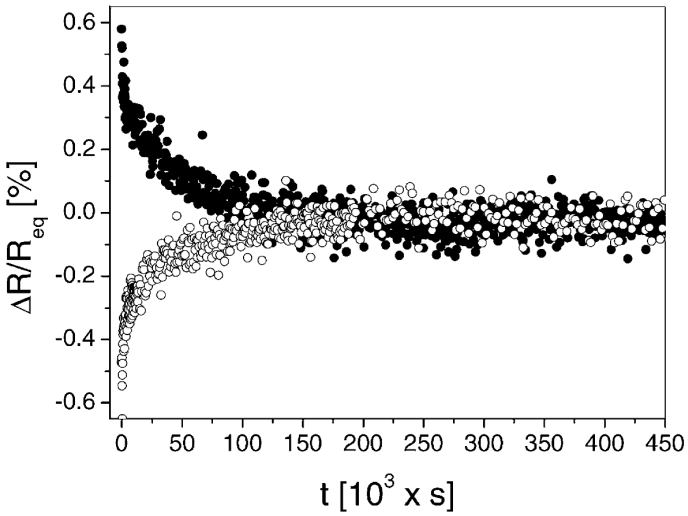

Figure 1.4: Relaxation of the electrical resistivity for $B2\ Ni_{50.5}Al_{49.5}$ sample in $T_2 = 1060\ K$. Hollow circles refer to $T_1 = 1011\ K$; Black circles refer to $T_1 = 1105\ K$.

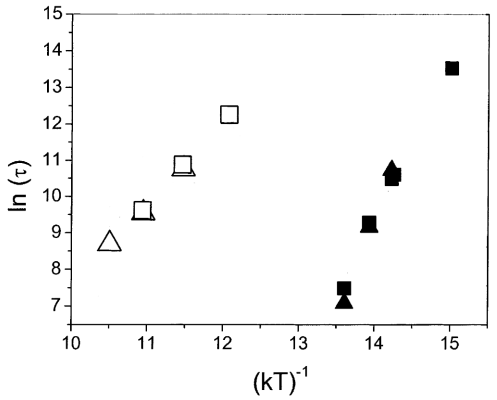

Figure 1.5: Arrhenius plots for $B2NiAl$ (hollow symbols) and $L1_2Ni_3Al$ (black symbols): squares denote ordering while triangles disordering for both samples consecutively

approximately equal. This happens, however, provided probabilities $P(X^{(\nu)})$ for both antisite formation events are assumed to be close to each other:

$$P(A^{(\beta)}) \approx P(B^{(\alpha)}) \Longrightarrow \left(\triangle N_A^{(\beta)} \approx \triangle N_B^{(\alpha)}\right) \wedge \left(N_V^{(\alpha)} \approx N_V^{(\beta)}\right) \tag{1.5}$$

where $N_X^{(\nu)}$ denotes the number of atoms/vacancies occupying ν sub-lattice. However, let us assume now that probabilities are significantly different:

$$P(A^{(\beta)}) \gg P(B^{(\alpha)}) \tag{1.6}$$

This implies, that the production of antisites being of type $B^{(\alpha)}$ will be incidental in comparison to the creation of the $A^{(\beta)}$ ones (see the configuration in the Fig.1.6c):

$$P(A^{(\beta)}) \gg P(B^{(\alpha)}) \Longrightarrow \left(\triangle N_A^{(\beta)} \gg \triangle N_B^{(\alpha)}\right) \wedge \left(2N_A^{(\beta)} \approx N_V^{(\alpha)}\right) \tag{1.7}$$

Hence, most vacancies are "trapped" on α sub-lattice (since $P(A^{(\beta)}) \gg P(B^{(\alpha)})$) and become very inefficient as atomic migration agents in a further disordering relaxation.

It leads to the conclusion that vacancies mostly occupy the α sub-lattice, contrary to antisites being only of $A^{(\beta)}$ kind ($N_A^{(\beta)}/N_V^{(\alpha)} \approx 1/2$). A complex of three point defects: two vacancies and one antisite is called a *triple defect* (after Wasilewski [11]).

According to the definition given by Wasilewski, the tendency for the generation of triple defect implies that for $\delta > 0.5 \Longleftrightarrow N_B > N_A$ the deviation from stoichiometry will be compensated by the so-called constitutional vacancies remaining in the system after the decay of thermal point defects (low temperatures). On the other hand, if $\delta < 0.5 \Longleftrightarrow N_B < N_A$ the deviation is compensated by A-atoms residing onβ sub-lattice.

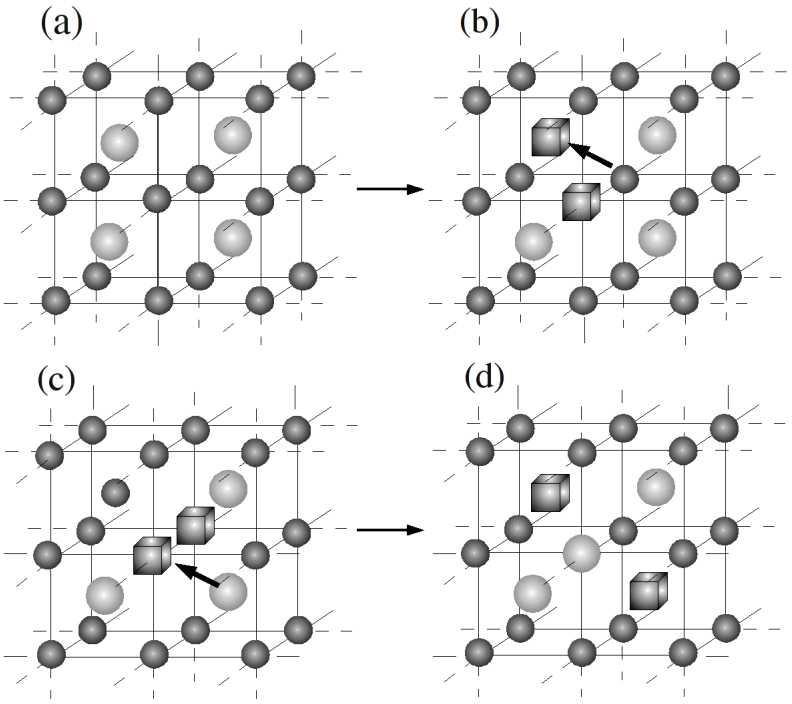

Figure 1.6: The scheme of disordering in B2 superstructure.

Concluding, the triple defect mechanism was proposed as a possible explanation for low rate kinetics of chemical disordering in the referred resistometry experiment [8]. Although the single crystalline sample examined was supposed to be characterized by high vacancy concentration (according to the experimental results reported in Refs. [9, 10]), most vacancies were suspected to be "trapped" on α sub-lattice hence remained inactive in further processes. Although one may argue that effects observed in resistometry experiment referred to the relaxing vacancy concentration, comparison of the relaxation times between resitometry experiment dedicated to "order-order" phenomena [8] and dilatometry measurements dedicated to the equilibrium vacancy concentration [9] allows to exclude this option. The relaxation times of "order-order" transformations were approximately two orders of magnitude longer (Fig.1.7)[5].

This work is model-oriented investigation of chemical ordering processes in triple defect type systems by means of computer simulation techniques.

[5]It must be noted that though different chemical composition where regarded in both experiments ($Ni_{50.5}Al_{49.5}$ in the resistometry, $Ni_{47}Al_{53}$in the dilatometry) the conclusion given is still valid if the context of constitutional vacancies is complied, see Ref. [8])

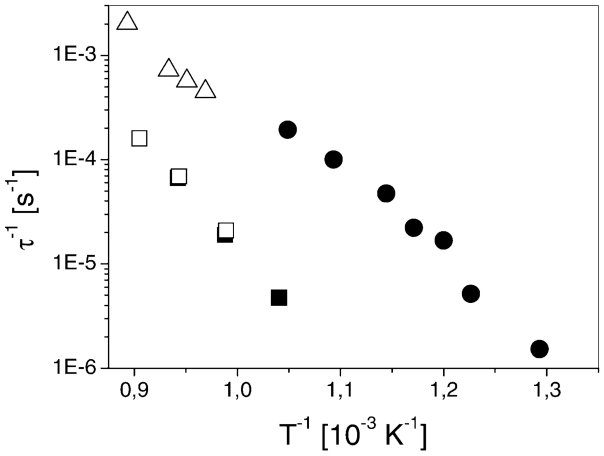

Figure 1.7: The comparison between length of time relaxations in resistometry experiment (squares) and dilatometry (triangles and circles)

1.3 Scheme of the study. General tasks.

The main task of this work is to model the kinetic processes of disordering in the B2 A-B system exhibiting triple defect type behavior. *Monte Carlo* (MC) techniques supported by *Molecular Statics* (MS) calculations are the main tool chosen to perform the simulations in a atomistic scale.

In the preceding sections it was demonstrated that the mechanism of antistructural defect creation may be of triple defect type which implies specific correlation between antisite and vacancy concentrations. Thus, it is clear that in *Kinetic Monte Carlo* (KMC) simulations performed for the systems being of interest temperature dependence of the equilibrium vacancy concentration has to be taken into account.

The modelling tasks for B2 superstructure based intermetallics is an area being deeply studied by many authors in various contexts. Most of them focused on equilibrium aspects (investigating the triple defect as well). However, there is no complete elaboration of methodology, which allows for investigating chemical ordering processes in view of atomic kinetics by means of MC techniques taking into account vacancy thermodynamics.

The present study consists of two main modelling stages:

- Vacancy thermodynamics
  - Equilibrium vacancy concentration in a wide range of temperatures is found for B2 triple defect binaries
- Kinetics of "order-order" processes simulations
  - Chemical disordering processes in a triple defect type system is simulated taking into account equilibrium vacancy concentration

The methodology for vacancy thermodynamics had to be compatible with kinetic MC simulations performed in the second stage of project. The use of analytical methods for obtaining equilibrium vacancy concentration would undoubtedly violate the consistency of the treatment. Therefore, the methodology based on the MC techniques had to be elaborated as one of the main task in the study. However, an analytical model, based on the *Bragg - Williams* approximation was also applied and was found very helpful in the very first stage of project realization. The methodology applied in both stages is presented in a Tab.1.1.

Stage	Task	Applied Methodology
I	Vacancy Thermodynamics	Bragg Williams approximation MC Simulations in *Semi Grand Canonical Ensemble*
II	Kinetic of disordering processes	Molecular Static Simulations Kinetic Monte Carlo (KMC) Simulations in *Canonical Ensemble*

Table 1.1: The scheme of this study and applied methodology.

Part I

Theoretical Background

Chapter 2

Chemical Ordering - Statistical Models

Of interest is atomic arrangement in a crystal corresponding to chemical order. Therefore, necessary simplifications making the model solvable by means of existing techniques have to be established. The branch of statistical physics dealing with the chemical ordering in multicomponent systems is *configurational thermodynamics*. In the context of triple defect type systems - where vacancy thermodynamics cannot be neglected - equilibrium configuration consists of atomic arrangement correlated with the particular amount of vacancies. Therefore, vacancy distribution over lattice sites is an integral part of equilibrium chemical order.

Non - equilibrium kinetics processes are also of interest. This aspect may be treated by means of *Transition State Theory*, known mainly for its application in the description of chemical reactions processes.

The chapter is organized as follows: firstly basics of configurational thermodynamics are given. Secondly the concept of obtaining equilibrium vacancy concentration (correlated with the equilibrium atomic configuration) is described, at the very end of this chapter, principles of the Transition Rate Theory in a context of kinetics of vacancy mediated processes in the intermetallics are discussed.

2.1 Basics of configurational thermodynamics.

Complete description of intermetallic phases requires that both configurational and non-configurational degrees of freedom [3] such as the lattice vibrations, electronic motions are considered. However non-configurational phenomena are characterized by a time scale which is orders of the magnitude shorter than that for the configurational degrees of freedom. Hence, it is justified to claim that total energy of crystal attributed to particular microstate Γ considered as the sum of terms referring to configurational and non-configurational contributions is given by the following formula:

$$E_{tot}(\Gamma) = E_c(\sigma) + E_{other}(\sigma) \tag{2.1}$$

Where $E_c(\sigma)$ is configurational energy and $E_{other}(\sigma)$ is non-configurational energy (associated with non-configurational degrees of freedom), both given for

the particular configuration σ related to microstate Γ.

Above equation states that average of observable can be performed for non-configurational degrees of freedom independently to configurational ones at a given configuration σ. Therefore, if total number of particles, composition, volume and temperature are fixed (crystal is in a thermal equilibrium with surrounding) the partition function may be presented in a following form:

$$Z_N = \sum_{\sigma} \left(e^{-\beta E_C(\sigma)} \times \sum_{other} e^{-\beta E_{other}(\sigma)} \right) = \sum_{\sigma} e^{-\beta [E_C(\sigma) + F^*_{other}(\sigma)]} \equiv \sum_{\sigma} e^{-\beta E(\sigma)} \tag{2.2}$$

Where $E(\sigma) \equiv E_c(\sigma) + F^*_{other}(\sigma)$ is "effective" configurational energy and $F^*_{other}(\sigma)$ relates to the non-configurational degrees of freedom associated with given configuration σ and is usually assumed to be temperature independent. However, the sum above may be rewritten respecting the number of configurations $g(E_k(\sigma))$ [12] associated with particular $E_k(\sigma)$ and approximated by its maximal term (see e.g. [12]):

$$Z_N = \sum_{k} g(E_k(\sigma)) e^{-\beta E_k(\sigma)} \approx max \left(g(E_l(\sigma)) \times e^{-\beta E_l(\sigma)} \right) \tag{2.3}$$

Defining free energy functional as:

$$F(\sigma) \equiv -\frac{1}{\beta} ln \left(g(E(\sigma)) \times e^{-\beta E(\sigma)} \right) \tag{2.4}$$

one realizes that its minimization allows to find configuration referring to the equilibrium state - it means that conventional variational problem needs to be solved. However, the forms of $E(\sigma)$ and $g(E(\sigma))$ have to be known.

According to the arguments given in the first part of this section, one notes that configurational problem can be considered in the framework of pairwise interactions, where $E(\sigma)$ is represented by Eq.2.5.

$$E(\sigma) = \frac{1}{2} \sum_{i,j} \phi_{ij} \left(r_{ij}(\sigma) \right) \tag{2.5}$$

The indices "i" and "j" number all particles present in the system and include particle identity (A,B,C,...). The function ϕ_{ij} describes the strength of bonding between particles being separated by the distance r_{ij} (including non-configuarational degrees of freedom). However, if degrees of freedom associated with "elasticity" (e.g. thermal expansion) are effectively incorporated into interactions, and only point defects are taken into account, rigid lattice approach may be considered. Then, interactions between atoms and non-configurational contribution to energy can be expressed in one term $V^{(k)}_{pq}$ where "p" and "q" denote atomic species and "k" refers to label of co-ordination zone (since the rigid lattice is taken into account $r_{ij} \rightarrow k$)

Hence, if the above assumptions are taken into account the Eq.2.5 may be rewritten in a form of Ising type model:

$$E(\sigma) = \frac{1}{2} \sum_{p,q} \sum_{k} V^{(k)}_{pq} N^{(k)}_{pq}(\sigma) \tag{2.6}$$

where $N_{pq}^{(k)}$ denotes the number of p-q atomic pairs being neighbours in the k-th coordination zone.

Although numerous approximations leading to purely configurational treatment were assumed, the problem of obtaining equilibrium state is still in question since direct solution of Ising model given by Onsager refers only to two-dimensional case [13]. Direct minimization of the $F(\sigma)$ functional (Eq.2.4) with the configurational energy $E(\sigma)$ (Eq.2.6) is impossible.

The approximate solution may be found by using an approach in which configuration σ is expressed as a set of smaller atomic clusters $\{\sigma_i\}$ related to all lattice sites "i". The size, geometry and general complexity of cluster depends on the type of structure and desired accuracy.

This method is called in the literature *Cluster Variation Method (CVM)*(see e.g. Refs. [14, 3, 15]). The complexity (size) of introduced clusters refers to the CVM hierarchy e.g. if the maximal cluster is simple a single lattice site then well known Bragg-Williams (B-W) approximation is formulated. If one considers two-site clusters, Bethe-Peierls or quasichemical approximation in CVM hierarchy is considered. Analogously, bigger clusters can be introduced and better approximation of the exact configuration is obtainable.

It must be mentioned that CVM formalism referred to quantum mechanical calculations of configurational energy based on the Density Functional Theory (DFT) forms *Cluster Expansion Method (CEM)* [16]. Therefore direct link between CVM formalism and real systems may be achieved.

2.2 Equilibrium vacancy concentration. Lattice-gas decomposition.

The origins of vacancy production are localized in grain boundaries, dislocations, surfaces etc. These are also sinks where vacancies may be annihilated. Hence, in the equilibrium the concentration of vacancies in a crystalline phase is statistically constant, though the fluctuations referred to dynamical character of production/annihilation events appear.

Despite the physical picture given above, equilibrium vacancy concentration models are usually situated in strictly thermodynamical context. It means, that microscopic mechanism of vacancy creation/annihilation is not directly considered.

A brief summary of the most common approaches to thermodynamics of vacancies in intermetallics was given in 1992 by Lim et al. (see Ref.[17] and references therein). The method proposed by most of the authors Refs.[18, 19, 20, 21, 22, 23, 24] and [24] consists of a construction, a free energy functional parametrized by the numbers (concentrations) of point defects, which are usually vacancies and antisites. The particular chemical composition of the system requires that either the total number of atoms, or at least the proportion of the numbers of component atoms, is fixed. Equilibrium values of the parameters are then obtained by minimizing the functional with respect to the numbers of defects. In such approach vacancies are not explicitly treated as an additional system component, but rather as a structural feature. Considering them as a component would mean that their equilibrium concentration corresponds to zero value of chemical potential ("$\mu_V = 0$" method according to Lim et al. [17] and[25]). It is worth mentioning that, because of the fixed

number/proportion of atoms, the latter does not apply to the chemical potentials of antisites: minimization procedure yields only zero values of differences of appropriate chemical potentials of atoms residing on different sub-lattices. The more rigorous formulation of the problem involving Grand Canonical Potential has been proposed by Fu et al.[26] and then by Mayer and Fähnle in Refs.[27, 28] and [29].

An approach allowing to deal with equilibrium point defects concentrations, can be based on rigid lattice approach. This simplification, encapsulated in the framework of configurational thermodynamics gives an additional benefit in the practical point view. If a rigid lattice is assumed, vacancy can be considered as an empty lattice site. Thus, it is possible to say that vacancy may be treated as an additional component. It must be emphasized that it is not claimed that vacancy is a "real" object but that it may be assumed to be an "atom" in the rigid lattice approach. Therefore, the model of interemetallic system characterized by a certain concentration of vacancies may be consequently mapped into the Ising type one [30, 31]. It gives an opportunity to deal with vacancies in the framework of standard thermodynamics of solid solutions.

Basing on the fact that vacancy is treated as an atom (empty lattice site), the idea firstly given by Schapink [32, 21] and followed only by few authors (see e.g. [33, 17] was developed in the present work. The Schapink's concept states that in question is if the system consisting of "c" components (including vacancies) in the rigid iso-structural lattice (*lattice-gas*) may decompose into vacancy poor and vacancy-rich phases. Therefore, if such decomposition occurs vacancy-poor phase may be interpreted as a crystal characterized by a particular vacancy concentration being in equilibrium with nearly pure vacancy lattice-gas. The phase decomposition phenomena may be investigated by methods commonly known from classical thermodynamics. Both, analytical and stochastic methods referring to the MC techniques are available. The methodology based on so called Semi Grand Canonical Ensemble in framework of MC is discussed in details in the chapter dedicated to MC techniques.

Let us assume that known is a functional of thermodynamic potential calculated per lattice site - e.g. a CVM free energy:

$$f(\{\sigma_i\}) \equiv \frac{F(\{\sigma_i\})}{N} \tag{2.7}$$

where N denotes number of lattice sites. The cluster variables σ_i depend on the concentrations c_p:

$$c_p \equiv \frac{N_p}{N} \tag{2.8}$$

Where "p" denotes kind of atomic element. According to the definition given above the following relation is fulfilled:

$$\sum_{p}^{c} c_p = 1 \tag{2.9}$$

Let us introduce generalized chemical composition parameters $\{\chi_p\}$ by means of the following equation:

$$\chi_p \equiv \frac{c_p}{\sum_{q\neq V}^{c} c_q} \tag{2.10}$$

where "V" denotes vacancies and "c" in a number of components (atomic species). Therefore:

$$\sum_{p\neq V}^{c} \chi_p \sum_{q\neq V}^{c} c_q + c_V = 1 \tag{2.11}$$

Free energy of the system at given chemical composition $\{\chi_p\}$, vacancy concentration c_V and temperature is obtainable by means minimization of free energy functional with respect to cluster functions describing configuration of system (which form depends on level in CVM hierarchy):

$$f_{\{\chi_p\},c_V}(T) = min\left[f(\{\sigma_i\})\right]_{T,\{\chi_p\}} \tag{2.12}$$

The minimization for the range of compositions and vacancy concentrations results in hyper-surface of free energy. The further analysis is based on a well known *common tangent construction* (see e.g. Ref.[34]). Hence, finding the "lowest boundary" of convex hull for free energy hyper-surface gives an opportunity to identify coexisting phases, since tangential points are related to the phases associated with identical set of chemical potentials $\{\mu_p\}$. Therefore, the possible coexistence of atom-rich and vacancy-rich phases may be investigated.

2.3 Bragg - Williams approximation

The simplest, "zero" approximation in CVM hierarchy is Bragg - Williams (B-W) one [35, 36, 37]. Since free energy of the system is desired the formulas for both configurational energy and configurational entropy functionals must be known. Only general ideas and formulas will be given and it will be assumed that interactions between atoms exist only for the 1st co-ordination zone.

The configurational energy $E(\sigma)$ of the system is calculated by assuming that the number of nearest neighbours (nn) pairs N_{pq} in the Ising-type Hamiltonian (Eq.2.6) is approximated by specifically calculated average numbers:

$$N_{pq} \approx < N_{pq} > = \sum_{\mu,\nu} N_p^{(\mu)} \times \frac{N_q^{(\nu)}}{N^{(\nu)}} \times z_{\mu\nu} \tag{2.13}$$

Where $N_p^{(\mu)}$ and $N_q^{(\nu)}$ are numbers of $p(q)$-atoms on $\mu(\nu)$ sub-lattice, $N^{(\nu)}$ is the number of ν sub-lattice sites and $z_{\mu\nu}$ is the nn co-ordination matrix giving numbers of ν sub-lattice sites being nearest neighbours of μ sub-lattice sites. Therefore, the configurational energy may be given in a form:

$$E\left(\left\{N_p^{(\mu)}\right\}\right) = \frac{1}{2}\sum_{\mu,\nu}\sum_{p,q} V_{pq} N_p^{(\mu)} \times \frac{N_q^{(\nu)}}{N^{(\nu)}} \times z_{\mu\nu} \tag{2.14}$$

According to Eq.2.4 the number of configurations $g\left(E\left\{N_p^{(\mu)}\right\}\right)$ referring to identical values of configurational energy must be known in order to formulate functional of the configurational entropy $k_B \times ln\left[g\left(E\left\{N_p^{(\mu)}\right\}\right)\right]$. In B-W treatment it is given by means of combinatorial formula and Stirling approximation:

$$S_{conf} \equiv k_B \times ln \left(\frac{\prod\limits_{\mu} N^{(\nu)}!}{\prod\limits_{\mu}\prod\limits_{p} N_p^{(\mu)}!} \right) \overset{Stirling}{\approx} -\sum_{\mu}\sum_{p} N_p^{(\mu)} ln \left(\frac{N_p^{(\mu)}}{N^{(\mu)}} \right) + const \tag{2.15}$$

It is convenient to deal with intensive variables - therefore, concentrations of constituents per sub-lattice site are defined as:

$$c_p^{(\mu)} \equiv \frac{N_p^{(\mu)}}{N^{(\mu)}} \tag{2.16}$$

Introducing additional parameter describing the contribution of the number of sub-lattice sites to the total number of lattice sites as:

$$n^{(\mu)} \equiv \frac{N^{(\mu)}}{N} \tag{2.17}$$

the free energy functional per lattice site in B-W approximation may be written in a form:

$$\frac{F(\{N_p^{(\mu)}\})}{N} = f(\{c_p^{(\mu)}\}) = \frac{1}{2}\sum_{\mu,\nu}\sum_{p,q} V_{pq} c_p^{(\mu)} c_q^{(\nu)} \times z_{\mu\nu} n_\mu + k_B T \times \sum_{\mu}\sum_{p} c_p^{(\mu)} ln\left(c_p^{(\mu)}\right) + const \tag{2.18}$$

Since the composition of the system is fixed the number "n" of independent variables $c_p^{(\mu)}$ equals:

$$n \equiv c \times m - c - m + 1 \tag{2.19}$$

where "c" denotes the number of constituents and m is the number of sub-lattices in the system. Therefore, minimization of above functional with respect to the arbitrary chosen set of $c_p^{(\mu)}$ variables at a given temperature and composition allows to find free energy of the system.

Particular parametrization suitable for the B2 superstructure calculations and details of the procedure are described in a Chapter 4 devoted to the equilibrium vacancy concentration results.

2.4 Kinetics and Transition State Theory

The equilibrium of the system in a context of chemical ordering phenomena refers to the particular atom arrangement over the lattice sites. As equilibrium configurational thermodynamics gives no opportunity to study how equilibrium is achieved, a dynamical model of atomic rearrangement processes is desired. Presuming that kinetic processes in intermetallic systems are based on the vacancy migration mechanism, the model being of interest may be formulated in the framework of Transition State Theory (TST) originally established for the description of chemical reactions. In this section only the main ideas of TST will be presented, more detailed mathematical description may be found, for example in the Ref. [2].

Let us consider particular configuration of model crystal with equilibrium vacancy concentration. The number of particles (and vacancies as well) is fixed and a system is in thermal equilibrium with surrounding. The atoms are vibrating in vicinity of the minima of potential. Within the Born-Oppenheimer approximation decoupling interactions of nuclei and electronic degrees of freedom, each particular configuration with atoms being in a minima of potential (in a statistical sense since atoms are vibrating) refers to a particular *microstate* $\Gamma_i(\{\alpha_k\})$ where $\{\alpha_k\}$ is a set of variables defining point Γ_i in a phase space. Let's assume that atom of type A is a nearest neighbour of a vacancy. The atom may force energetic barrier (*saddle point energy*) denoted as $E^{(s,j)}$ and jump to the vacancy which would mean a transition to a new microstate Γ_j. The probability of a jump referring to $\Gamma_i \rightarrow \Gamma_j$ microstate transition is thus in interest. Instead of treating the evolution of the single vibrating atom "trying to enforce" barrier, the ensemble of systems being in vicinity of Γ_i microstate is considered in the TST. Let us denote such "constrained" microstates as $\Gamma_{s,i}$.

It is an important assumption incorporated in TST that if the thermal fluctuation drives atom to the position referring to $E^{(s,j)}$ then the jump related to the microstate Γ_j is performed. Therefore, the frequency ω_{ij} of successful atomic jump referring to $\Gamma_i \rightarrow \Gamma_j$ is proportional to the ratio between the number of systems in the ensemble being in vicinity of the barrier $E^{(s,j)}$ denoted as $n_{s,\epsilon}$ (where ϵ emphasizes that infinitesimally small "strip" in a phase space is considered) and number of systems being in vicinity of Γ_i state denoted as ϵn_A.

$$\omega_{ij} \sim \frac{n_{s,\epsilon}}{\epsilon n_A} \tag{2.20}$$

However, if the average velocity $\overline{u}$ of the positive flux of atoms attempting to force the barrier and jump into vacancy is calculated from Maxwellian velocity distribution, the frequency is given by:

$$\omega_{ij} = \frac{\overline{u} n_{s,\epsilon}}{\epsilon n_A} \tag{2.21}$$

Performing necessary integrations and expanding the potential in Taylor series around $E^{(i)}$ (the energy referring to the microstate Γ_i) and $E^{(s,j)}$ yields:

$$\omega_{ij} = \tilde{\nu} \times e^{-\beta(E^{(s,j)} - E^{(i)} - T\Delta S_{vib}^{(s,i)} + P\Delta V^{(s,i)})} \tag{2.22}$$

Where $\tilde{\nu}$ refers to an effective vibration frequency (attempt of the jump), $\Delta S_{vib}^{(s,i)}$ is the change of the vibrational entropy, P is an external pressure and $\Delta V^{(s,i)}$ is the change of the volume. However, simplifications relying on fixing zero external pressure and constant volume may be introduced. Additionally, it may be assumed that the change of vibrational entropy is very small and $T\Delta S_{vib}^{(s,i)}$ is negligible in comparison to energy change. Then frequency of atomic jumps into vacancies maybe rewritten in a simple form:

$$\omega_{ij} = \tilde{\nu} \times e^{-\beta(E^{(s,j)} - E^{(i)})} \tag{2.23}$$

The equation given above is directly applicable in MC simulations. It will be shown in the chapter dedicated to MC methodology that appropriately applied formula 2.23 allows to model kinetic processes leading to equilibrium

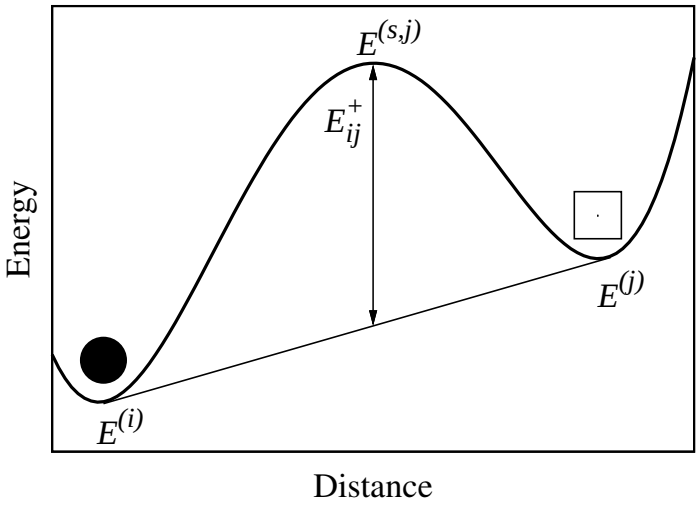

Figure 2.1: The general idea of application of TST in kinetic processes in intermetallics: atom (black circle) is vibrating in the vicinity of minium of potential and attempts to force the saddle energy and jump into the nearest neighboring vacancy (empty square).

configuration of atoms. Moreover, such simplifications allow for application of TST into the Ising type model.

It must be mentioned that in view of the simulation techniques application it is convenient to define a parameter :

$$E^{+}_{ij} \equiv E^{(s,j)} - \frac{E^{(j)} + E^{(i)}}{2} \tag{2.24}$$

Thus the Eq.2.22 maybe rewritten in a form:

$$\omega_{ij} = \tilde{\nu} \times e^{-\beta(E^{+}_{ij} + \frac{1}{2}\Delta E_{ij})} \tag{2.25}$$

where:

$$\Delta E_{ij} \equiv E^{(j)} - E^{(i)} \tag{2.26}$$

The general idea of application of TST in the context of ordering/disordering kinetics phenomena by vacancy migration mechanism is presented on Fig 2.1.

Chapter 3

Monte Carlo Simulation techniques - theoretical background

The term "Monte Carlo" (MC) refers to a class of stochastic calculation methods firstly proposed by Stanisław Ulam and John von Neumann during the realization of the "Manhattan Project". The fundamental idea of MC is random sampling of microstates with a given probability distribution allowing to obtain the most probable value of parameter(s) being of interest - hence the given solution has a statistical nature.

One of the simplest, "textbook" example of MC method is estimating π number by calculating the area of a circle with a known radius. If a circle is inscribed in a square denoted by Sq and coordinates $(x_i, y_i) \epsilon Sq$ are generated randomly, it is straightforward to approximate the area of the circle by observing the ratio N_s/N_{tot} where N_s denotes the number of $(x_i, y_i) : x_i^2 + y_i^2 < r^2$ points and N_{tot} is a total number of generated (x_i, y_i) pairs. Random sampling is essential for MC methods. This procedure formally realizes numerical integration. However, for low dimensional tasks (less than or equal four) more accurate deterministic algorithms for the numerical integration exist. On the other hand, if the dimensionality of the addressed problem is higher, MC methods become one of the most powerful tool. Such situation is regular for standard problem of statistical physics (discrete mixture problems, lattice models of solid state, classical gases, high energy physics etc.). Every physical observable A in statistical physics is to be estimated as its average value. Keeping in mind that configurational thermodynamics is formulated in a manner of statistical physics one concludes that MC method appears to be suitable in the field of interest. Moreover, not only equilibrium properties could be analyzed but also a "path" of reaching equilibrium if it is physically justified to investigate the time evolution of the system modelled by means of stochastic processes (e.g. kinetic aspects of chemical ordering phenomena in intermetallics governed by vacancy migration mechanism may be modelled see e.g. Refs.[38, 39]).

In the following sections foundations of MC simulations techniques will be presented. Firstly general overview, assumptions and fundamental formulas will be given. In the second section, algorithms for simulations in Semi Grand Canonical Ensemble will be presented and aspect of phase separation modelling will be discussed. Subsequently other methods based on *thermodynamic integration* and some of algorithms suitable for the simulations of kinetic processes

will be presented. Finally, supporting (in view of this study) Molecular Statics technique will be shortly described.

3.1 Basic ideas

Let us consider system consisting of N interacting particles at temperature T given P or V and external field (magnetic field, chemical potential etc.). Each "i" particle posses its own set of variables α_i (position, momentum), referring to microstate $\Gamma(\{\alpha_i\})$ defining the point in the phase space Ω. The microstate of the system may be expressed as $\Gamma(\{\sigma_i\})$ since in the context of alloy models adopted in this study, the phase space is limited to the configurational degrees of freedom. In other words microstates $\Gamma(\{\sigma_i\})$ correspond to atomic configurations $\{\sigma_i\}$. The system is described by the Hamiltonian $H_N(\Gamma)$ and an average value of any observable A is thus given by:

$$< A >\equiv \frac{\int_\Omega A(\Gamma) f(H_N(\Gamma)) d\Gamma}{\int_\Omega f(H_N(\Gamma)) d\Gamma} = \frac{1}{Z_N} \int_\Omega A(\Gamma) f(H_N(\Gamma)) d\Gamma \tag{3.1}$$

where $f(H_N(\Gamma))$ is equilibrium density of probability distribution function of microstates (given in a particular, physical context). Though the most intuitive procedure suggests to sample Ω space with the uniform probability distribution, such method suffers for big inefficiency - huge amount of the microstates sampled would give negligible contribution to the integrals. The efficiency is improved if the sampling procedure is performed with probability distribution function $P(\Gamma)$. Then, an average value $< A >$ may be approximated by the weighted integral (or sum if the discrete phase space is considered e.g. lattice models):

$$< A >\cong \overline{A} = \frac{\int_\Omega A(\Gamma) P(\Gamma)^{-1} f(H_N(\Gamma)) d\Gamma}{\int_\Omega f(H_N(\Gamma)) P(\Gamma)^{-1} d\Gamma} \tag{3.2}$$

Moreover, if $P(\Gamma)$ is chosen as:

$$P(\Gamma) \propto f(H_N(\Gamma)) \tag{3.3}$$

Then $\overline{A}$ is obtainable by means of arithmetic average of sampled microstates:

$$\overline{A} \cong \frac{1}{n_{MCS}} \sum_{i=1}^{n_{MCS}} A(\Gamma_i) \tag{3.4}$$

where n_{MCS} is the number of the microstates sampled. The procedure presented above is called in MC terminology *importance sampling*. However, it is cruxial to generate the microstates with the equilibrium probability distribution $f(H_N(\Gamma))$. It is possible to generate a random sequence of microstates by means of Markov chain, considering *transition probability rates* between microstates $W_{ij}(\Gamma_i \to \Gamma_j)$ fulfilling following conditions[40]:

- $\exists(\Gamma_i, \Gamma_j)\, \epsilon\, \Omega \times \Omega : W_{ij}(\Gamma_i \to \Gamma_j) \neq 0$ Every microstate in phase space Ω is attainable
- $\forall(\Gamma_i, \Gamma_j)\, \epsilon\, \Omega \times \Omega : W_{ij}(\Gamma_i \to \Gamma_j) \geq 0$ Probability must be greater than or equal to zero

- $\forall \Gamma_i \epsilon \Omega : \sum_{\Gamma_j} W_{ij}(\Gamma_i \rightarrow \Gamma_j) = 1$ Probability that system will evolve to any microstate must be normalized to the unity

Assuming that $W_{ij}(\Gamma_i \rightarrow \Gamma_j)$ were defined an evolution of the system may be described by the *master equation* (*fundamental equation*):

$$\frac{dP(\Gamma_i, t)}{dt} = -\sum_{\Gamma_j} W_{ij}(\Gamma_i \rightarrow \Gamma_j)P(\Gamma_i, t) + \sum_{\Gamma_j} W_{ji}(\Gamma_j \rightarrow \Gamma_i)P(\Gamma_j, t) \quad (3.5)$$

It must be mentioned that a time is supposed to be a continuous variable here and that above approximation becomes exact in the thermodynamical limit.

A stationary solution of the Master equation refers to the equilibrium state of the system:

$$\frac{dP(\Gamma_i, t)}{dt} = 0 = -\sum_{\Gamma_j} W_{ij}(\Gamma_i \rightarrow \Gamma_j)P(\Gamma_i) + \sum_{\Gamma_j} W_{ji}(\Gamma_j \rightarrow \Gamma_i)P(\Gamma_j) \quad (3.6)$$

One concludes that sufficient (but not necessary) condition to find such solution is to assume *detailed balance condition (microscopic reversibility)*:

$$W_{ij}(\Gamma_i \rightarrow \Gamma_j)P(\Gamma_i) = W_{ji}(\Gamma_j \rightarrow \Gamma_i)P(\Gamma_j) \quad (3.7)$$

Which implies that transition rate probabilities $W(\Gamma_i \rightarrow \Gamma_j)$ leading to the equilibrium distribution $f(\Gamma_i)$ have to be chosen in such a way that following relation is fulfilled:

$$\frac{W_{ij}(\Gamma_i \rightarrow \Gamma_j)}{W_{ji}(\Gamma_j \rightarrow \Gamma_i)} = \frac{P(\Gamma_j)}{P(\Gamma_i)} = \frac{f(\Gamma_j)}{f(\Gamma_i)} \quad (3.8)$$

The transition probability rate, may be factorized and written in a form[40]:

$$W_{ij} = a_{ij} w_{ij} \quad (3.9)$$

Where a_{ij} is probability of sampling the transition between microstates per MC time unit and w_{ij} is the probability of transition $\Gamma_i \rightarrow \Gamma_j$. Both a_{ij} and w_{ij} have to be chosen carefully to maintain the conservation of detailed balance condition.

3.2 Monte Carlo simulation in Semi Grand Canonical ensemble

In a first part of the previous section while describing the general idea of MC it was assumed that a total number of interacting particles is constant. However the scheme for MC simulation in Grand Canonical Ensemble (GCE) mode also exist (see e.g. Refs. [41, 42] and naturally that constraint is not longer valid.

One may consider possibility of keeping the total number of particles constant and let the system change only its composition. This is achievable by "mutating" one kind of the particle to another instead their physical insertion/subtraction. The statistical ensemble adopting this idea, known as *Semi*

Grand Canonical [43, 44, 45] or *Transmutation Ensemble*[45] (here the Semi Grand Canonical Ensemble (SGCE) terminology will be used) gives an opportunity to perform such kind of simulations. Semi Grand Canonical Monte Carlo (SGCMC) simulations were applied by many authors particularly in view of phase equilibria problems (see e.g. Refs. [46, 47, 48, 49])

In the following sub-sections the general idea of simulation in SGCE and assisting techniques (in view of this study) are described. However, the considerations are limited to the lattice-gas models, the more generalized version, describing the application of SGCE techniques in a context of the off-lattice models may be found in the Ref.[43].

3.2.1 Semi Grand Canonical Ensemble

Thermodynamic potential, suitable for the description of opened systems description is the grand canonical one[1]:

$$\Omega\left(\{\mu_p\},T\right) \equiv F\left(T\right) - \sum_{p=1}^{c} \mu_p N_p \tag{3.10}$$

Where μ_p denotes chemical potential of constituent labeled by "p" index. Expressing the number of arbitrary chosen particles "r" as:

$$N_r \equiv N - \sum_{p\neq r}^{c} N_p \tag{3.11}$$

The grand potential may be rewritten in a slightly different but equivalent form:

$$\begin{aligned}\Omega\left(\{\mu_p\},T\right) = F(T) - \sum_{p\neq r}^{c} \mu_p N_p - \mu_r \left(N - \sum_{p\neq r}^{c} \mu_p N_p \right) = \\ = F(T) - \sum_{p\neq r}^{c} \left(\mu_p - \mu_r\right) N_p - \mu_r N = \\ = F(T) - \sum_{p=1}^{c} \triangle\mu_{pr} N_p - \mu_r N \end{aligned} \tag{3.12}$$

where:

$$\Delta\mu_{pr} \equiv \mu_p - \mu_r \tag{3.13a}$$

and then:

$$\Delta\mu_{pq} \equiv \triangle\mu_{pr} - \Delta\mu_{qr} \tag{3.13b}$$

However, in the simulations performed in SGCE mode it holds:

[1]Since the lattice-gas approach is of interest and the external pressure equals zero, in a following considerations Gibbs free energy is replaced by Helmholtz free energy.

$$\sum_{p=1}^{p=c} N_p = N = const \tag{3.14}$$

where N_p denotes the number of p-atoms. Then, introducing above constraint, and assigning μ_r as the reference value for other chemical potentials, one may define SGC potential:

$$\tilde{\Omega}\left(\{\triangle\mu_{pr}\}, N, T\right) \equiv F(T) - \sum_{p=1}^{c} \triangle\mu_{pr} N_p \tag{3.15}$$

Since $\mu_r N = const$.

The Grand Canonical partition function for the rigid lattice model may be expressed as:

$$\Xi\left(\{\mu_p\}, T\right) \equiv \sum_{p=1}^{c} \sum_{N_p=0}^{\infty} \prod_{p=1}^{c} \frac{e^{\beta\mu_p N_p}}{N_p!} \times Z_{\{N_p\}} \tag{3.16}$$

Where $Z_{\{N_p\}}$ (Eq.3.17) is the Canonical partition function and $H_{\{N_p\}}\left(\Gamma_k\right)$ is a Hamiltonian describing the system consisting of certain number of particles.

$$Z_{\{N_p\}} = \sum_{k} e^{-\beta H_{\{N_p\}}(\Gamma_k)} \tag{3.17}$$

Applying the quantity $\triangle\mu_{pr}$ defined in Eq.3.13 into the Grand Canonical partition function, one obtains:

$$\Xi\left(\{\triangle\mu_{pr}\}, \mu_r, T\right) = \sum_{N=0}^{\infty} \sum_{p=1}^{c} \sum_{N_p=0}^{\infty} e^{\beta\mu_r N} \prod_{p=1}^{c} \frac{e^{\beta\triangle\mu_{pr} N_p}}{N_p!} \times Z_{\{N_p\}} \tag{3.18}$$

Introducing the constraint (3.14) into above formula and assuming that μ_r is an arbitrary chosen reference value, Semi Grand Canonical Ensemble partition function is defined as [43]:

$$\Upsilon\left(\{\Delta\mu_{pr}\}, N, T\right) \equiv \sum_{p=1}^{c} \sum_{N_p=0}^{N-\sum_{q\neq p}^{c} N_q} \prod_{p=1}^{c} \frac{e^{\beta\triangle\mu_{pr} N_p}}{N_p!} \times Z_{\{N_p\}} \tag{3.19}$$

An alternative way to formulate partition function for GCE (and SGCE also) is to assume that summation in Eq.3.16 is taken over all N particles/lattice sites separately assuming that every lattice site may be in one of the "c" "state". Then over-counting of microstates has to be compensated applying $\frac{\prod_{p=1}^{c} N_p!}{N!}$ factor [50], to ensure the proper summation:

$$\Xi\left(\{\Delta\mu_{pr}\}, \mu_r, T\right) \equiv \sum_{N=0}^{\infty} \sum_{i=1}^{N} \sum_{I_i=1}^{c} e^{\beta\mu_r N} \prod_{p=1}^{c} \frac{e^{\beta\triangle\mu_{pr} N_p(\{I_i\})}}{N!} \times Z_{\{N_p\}} \tag{3.20}$$

where I_i denotes a kind of particle being at site labeled by index "i". Therefore SGCE partition function may be also rewritten in a different form:

$$\Upsilon\left(\{\Delta\mu_{pr}\}, N, T\right) \equiv \sum_{i=1}^{N}\sum_{I_i=1}^{c}\prod_{p=1}^{c}\frac{e^{\beta\triangle\mu_{pr}N_p(\{I_i\})}}{N!}\times Z_{\{N_p\}} \tag{3.21}$$

Although the two forms of the partition function given in Eq.3.19 and Eq.3.21 are equivalent, each of them suggests different MC simulation algorithm[43] (see next section).

3.2.2 Monte Carlo Algorithms

Independently of the form of partition function chosen, the probability of occurrence of Γ_i microstate is given by:

$$P(\Gamma_i) = \frac{e^{-\beta H(\Gamma_i)+\beta\sum_p^c \triangle\mu_{pr}N_p(\Gamma_i)}}{\Upsilon} \tag{3.22}$$

where the system consisting of $N = const$ lattice site, being at temperature given by $\beta = 1/k_BT$, external pressure $P = 0$ and with assumed linear combinations chemical potentials $\{\triangle\mu_{pr}\}$ is considered. Two equivalent algorithms, partition function form dependent and obeying detailed balance condition, exist for SGC mode simulations[43].

Microscopic reversibility condition demands that transition probabilities W_{ij} must be chosen in such a way that if atom of kind "p" is replaced by an atom of kind "q", the following relation is fulfilled:

$$\frac{W_{ij}}{W_{ji}} = \frac{a_{ij}w_{ij}}{a_{ji}w_{ji}} = \frac{P(\Gamma_j)}{P(\Gamma_i)} = e^{-\beta[H(\Gamma_j)-H(\Gamma_i)+\triangle\mu_{pq}]} \tag{3.23}$$

The form of the partition function given in Eq.3.19 suggests that a kind of atomic specimen should chosen firstly [43]. Hence, the algorithm is realized by means of performing the following steps:

1. Choose the kind of atom p with the uniform probability distribution $\left(a_{ij}^{(1)} = \frac{1}{c}\right)$
2. Choose the atom from the list consisting of N_p atoms $\left(a_{ij}^{(2)} = \frac{1}{N_p}\right)$
3. Choose the kind of possible mutation $p \rightarrow q$ with the uniform probability distribution $\left(a_{ij}^{(3)} = \frac{1}{c}\right)$
4. Calculate $[H(\Gamma_j) - H(\Gamma_i) + \triangle\mu_{pq}]$
5. Calculate the acceptance probability $w_{ij} = min\left[1, \frac{N_p}{N_q+1}\times e^{-\beta[H(\Gamma_j)-H(\Gamma_i)+\triangle\mu_{pq}]}\right]$
6. Generate random number $u\epsilon(0,1]$, if $u \leq w_{ij}$ accept mutation
7. Repeat until system relaxes to the equilibrium

In the above procedure the transition probability rate equals: $W_{ij} = w_{ij} \prod_{k=1}^{n=3} a_{ij}^{(k)} = w_{ij} \frac{1}{N_p c^2}$. Let assume that $w_{ij} < 1$ then obviously $w_{ji} = 1$, hence:

$$\frac{W_{ij}}{W_{ji}} = \frac{\frac{N_p}{N_q+1} \times e^{-\beta[H(\Gamma_j)-H(\Gamma_i)+\triangle\mu_{pq}]} \frac{1}{N_p c^2}}{\frac{1}{(N_q+1)c^2}} = e^{-\beta[H(\Gamma_j)-H(\Gamma_i)+\triangle\mu_{pq}]}$$

and detailed balance condition is fulfilled.

The second version of algorithm is based on partition function form referring to Eq.3.21, which provokes that particular site among N possibilities should be chosen as first to perform a MC attempt.

1. Choose any atom in the system with the uniform probability distribution $\left(a_{ij}^{(1)} = \frac{1}{N}\right)$
2. Choose the kind of possible mutation $p \rightarrow q$ with the uniform probability distribution $\left(a_{ij}^{(2)} = \frac{1}{c}\right)$
3. Calculate $[H(\Gamma_j) - H(\Gamma_i) + \triangle\mu_{pq}]$
4. Calculate the acceptance probability $w_{ij} = min\left[1, e^{-\beta[H(\Gamma_j)-H(\Gamma_i)+\triangle\mu_{pq}]}\right]$
5. Generate random number $u \epsilon (0, 1]$ with uniform distribution probability
6. if $u \leq w_{ij}$ accept mutation
7. Repeat until system relaxes to the equilibrium

The algorithm presented above refers to the transition rate : $W_{ij} = w_{ij} \prod_{k=1}^{n=2} a_{ij}^{(k)} = w_{ij} \frac{1}{Nc}$. If $w_{ij} < 1$ then $w_{ji} = 1$ and algorithm given above obeys detailed balance condition:

$$\frac{W_{ij}}{W_{ji}} = \frac{e^{-\beta[H(\Gamma_j)-H(\Gamma_i)+\triangle\mu_{pq}]} \frac{1}{Nc}}{\frac{1}{Nc}} = e^{-\beta[H(\Gamma_j)-H(\Gamma_i)+\triangle\mu_{pq}]}$$

According to the remarks given by Kofke in Ref.[43] the efficiency of both algorithms depends on the context of their application. In this work, the second version was chosen as more convenient in its application. The simulation properly performed by means of any of the algorithms described above leads to the minimum of a Semi Grand Canonical Potential value at given temperature and the chemical potential differences.

3.3 Study of phase separation.

3.3.1 SGCMC procedure

The MC simulations preformed in the SGCE mode allow to test if the phase separation of the system being of interest may occur at given external parameters (only temperature in the context of lattice-gas model). Investigation of decomposition is based on scanning the sub-space of relative chemical potentials resulting in $c_p\left(\{\triangle\mu_{pr}\}\right)\Big|_{T,N}$ dependencies. The co-existing phases must

show equal values of relative chemical potentials of all constituents (since μ_r is fixed at a given temperature). In a context of interest, co-existing phases in question are distinguishable by means of significant differences of compositions (since iso-structural lattices are considered). Hence, the decomposition may be observed by means of discontinuous transition (characteristic "jump") of $c_p\{\triangle\mu_{pr}\}$ for particular values of $\left\{\triangle\mu_{pr}^{(eq)}\right\}$.

The idea of procedure may be presented by means of an example of A-V binary system (A-atoms and vacancies). In this the simplest case, only one chemical potential linear combination (differences defined in Eq.3.13) is needed to fix the composition of the system. Therefore, at a given temperature and fixed number of the lattice sites, the simulations are performed by means of one of the algorithm described above for chemical potential differences ordered in a n-elements-long sequence:

$$\left(\Delta\mu_{AV}^{(i)}\right)_{i\epsilon<1,n>} : \Delta\mu_{AV}^{(i-1)} < \triangle\mu_{AV}^{(i)}\ for\ i\epsilon < 2, n > \tag{3.24}$$

Those values may be chosen "experimentally" (by means of performing testing simulations) and if it is possible, one should ensure that:

$$c_A\left(\triangle\mu_{AV}^{(1)}\right)\Big|_{T,N} \approx 0,\ c_A\left(\triangle\mu_{AV}^{(n)}\right)\Big|_{T,N} \approx 1 \tag{3.25}$$

Hence, the extremal values of chemical potential differences have to refer to pure, mono-atomic (pure-vacancy) phases. When the sequence (Eq.3.24) is fixed, the simulations are performed in a "step-by-step" mode. It means that the simulation for a given $\triangle\mu_{AV}^{(1)}$ is performed firstly, after the saturation, the finally obtained configuration becomes the initial one for the following simulation and $\Delta\mu_{AV} = \Delta\mu_{AV}^{(2)}$. This procedure is repeated until $i \leq n$. When $i = n$ the simulations are performed in the reversed order, until $i \geq 1$.

The above procedure finds its continuation in analysis of $c_V(\triangle\mu_{AV})$ (or alternatively $c_A(\Delta\mu_{AV})$) dependence. According to considerations presented at a beginning of this section, if decomposition occurs one may expect discontinuous transition in $c_V(\triangle\mu_{AV})$ dependence. However, hysteresis loop in $c_V(\triangle\mu_{AV})$ dependency - caused by the meta-stable states in the vicinity of chemical potentials referring to the phase equilibria - may be detected. The existence of hysteresis loop (Fig.3.1) confirms phase separation and allows to find the approximate values of concentrations in both phases since limits of the loop indicate approximate width of the miscibility gap. However, in many cases more precise values of concentrations referring to co-existing phases are desired. Then, further analysis by means of dedicated MC simulation techniques should be performed.

3.3.2 Refinement of SGCMC results

3.3.2.1 Thermodynamic integration techniques.

If a hysteresis loop is "sharp" but "thin" equilibrium values of concentrations, degrees of order etc. are to be estimated by arithmetic average over values reproducing characteristically "jumps" in a hysteresis loop.

However, in some cases, the more detailed analysis of a hysteresis loop allows to find equilibrium compositions (and configurations as well) more pre-

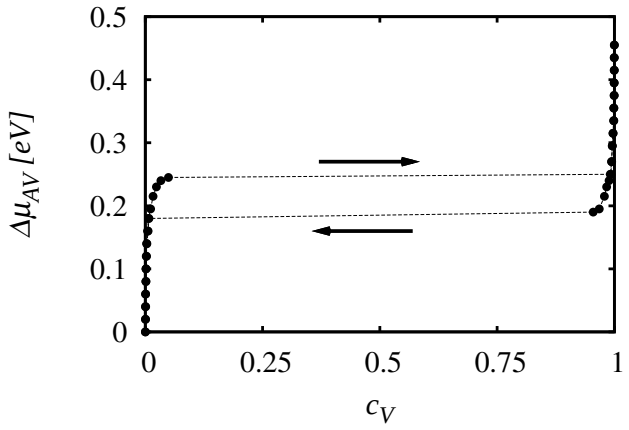

Figure 3.1: Hysteresis loop obtained for A-V binary system with the Ising type energetics ($V_{AA} < 0$, $V_{AV} = V_{VV} = 0$). Arrows indicate the direction of scanning the chemical potential differences sequence. Lines serve as a guide.

cisely than by simple averaging over concentrations referring to the points of characteristic jump (Fig.3.1) . The procedure stems from the fact that hysteresis loop in view of the context of phase separation reflects first order phase transition, hence Semi Grand Canonical (SGC) potential per particle (lattice site) is equal in equilibrium[2] for both phases:

$$\omega^{(I)}\left(\left\{\triangle\mu_{pr}^{(eq)}\right\},T\right) = \frac{\tilde{\Omega}^{(I)}(N,\{\Delta\mu_{pr}\},T)}{N} = \\ = \frac{\tilde{\Omega}^{(II)}(N,\{\Delta\mu_{pr}\},T)}{N} = \omega^{(II)}\left(\left\{\triangle\mu_{pr}^{(eq)}\right\},T\right) \quad (3.26)$$

In formula given above, Roman numbers in brackets denote both phases. The dependencies $\omega^{(I)}\left(\triangle\mu_{AV}^{(1)}\right)$ and $\omega^{(II)}\left(\triangle\mu_{AV}^{(n)}\right)$ may be determined basing on the thermodynamic relation (in a context of SGCE see e.g. Ref.[45]):

$$\frac{\partial\tilde{\Omega}}{\partial\Delta\mu_{pr}} = -\bar{N}_p \quad (3.27a)$$

or:

$$\frac{\partial\omega}{\partial\Delta\mu_{pq}} = -\bar{c}_p \quad (3.27b)$$

[2]It is worthy to notice the analogy to the typical Ising anti-ferromagnet model where the transition occurs due to the increasing/decreasing external magnetic field (see Ref. [51]).

Where the bar over number of constituents (concentration) denotes an average value.

Denoting:

- $\Delta\mu_{pr}^{(I),init} = \Delta\mu_{pr}^{(1)}$ and $\Delta\mu_{pr}^{(I),fin}$ as the last point before the "jump" to the second (II) phase
- $\Delta\mu_{pr}^{(II),init} = \Delta\mu_{pr}^{(n)}$ and $\Delta\mu_{pr}^{(II),fin}$ as the last point before the "jump" to the first (I) phase

The differences of the SGC potential per lattice site for both phases are:

$$\begin{aligned}\Delta\omega^{(I)}\left(\left\{\triangle\mu_{pr}^{(I)}\right\}\right) &= \omega\left(\left\{\triangle\mu_{pr}^{(I)}\right\}\right) - \omega\left(\left\{\triangle\mu_{pr}^{(I),init}\right\}\right) \\ &= -\sum_{p\neq r}^{c}\int_{\triangle\mu_{pr}^{(I),init}}^{\triangle\mu_{pr}^{(I)}} \bar{c}_p\left(\triangle\mu_{pr}\right) d\left(\Delta\mu_{pr}\right) \qquad (3.28a)\\ \Delta\omega^{(II)}\left(\left\{\triangle\mu_{pr}^{(II)}\right\}\right) &= \omega\left(\left\{\triangle\mu_{pr}^{(II)}\right\}\right) - \omega\left(\left\{\triangle\mu_{pr}^{(II),init}\right\}\right) \\ &= -\sum_{p\neq r}^{c}\int_{\triangle\mu_{pr}^{(II),init}}^{\triangle\mu_{pr}^{(II)}} \bar{c}_p\left(\triangle\mu_{pr}\right) d\left(\Delta\mu_{pr}\right) \qquad (3.28b)\end{aligned}$$

Therefore, $\omega^{(I)}\left(\left\{\triangle\mu_{pr}^{(I)}\right\}\right)$ and $\omega^{(II)}\left(\left\{\triangle\mu_{pr}^{(II)}\right\}\right)$ for $\triangle\mu_{pr}\epsilon < \Delta\mu_{pr}^{init}, \Delta\mu_{pr}^{fin} >$ might be evaluated by means of the following formulas:

$$\omega\left(\left\{\triangle\mu_{pr}^{(I)}\right\}\right) = \triangle\omega^{(I)}\left(\left\{\triangle\mu_{pr}^{(I)}\right\}\right) + \omega\left(\left\{\triangle\mu_{pr}^{(I),init}\right\}\right) \qquad (3.29a)$$

$$\omega\left(\left\{\triangle\mu_{pr}^{(II)}\right\}\right) = \triangle\omega^{(II)}\left(\left\{\triangle\mu_{pr}^{(II)}\right\}\right) + \omega\left(\left\{\triangle\mu_{pr}^{(II),init}\right\}\right) \qquad (3.29b)$$

Taking into account that ω may be expressed as:

$$\omega\left(\{\Delta\mu_{pr}\}\right) = f(T) - \sum_{p\neq r}^{c}\bar{c}_p\triangle\mu_{pr} \qquad (3.30)$$

it may be evaluated if the value of free energy referring to configuration obtained for $\triangle\mu_{pr}^{(I),init}$ is known. Although the internal energy (configurational energy in context of lattice-gas) is directly available from the simulations, the configurational entropy is not. However, in some cases it may be obtained basing on thermodynamic relation:

$$S(T) = \int_{T\to 0}^{T}\frac{1}{T'}\frac{\partial U\left(T'\right)}{\partial T'}dT' \qquad (3.31)$$

Therefore, to obtain configurational entropy, for ordered phase[42] by means of the MC techniques one has to perform additional set of SGCMC simulations

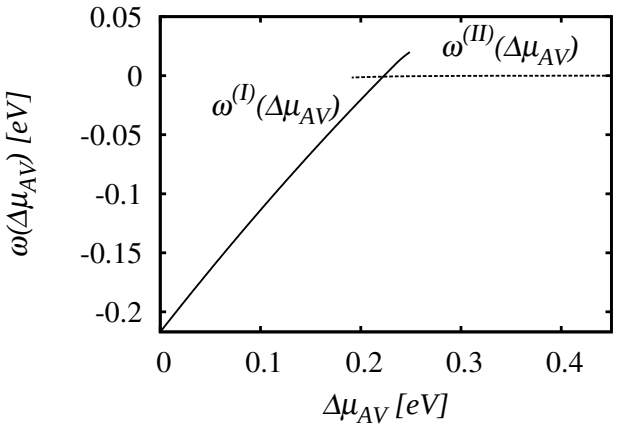

Figure 3.2: Semi Grand Canonical potential (per lattice site) $\omega^{(I)}\left(\triangle\mu_{AV}^{(I)}\right)$ (solid line) and $\omega^{(II)}\left(\triangle\mu_{AV}^{(II)}\right)$ (dashed line) obtained for the system described in Fig.3.1. The intersection indicates equilibrium value of $\triangle\mu_{AV}^{(eq)}$ and allows to obtain precise concentration in both phases.

for temperatures in range $(0, T >$ assuming fixed chemical potential differences $\left\{\Delta\mu_{pr}^{(phase),init}\right\}$ in every single simulation.

At low temperatures free energy of ordered (or mono-atomic) phase of may be safely estimated by its configurational energy at $T \to 0$ (in rigid lattice approach[42]).

The typical result obtained by means of performing scheme described above and applied to the A-V lattice system considered in the previous section is presented in Fig.3.2. Free energies calculated "deeply" in both A-atom-rich and vacancy-rich phases were estimated assuming their equality to the internal configuarational energy. Subsequently, integrations by means of Eqs.3.28 were performed and $\omega^{(I)}\left(\triangle\mu_{AV}^{(I)}\right)$ and $\omega^{(II)}\left(\triangle\mu_{AV}^{(II)}\right)$ were obtained after combining the values of integrals. Their intersection indicates precisely the chemical potential difference referring to the phase co-existence[52, 42] and allows to find equilibrium concentrations in both phases.

The procedure described should not be considered as universal one, since it was e.g. assumed that the range of temperatures taken into account in the integration does not "cross" any phase transition - e.g. order-disorder[52]. Another scheme of integration is useful if e.g. the co-existence between ordered and disordered phase is investigated[42]:

$$F(T) = TS(T \to \infty) + \int_0^{1/k_B T} U d(1/k_B T) \tag{3.32}$$

One notes that above scheme of obtaining free energy demands proper estimation of the configuarational entropy at high temperatures.

3.3.2.2 Other methods.

Though thermodynamic integration schemes are the powerful methods applicable in view of many simulation tasks they cannot be considered - as it was mentioned - as universal. The problem of meta-stable states (e.g. hysteresis loop) should be handled by methods - possibly others than those based on the thermodynamic integration techniques - chosen for a particular computational problem. In this work only a short review of other known techniques is given below. An interested reader is encouraged to find comprehensive description of various techniques in a Ref. [42].

- Re-weighting methods (histogram and multi-histogram methods) - statistical group of methods allowing to predict transition point. Those techniques in view the phase co-existence phenomena simulations may be applied if the local minima of thermodynamical potential are shallow. Then, simulated sample may "switch" between phases in the vicinity of equilibrium values of chemical potential with sufficient frequency, allowing to collect proper statistics of such events. The further analysis is based on statistics of the data obtained and adopts numerical extrapolation techniques.
- Direct estimation of partition function of system - this technique demands proper classification of microstates counting which can be problematic in view of criteria assumed

At the end of this section describing the possibility of application of SGCMC simulation into the phase separation modelling, another interesting method involving simulations in both Canonical and Grand Canonical ensembles has to be mentioned. This method described by Lim, Murch and Oates in Ref. [53, 54] relies on direct calculation of chemical potentials of constituents in both phases by means of simulations performed in Canonical Ensemble (constant number of particles within two phases investigation) and then followed by simulations performed in Grand Canonical mode. The procedure is repeated until system converges corresponding to equilibrium concentrations in both phases. The chemical potentials are obtainable by means of *test-particle method* (or *Widom insertion method*) (see e.g. Refs. [55] [42]). It must be pointed out that elaborated procedure was also applied by Lim, Murch and Oates [17] into investigations concerning equilibrium vacancy concentration in non-stoichiometric B2 compounds.

3.4 Kinetics of structural transformations: Kinetic Monte Carlo algorithms

In this section, the best known algorithms suitable for modelling of kinetics of chemical ordering phenomena via vacancy mechanism in alloys are presented. The system at a given temperature T, fixed number of lattice sites and composition (including vacancies) is considered. Therefore, the probability of occurrence of microstate Γ_i is proportional to Boltzmann factor:

$$P(\Gamma_i) \sim e^{-\beta H(\Gamma_i)} \tag{3.33}$$

Probably the most famous algorithm, allowing to sample the transitions between microstates is based on Metropolis transition rate formula[56]:

$$W_{ij} = min\left[\tau^{-1}, \tau^{-1} e^{-\beta[H(\Gamma_j) - H(\Gamma_i)]}\right] \tag{3.34}$$

where τ is a constant time coefficient related to the attempt of transition in a single MC step (usually fixed to unity).

It must be mentioned that Metropolis type scheme has been already presented in view of SGCMC, however, in author's opinion it is worthy presenting it once more but in a "traditional" form for comparison purposes (Residence Time Algorithm - see further considerations). The algorithm, is performed by means of the following procedure, starting from initial microstate Γ_i and $MC\ Time = 0$:

1. Randomize $\Gamma_i \rightarrow \Gamma_j$ transition (from "n_T" possible transitions) with the uniform number distribution $\left(a_{ij} = \frac{\tau^{-1}}{n_T}\right)$
2. Calculate $\Delta H_{ij} = H(\Gamma_i) - H(\Gamma_j)$
3. Calculate transition probability $w_{ij} = min\left[1, e^{-\beta[\Delta H_{ij}]}\right]$
4. Generate random number $u \epsilon (0, 1]$ with uniform distribution probability
5. If $u \leq w_{ij}$ accept transition
6. Increase MC time $MC\ Time = MC\ Time + \triangle t,\ \triangle t = \tau / n_T$
7. Repeat until system relaxes to the equilibrium

Hence, the system evolution is associated with MC time increment τ / n_T. However, if $n_T = const$ the number of possible transitions in every MC step does not change, and the algorithm obeys detailed balance condition:

$$\frac{W_{ij}}{W_{ji}} = \frac{w_{ij} a_{ij}}{w_{ji} a_{ij}} = \frac{e^{-\beta[\Delta H_{ij}]} \tau^{-1} / n_T}{\tau^{-1} / n_T} = \frac{P(\Gamma_j)}{P(\Gamma_i)} = e^{-\beta \Delta H_{ij}} \tag{3.35}$$

Since if $w_{ij} < 1$ then $w_{ji} = 1$.

In some particular cases, at high temperatures, where the transition probabilities approaches "1", the algorithm given above may not work properly, due to the lack of ergodicity[42].

However, the Metropolis transition rate formula, may be replaced by the Glauber one[57]:

$$W_{ij} = \tau^{-1} \frac{e^{[-\beta H(\Gamma_j)]}}{e^{[-\beta H(\Gamma_j)]} + e^{[-\beta H(\Gamma_i)]}} = \tau^{-1} \frac{e^{[-\beta \triangle H_{ij}]}}{1 + e^{[-\beta \triangle H_{ij}]}} \tag{3.36}$$

obviously satisfying the detailed balance condition. In the most of applications, the use of both formulas is somewhat arbitrary (despite disadvantage mentioned above).

However, regardless of formula chose for transition, in the scheme given above, the transition to another microstate may be rejected or accepted. Therefore, if the values of the rates W_{ij} are low the efficiency in view of computational time may be found very poor, even making equilibrium unreachable in reasonable time. Then, an alternative simulation tool is the *Residence Time Algorithm*[3] (RTA) [58, 59], ensuring that in each single MC step the transition between microstates is performed. Let us to present RTA basing on Glauber formula. As previously, the simulation starts at a given initial microstate and with the MC "clock" reset ($MCT = 0$). The algorithm is realized performing the following steps:

1. Create the catalogue of all the possible transitions and their probabilities:

$$w_{ik} = \frac{1}{R^{(i)}_{n_T}} \times \frac{e^{[-\beta H(\Gamma_j)]}}{e^{[-\beta H(\Gamma_j)]} + e^{[-\beta H(\Gamma_i)]}}$$

   where:

$$R^{(i)}_{n_T} = \sum_{j \neq i}^{j=n_T} \frac{e^{[-\beta H(\Gamma_j)]}}{e^{[-\beta H(\Gamma_j)]} + e^{[-\beta H(\Gamma_i)]}}$$

   is the cumulative function of all possible transitions

2. Generate sequence of series w_k consisting of $n_T + 1$ elements:

$$w_k = \sum_{l=0}^{l=k} w_{ik}$$

   where $k = 0, 1, 2...n_T$ and $w_0 \equiv 0$

3. Generate random number $u \epsilon (0, 1]$ with uniform probability distribution

4. Find the element w_j where $j = 1, 2..n_T$ fulfilling the following relation: $w_{j-1} < u \leq w_j$

5. Perform transition referring to w_{ij}

6. Increase MC time by an increment $\Delta t^{(i)}$ where[4]:

$$\Delta t^{(i)} = \frac{\tau}{R^{(i)}_{n_T}}$$

7. Repeat until system relaxes to the equilibrium

Performing above procedure, one ensures that in every MC step the transition occurs. However, the time scale is induced by means of the incrementation with a time interval given in step 6 (dependent on the transition probabilities). It may be proved (see e.g. Ref. [60] and references therein), that the time increment $\Delta t^{(i)}$ is equivalent to the MC time obtained in the Metropolis type

[3] Bortz-Kosterlitz-Lebowitz algorithm and n-fold algorithm are synonyms

[4] The time increment may be also given by $\Delta t = \tau \frac{-log(u_2)}{R^{(i)}_{n_T}}$ where "u_2" is a random number normalized to the unity, note that $< \frac{-log(u)}{R^{(i)}_{n_T}} >= \frac{1}{R^{(i)}_{n_T}}$.

scheme, referring to the number of rejected transitions preceding the transition from the microstate Γ_i.

It is important that RTA applied into TST obeys detailed balance condition. Denoting that $\triangle H_{ij} = \triangle E_{ij}$ (Eq.2.47) and assuming that barriers are the same for the forward and reversal transition: $E^+_{ij} = E^+_{ji} = E^+$, the probability of transition acceptance may be given in a form:

$$w_{ij} = \frac{e^{-\beta\left[E^+ + \frac{1}{2}\triangle E_{ij}\right]}}{R^{(i)}_{n_T}} \tag{3.37}$$

with $R^{(i)}_{n_T} = \sum_{j\neq i}^{j=n_T} e^{-\beta\left[E^+ + \frac{1}{2}\triangle E_{ij}\right]}$.

Taking into account, that the probability of sampling the transition per MC time unit is simply given in RTA by $a_{ij} = \left(\frac{\tau}{R^{(i)}_{n_T}}\right)^{-1}$ the transition rate equals:

$$W_{ij} = a_{ij}w_{ij} = \left(\frac{\tau}{R^{(i)}_{n_T}}\right)^{-1} \times \frac{e^{-\beta\left[E^+ + \frac{1}{2}\triangle E_{ij}\right]}}{R^{(i)}_{n_T}} = \tau^{-1}e^{-\beta\left[E^+ + \frac{1}{2}\triangle E_{ij}\right]} \tag{3.38}$$

and:

$$\frac{W_{ij}}{W_{ji}} = \frac{\tau^{-1}e^{-\beta\left[E^+ + \frac{1}{2}\triangle E_{ij}\right]}}{\tau^{-1}e^{-\beta\left[E^+ + \frac{1}{2}\triangle E_{ji}\right]}} = \frac{e^{-\beta\left[E^+ + \frac{1}{2}\triangle E_{ij}\right]}}{e^{-\beta\left[E^+ - \frac{1}{2}\triangle E_{ij}\right]}} = e^{-\beta[\triangle E_{ij}]} \tag{3.39}$$

obeying detailed balance condition.

3.4.1 Molecular Statics

The typical problem demanding the solution in Kinetic MC simulations concern evaluation of saddle point energies which are usually treated as input parameters. It is the case for simulations based on the Ising type Hamiltonian. The calculations based on energetics properly describing realistic system (e.g. alloy) may give an opportunity to model the energetic barriers (see e.g. Refs. [61, 62]). Obviously, the results obtained depend on the quality of potential (e.g. DFT techniques, many-body quasi-empirical Embedded Atom Method potentials etc.) applied.

If the potential describing complex physical system is known, the minimum of potential energy with respect to particle/atoms positions and volume is obtainable. As the "statical" properties are of interest, hence the desired minimum refers to "quenched" ($T \to 0$) system. Therefore the kinetic energies of particles (and of the center of mass as well) are zero valued and total energy is identified with its minimum. Those "static" or "quenched" characters of calculations are the source of terminology: Molecular Statics (MS) or Quenched Molecular Dynamics (QMD). The typical task considered in a framework of MS in view of field of interest is e.g. finding the lattice constant of crystal at $T \to 0$, or searching the optimal positions of atoms in a crystal with the artificially introduced antistructural defect(s).

Though, "statical" properties are of interest, the schemes of numerical solution of the equations of motion may be applied for the addressed problem. However, those schemes demand the modification allowing to "lose" the excess

kinetic energy. It can be done, by reducing the velocity of a particle to zero (or by arbitrary chosen factor) if the scalar product of current velocity and of acting force is negative (the particle "crosses" the local minimum of potential). The procedure may be performed e.g. by means of the *Velocity Verlet Algorithm* (VVA) [63].

Let us denote the position, velocity and acceleration referring to a force acting on a particle labeled by index "i" as $\vec{r_i}, \vec{v_i}, \vec{a_i}$, modified VVA is executed by means of the following steps:

1. Select particle "i"
2. Calculate $\vec{r_i}(t + \triangle t) = \vec{r_i}(t) + \vec{v_i}(t)\triangle t + \frac{1}{2}\vec{a_i}(t)(\triangle t)^2$
3. Calculate $\vec{v_i}(t + \frac{1}{2}\triangle t) = \vec{v_i}(t) + \frac{1}{2}\vec{a_i}\triangle t$
4. Derive acceleration from the potential: $\vec{a_i}(t + \triangle t) = -\frac{1}{m_i}\vec{\nabla} V(\{\vec{r_k}\})$
5. Calculate $\vec{v_i}(t + \triangle t) = \vec{v_i}(t + \frac{1}{2}\triangle t) + \frac{1}{2}\vec{a_i}(t + \triangle t)\triangle t$
6. If $\vec{a_i} \circ \vec{v_i} < 0$ then set $\vec{v_i} = 0$

The above cycle is performed for every particle until system relaxes to configuration referring to minimum of total energy. Sometimes it is convenient to minimize the energy with respect to the volume of system and therefore an additional step after integration procedure should be introduced and the scheme repeated until configuration of atoms and volume refer to minimum of potential energy.

It must be mentioned that minimization is often performed with additional constraints assumed. A typical example (applied in a context of the present study) is fixing the possible movement of particle(s) to plane perpendicular to some direction (see Chapter 5 - devoted to calculations of saddle point energies). The atom being in the surrounding of vacancy is moved artificially along direction referring to vector "connecting" the atom and vacancy positions by arbitrary selected increment. In that new attained position the system is relaxed by means of performing minimization procedure (atomic position and volume relaxation). The mentioned constraint prevents atom from relaxing to its initial position. If procedure converges, both atom position and energy are registered and the atom is moved again. The algorithm is repeated until "energy profile" (see e.g. Fig.2.1) is obtained with desired resolution. This method allows to estimate the values of saddle point energies identified with maximal values of potential energy obtained for investigated jumps.

Part II

Chemical Ordering Kinetics and Thermal Vacancy Thermodynamics in B2 Binary Intermetallics: Results

Chapter 4

Equilibrium vacancy concentration from lattice-gas decomposition model

According to the arguments mentioned in the first chapter the modelling study of chemical ordering phenomena in B2 superstructure type alloys demanded elaboration of the methodology allowing to obtain equilibrium vacancy concentrations in a wide range of temperatures.

Firstly, the solution in the framework of B-W approximation will be presented as the preliminary study of vacancy thermodynamics in B2 superstrucutre. Secondly, the solution of lattice-gas decomposition model will be found by means of SGCMC simulations technique.

4.1 Bragg - Williams solution

The results presented in this section were published in Refs. [64, 65, 66].

The minimization of free energy functional (Eq.2.18) at given temperature, stoichiometry and vacancy concentration, requires the selection of independent configuration variables. Taking into account that B2 type super-lattice is considered as consisting of two interpenetrating simple cubic lattices denoted as α and β, and the number of constituents (consequently including vacancies) equals three, the number of independent variables equals two (see Eq.2.19). However, instead of considering $c_p^{(\mu)}$ explicitly, *long range order* (LRO) parameters are defined referring to atoms A and B:

$$\eta_A \equiv \frac{c_A^{(\alpha)} - c_A^{(\beta)}}{c_A^{(\alpha)} + c_A^{(\beta)}} \tag{4.1}$$

$$\eta_B \equiv \frac{c_B^{(\beta)} - c_B^{(\alpha)}}{c_A^{(\alpha)} + c_A^{(\beta)}} \tag{4.2}$$

Since the concentration of vacancies c_V is fixed in a single minimization procedure and the following relation is held:

$$\chi_B = \delta,\ \chi_A = 1 - \delta \tag{4.3}$$

the LRO parameter for vacancy species may be expressed as:

$$\eta_V \equiv \frac{c_V^{(\alpha)} - c_V^{(\beta)}}{c_V^{(\alpha)} + c_V^{(\beta)}} = \frac{(1 - c_V)}{c_V} \times (\eta_B \times \delta - \eta_A \times (1 - \delta)) \tag{4.4}$$

All six concentrations $c_p^{(\nu)}$ are obtainable from η_A and η_B, fixed total vacancy concentration c_V and stoichiometry parameter δ by means of simple formulas. According to geometrical properties of B2 superstructure the $n^{(\mu)}$ parameters and $z_{\mu\nu}$ matrix are:

$$n^{(\alpha)} = n^{(\beta)} = \frac{1}{2} \tag{4.5}$$

$$z_{\mu\nu} = 8 \times (1 - \delta_{\mu\nu}) \tag{4.6}$$

where $\delta_{\mu\nu}$ is Kronecker delta. Hence, free energy of a homogenous system at given temperature, vacancy concentration and composition is obtainable by means of solution of minimization problem:

$$\begin{cases} \frac{\partial f(\eta_A, \eta_B)}{\partial \eta_A}\Big|_{T, c_V, \delta} = 0 \\ \frac{\partial f(\eta_A, \eta_B)}{\partial \eta_B}\Big|_{T, c_V, \delta} = 0 \end{cases} \tag{4.7}$$

The calculations were performed for a wide range of model nn pair interaction parameters to find the energetic conditions promoting the triple defect type behaviour. The following requirements for the pair potentials were assumed:

- The ordering energy $W = 2V_{AB} - V_{AA} - V_{BB}$ had to be assumed as negative to maintain tendency for chemical ordering
- Vacancy - vacancy interaction was assumed to be zero valued: $V_{VV} = 0$ since chemical potential of pure vacancy phase (empty lattice) equals zero

In particular:

- The ordering energy W was assumed as $W = -0.08\,[eV]$ for all calculations as corresponding to "order-disorder" temperature $T_C \approx 1850$ K in B2 AB system without vacancies
- The pair interaction energy between the pair of B-atoms $V_{BB} = -0.05[eV]$ was applied
- The asymmetry energy defined as:

  $$E_{asym} \equiv V_{BB} - V_{AA} \tag{4.8}$$

  and responsible for asymmetric distribution of defects on sub-lattices ,varied in a range $E_{asym}\epsilon < -0.09, 0.0 > [eV]$
- The interaction between atoms and vacancies were assumed as antisymmetric: $V_{AV} = -V_{BV} \leq 0$

4.1.1 General procedure

The equilibrium vacancy concentration at a given temperature, composition and for the assumed set of pairwise interactions was obtainable by means of the following procedure:

1. Selection of representative vacancy concentrations $\{c_V^i\}, c_V^i \epsilon < 0, 1 >$
2. Numerical solution of minimization problem (Eq.4.7) for set of vacancy concentrations selected
3. Fitting the cubic spline functions to $\left\{\left(c_V^i, f(c_V^i)_{T,\delta}\right)\right\}$ points - generation of $f(c_V)_{T,\delta}$ curve
4. Finding the common tangent to $f(c_V)_{T,\delta}$ curve by means of numerical procedure
5. Recording "k" tangential point(s) $\{c_V^{k-eq}\}$ referring to the equilibrium concentration(s) of coexsiting phases
6. Fitting the cubic spline functions to $\left\{\left(c_V^i, \eta_p(c_V^i)_{T,\delta}\right)\right\}$, $p = A, B$ points - generation of $\eta_p(c_V)_{T,\delta}$ curves
7. Calculation of equilibrium values of the LRO parameters: $\eta_p^{k-eq} = \eta_p(c_V^{k-eq})$ and all $c_p^{(\mu),k-eq}$ concentrations

It must be mentioned that procedure given above refers to search of the possible phase co-existence assuming the chemical equi-composition in both phases in question ($\delta = const$). The procedure is justified as calculations show that concentration of atomic species in a vacancy-rich phase is negligible (at least at low temperature). The additional arguments, validating such approach will be given in the last part of this section and in a context of the SGMC simulation (see next section).

In other treatments of vacancy thermodynamics and triple defect formation, relying on minimization of analytical free energy functional (see e.g. Refs. [67, 68]), the triple defect behaviour is often assumed a-priori. Those manipulations are usually based on preventing the formation of $V^{(\beta)}$ or $B^{(\alpha)}$ (or both) simplifying the formula of the free energy functional. In this work the strategy of modelling is different: the space of pairwise interactions was scanned to find those promoting the triple defect behaviour.

4.1.2 Thermodynamic properties of the lattice-gas

The phase separation into atom-rich and vacancy-rich phases in question was the fundamental condition required from the applied lattice-gas decomposition model. It was found that for the examined pair interaction energy sets the principally desired property of phase separation was observed in the wide range of temperatures. The typical evolution of free energy curves as a function of vacancy concentration in three different temperatures is shown on the Fig.4.1.

The shape and evolution of free energy curves for diverse pair interaction energy sets applied, were found qualitatively similar. The convexity of free energy curves was vanishing with increasing temperature as it had been expected, since at $T \to \infty$ the lattice-gas tends to form the homogeneous mixture of atoms

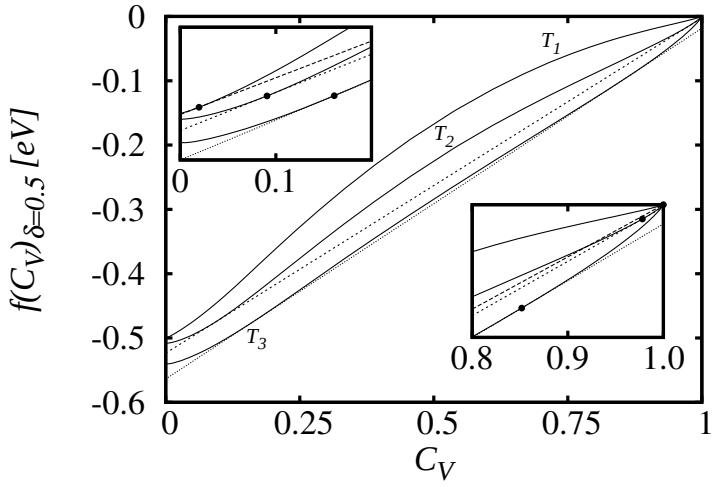

Figure 4.1: The evolution of free energy curves (solid lines) for $E_{asym} = -0.07$ [eV] and $V_{AV} = -0.04$ [eV] at $T_1 < T_2 < T_3$. Dotted and dashed lines are common tangents (for T_1 not marked to maintain the clarity). Insets present the ranges of vacancy concentration where the tangential points (filled circles) were found (equilibrium vacancy concentrations in both vacancy-poor and vacancy-rich phases).

and vacancies due to the domination of entropy contribution to free energy. However, in the range of temperatures being of interest (referring to those significantly lower than the order-disorder one) lattice-gas exhibited the tendency to decomposition into the two phases: atom and vacancy-rich (Fig.4.1). In low temperature regimes (in comparison to the T_C temperatures) the decomposition into nearly pure-atom and pure-vacancy phases was observed.

Therefore, the task of finding the equilibrium vacancy concentrations by means of proposed model was found promising. Moreover, the selection of the pairwise interactions promoting the triple defect formation became possible by means of equilibrium chemical order analysis in atom-rich phase interpreted as a crystal with equilibrium vacancy concentration.

4.1.3 Equilibrium vacancy concentrations and B2 atomic long range order in stoichiometric AB binary system

The detailed analysis of the results obtained for the tested pair-interaction energies will be presented for the three representative sets (Tab.4.1) This "representativity" refers to tendency for triple defect formation. The complete "energetic map" describing the tendency of systems to be of triple defect character will be shown in the next sub-section.

[eV]	E_{asym}	$V_{AV} = -V_{BV}$
A	0.01	0.00
B	0.07	0.00
C	0.07	0.04

Table 4.1: Pair interaction energy sets referring to the results presented in this section.

The pair-wise interactions denoted as "A" refer to relatively low E_{asym}, in sets "B" and "C" strong asymmetry between V_{AA} and V_{BB} interactions were assumed. In the energy set labeled as "C" non-zero interactions between atoms and vacancies were introduced to enhance promotion of asymmetry of defect formations on both sub-lattices.

The LRO parameters and vacancy distribution over the sub-lattices as function of reduced temperatures are presented in Fig.4.2. The continuous character of "order-disorder" transitions was observed.

The further analysis of LRO parameters and vacancy distribution over sub-lattices based on the dependencies shown in Fig.4.2 resulted in the following conclusions:

1. Set "A" of the pair interaction energies

   a) Both η_A and η_B parameters exhibited similar behaviour implied by relatively low value of E_{asym}. The weak promotion of $A^{(\beta)}$ formation was observed since $\eta_A(T/T_C) < \eta_B(T/T_c)$ for $T/T_C < 1$, implying non-zero η_V parameter. However, the chemical order of vacancies was found remarkably lower than for A- and B-atoms ($T/T_C < 1 \rightarrow \eta_V(T/T_C) \ll \eta_A(T/T_C) \lesssim \eta_B(T/T_C)$). Low vacancy concentrations in the low temperatures $T/T_C \lesssim 0.25$ influenced the quality of data obtained (the "noise" observed for the first part of $\eta_V(T/T_C)$ curve).

   b) Total vacancy concentration was smoothly increasing with increasing temperature. Only a small difference between $c_V^{(\alpha)}(T/T_C)$ and $c_V^{(\beta)}(T/T_C)$ was found - notably for t $T/T_C \gtrsim 0.5$.

2. Set "B" of the pair interaction energies

   a) In comparison to the results obtained for the set "A", the difference between atomic LRO parameters appeared significantly bigger. Consequently, the $A^{(\beta)}$ defects formation was found more preferable than for $B^{(\alpha)}$ones, exhibited by values of $\eta_A(T/T_C)$ lower than $\eta_B(T/T_C)$ for $T/T_C < 1$. The evolution of $\eta_V(T/T_C)$ differed significantly to that observed for the set "A", exhibiting higher chemical order of vacancies - $\eta_V(T/T_C) \approx \eta_A(T/T_C) \approx \eta_B(T/T_C)$ for the $T/T_C \lesssim 0.4$. However, the value η_V was found still lower than values of η_A and η_B in the range of temperatures referring to $0.4 \lesssim T/T_C < 1$.

b) As it might be supposed (taking into account the behaviour $\eta_V(T/T_C)$) vacancy distribution on the sub-lattices was found considerably different. The $V^{(\alpha)}$ vacancies were dominating though at higher temperatures difference between $c_V^{(\alpha)}$ and $c_V^{(\beta)}$ was vanishing.

3. Set "C" of the pair interaction energies

a) The chemical order of B-atoms referring to "C" variant energetics was found much higher than for A-atoms, even at lower temperatures. The tendency to form mainly $A^{(\beta)}$ defects, was found the strongest among considered cases ("A", "B", "C"). Obviously, this favorization was vanishing close to order-disorder temperature. It was found, that vacancies exhibited higher degree of order than A-atoms. The $\eta_V(T/T_C)$ values were closer to the $\eta_B(T/T_C)$ than to the $\eta_A(T/T_C)$ in the range of reduced temperatures referring to $0.2 \lesssim T/T_C \lesssim 0.8$.

b) Due to relatively high E_{asym} intensified additionally by introducing non-zero vacancy-atom interactions, the highest disproportion between sub-lattice site occupations by vacancies was found. Total vacancy concentration appeared as significantly higher at lower temperatures than in the cases previously described. Therefore, additional calculations were performed to clarify if vacancy concentration tends to zero assuming $T \to 0$ extrapolation (the inset) since no structural vacancies were supposed to exist for $\delta = 0.5$. The result obtained, confirmed vanishing formation of thermal vacancies in very low ($T/T_C < 0.2$) temperature regime.

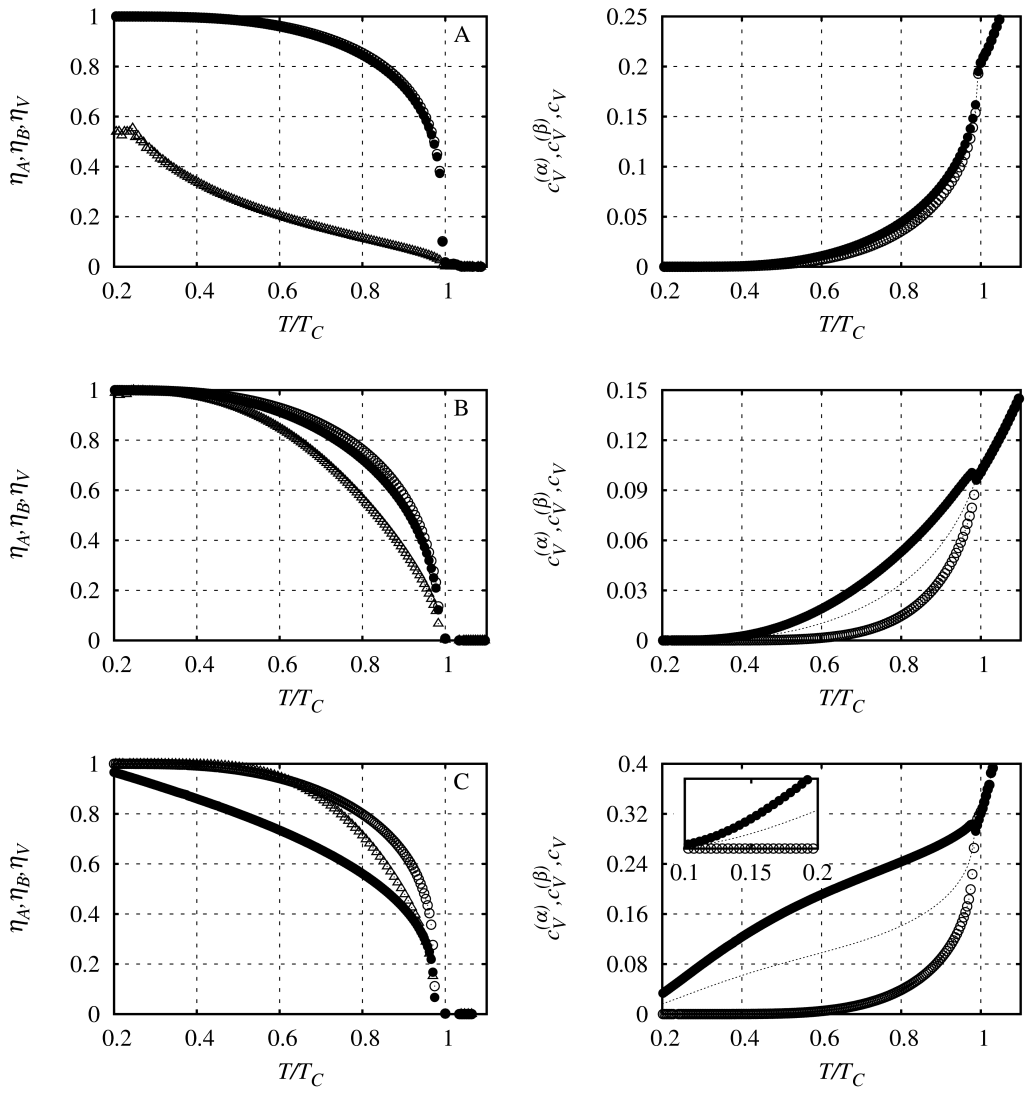

Figure 4.2: Long range order parameters (the left column) as a function of the reduced temperature (T_C is "order-disorder" temperature), obtained for atom-rich phases for "A", "B" and "C" sets of pairwise interactions: η_A- filled circles; η_B - empty circles; η_V - empty triangles. The right column refers to the distribution of vacancies over the sub-lattices: $c_V^{(\alpha)}$ - filled circles, $c_V^{(\beta)}$- empty circles, dotted lines refer to total equilibrium vacancy concentration c_V.

Results described above allowed to suppose the triple defect existence because of observed asymmetry in antistructural defect formations. However, "pure" triple defect behaviour in limited range of temperatures was expected for the strongly asymmetrical energetics ($E_{asym} \gg 0$) additionally intensified by "turning on" vacancy-atom interactions. Therefore, further analysis of additionally introduced parameters, allowing to arbitrate if triple defect type behaviour existed for scanned energetic space, was required.

4.1.4 Triple defect formation in stoichiometric AB binary system

The parameter giving the opportunity to judge if the triple defect appeared (in a statistical sense according to Mean-Field nature of B-W approximation), was defined as the ratio between antisite concentration and vacancy concentration and named *Triple Defect Indicator* (*TDI*). This parameter was considered in a variety of forms depending on a context of investigation and stoichiometry of the system (see next sub-section). In this sub-section two of them will be investigated:

- *TDI* referring to total concentration of thermally activated defects regardless of their kind:

$$TDI \equiv \frac{c_{ANT}}{c_V} = \frac{c_A^{(\alpha)} + c_B^{(\beta)}}{c_V^{(\alpha)} + c_V^{(\beta)}} \tag{4.9}$$

- *TDI* referring to concentrations of thermally activated $A^{(\beta)}$ and $V^{(\alpha)}$ defects:

$$TDI^{(A)} \equiv \frac{c_A^{(\beta)}}{c_V^{(\alpha)}} \tag{4.10}$$

The triple defect indicator referring to B-atom antisites, though directly obtainable, was not analyzed. It came from the fact that energetics applied was expected to promote A-atom defects and vacancies on α sub-lattice (preliminarily confirmed by means of analysis of LRO parameters and vacancy distribution over sub-lattices - see previous sub-section). Therefore the triple defect was supposed to relate to the formations of A-atom antisites and vacancies on α sub-lattice.

The triple defect indicators obtained for the pairwise-interactions "A","B" and "C" sets are presented in Fig.4.3. Irregularity of the points at lower temperatures referring to "A" and "B" variant are indicated by small vacancy concentration ($c_V < 1.0e-6$) resulting in lower accuracy of data obtained.

It was found that triple defect behaviour referred to those model pairwise interactions which adopted additional enhancement of asymmetry of defect formations by means of non-zero vacancy-atom interactions introduction (set "C" in Fig.4.3a). Such conclusion stems from the analysis of TDI's in the range of temperature lower than $\sim 0.4 \times T_c$. In that range the triple defect indicators for "C" energetics were valued nearly 1/2 and formed the characteristic "plateau". Hence, statistically one $A^{(\beta)}$ antistite per two $V^{(\alpha)}$ vacancies existed. It should be emphasized that such behaviour is not the trivial one, while even at temperatures referring to $T/T_c < 0.4$ the concentration of vacancies and antisites

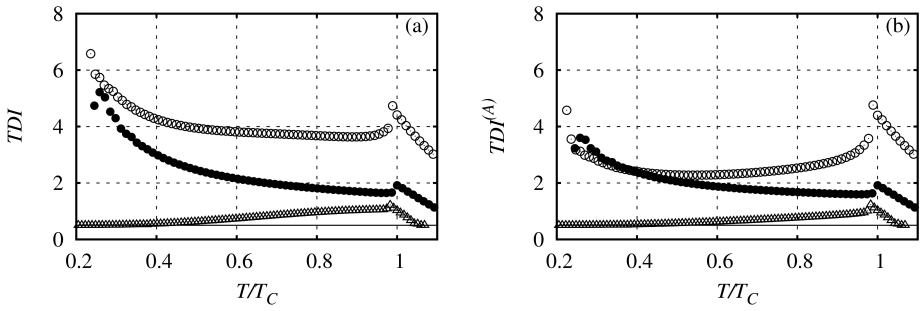

Figure 4.3: Triple defect indicators obtained for "A" (filled circles) ,"B" (empty circles) and "C" (empty triangles) energetic variants: (a) TDI; (b) $TDI^{(A)}$. The solid line indicates 1/2 level referring to triple defect type behaviour.

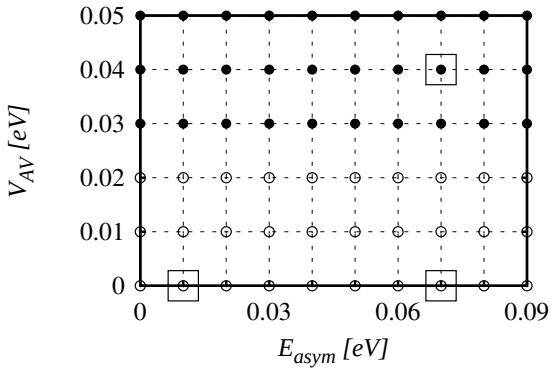

Figure 4.4: "Energetic map" describing triple defect behaviour in view of triple defect indicators. Filled circles refer to the triple defect behaviour; empty circles - no triple defect observed. The square boxes indicate A,B and C variants.

mutually increases with increasing temperature (see Fig.4.2). Therefore, the 1/2 level cannot be considered as an artefact of numerical procedure.

At higher temperatures the "plateau" was vanishing exhibiting increasing ratio between antisite and vacancy formations and leading to maximum value of TDI close to order-disorder temperature.

Neither "A" nor "B" variant characterized by the significantly higher values of TDI exhibited the triple defect behaviour even for the "B" variant referring to relatively big E_{asym}. However, kind of "plateau" for "B" variant was observed but its value did not refer to triple defect type behaviour.

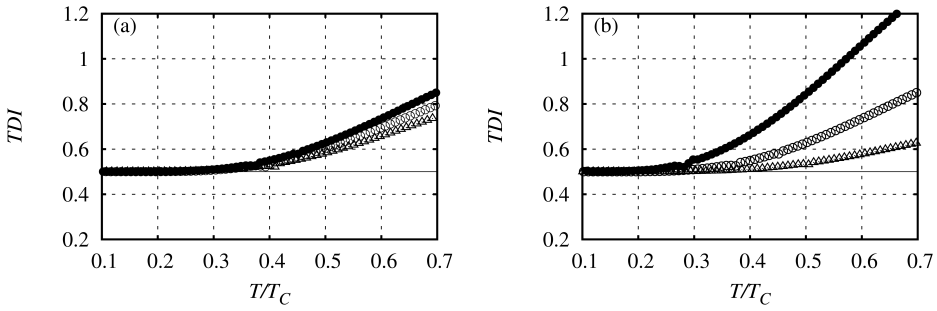

Figure 4.5: The evolution of TDI for different pair-interaction energies. (a) $V_{AV} = 0.04$ [eV]: $E_{asym} = 0.06$ [eV] - filled circles; $E_{asym} = 0.07$ [eV] - empty circles;$E_{asym} = 0.06$ [eV] - empty triangles;(b) $E_{asym} = 0.07$ [eV]: $V_{AV} = 0.3$ [eV] - filled circles,$V_{AV} = 0.4$ [eV] - empty circles, $V_{AV} = 0.5$ [eV] - empty triangles; Solid lines in both figures refer to $1/2$ level.

The results obtained for three sets of pair interaction energies are selected as giving an overview of calculations performed. However, "energetic map" referring to the considered sub-space of pair interactions energies was obtained by means of analysis presented above (Fig.4.4). The classification of pair interactions allowing to adopt them into the triple defect type group in view of triple defect indicators was somehow arbitrary. Only well marked, constant level - "plateau"- referring to the value of TDI being approximately $1/2$ was decisive criterion.

The main conclusion coming from the study of the "map" states that triple defect behaviour was definitely observed only for those energetic sets where non-zero vacancy-atom interactions were assumed. However, only higher valued $V_{AV} = -V_{BV} \geq 0.03\,[eV]$ exhibited the presence of triple defect behaviour.

It was interesting to compare the TDI dependencies for the selected systems found to be of triple defect type, in the range of temperatures referring to "$1/2$ plateau" existence. That evolution of triple defect indicators was compared for the following energetics (Fig.4.5):

- Firstly: the value $V_{AV} = 0.04\,[eV]$ was fixed and E_{asym} varied in the range $< 0.06, 0.08 >\ [eV]$ (Fig.4.5a)
- Secondly: constant value of $E_{asym} = 0.07$ was assumed and V_{AV} varied in the range $< 0.03, 0.05 >\ [eV]$ (Fig.4.5b)

It was found that both E_{asym} and V_{AV} influenced the range of temperatures where the 1/2 levels existed. However, the value of vacancy-atom interaction was found as a predominant factor (compare Fig.4.5a and Fig.4.5b) which might have been expected since non-zero vacancy atom interactions were found necessary condition for the existence of triple defects.

4.1.5 Properties of non-stoichiometric A-B systems

The results analyzed for the stoichiometric ($\delta = 0.5$) systems strongly suggested that model pair interactions promoting triple defect behaviour were found (i.e. "C" energy set). However the non-stoichiometric systems had to be investigated to inspect the behaviour of constitutional defects since the existence of structural vacancies for $\delta > 0.5$ are postulated for triple defect type alloys. The systems characterized by the composition deviation referring to $\delta < 0.5$ are claimed to posses a certain number of A-atom antistes even for temperatures close to ground state of an alloy ($T \to 0$ since the thermally activated defects vanish).

Therefore, if one assumes that for $\delta > 0.5$ and $T \to 0$ the only kind of point defect existing in a system are structural vacancies following formula may be derived:

$$c_V\big|_{\delta>0.5,T\to 0} = \frac{1}{2} \times \frac{2\delta - 1}{\delta} \tag{4.11}$$

In an analogical way, the concentration of A-atom antistes may be predicted for $\delta < 0.5$, $T \to 0$ as:

$$c_A^{(\beta)}\big|_{\delta<0.5,T\to 0} = 1 - 2\delta \tag{4.12}$$

The examined systems referred to $\delta = 0.48$ and $\delta = 0.52$. The vacancy and antisites distributions obtained for the "A","B" and "C" energetics sets referring to $\delta = 0.52$ are presented in Fig.4.6. As expected, neither "A" nor "B" energetics yielded the existence of structural vacancies at lower temperatures. The concentrations of B-atom antisites $c_B^{(\alpha)}$ were found significantly higher in comparison to non-stoichiometry deviated cases and became dominating over $c_A^{(\beta)}$. In the case of "C" energetics the concentration of vacancies did not seem to decrease to zero value with decreasing temperature and became nearly constant up to $T/T_c \approx 0.2$. According to higher vacancy concentration than for "A" and "B" energetics at the lower temperatures, it was possible to obtain reasonable results for $T/T_c < 0.2$ (the inset in Fig.4.6e) (estimated as not significantly influenced by the numerical error in view of vacancy concentration). Therefore, vacancy concentration, in $T \to 0$ extrapolation was found non-vanishing. The formation of $A^{(\beta)}$ defects remained favored up to temperatures close to the order-disorder.

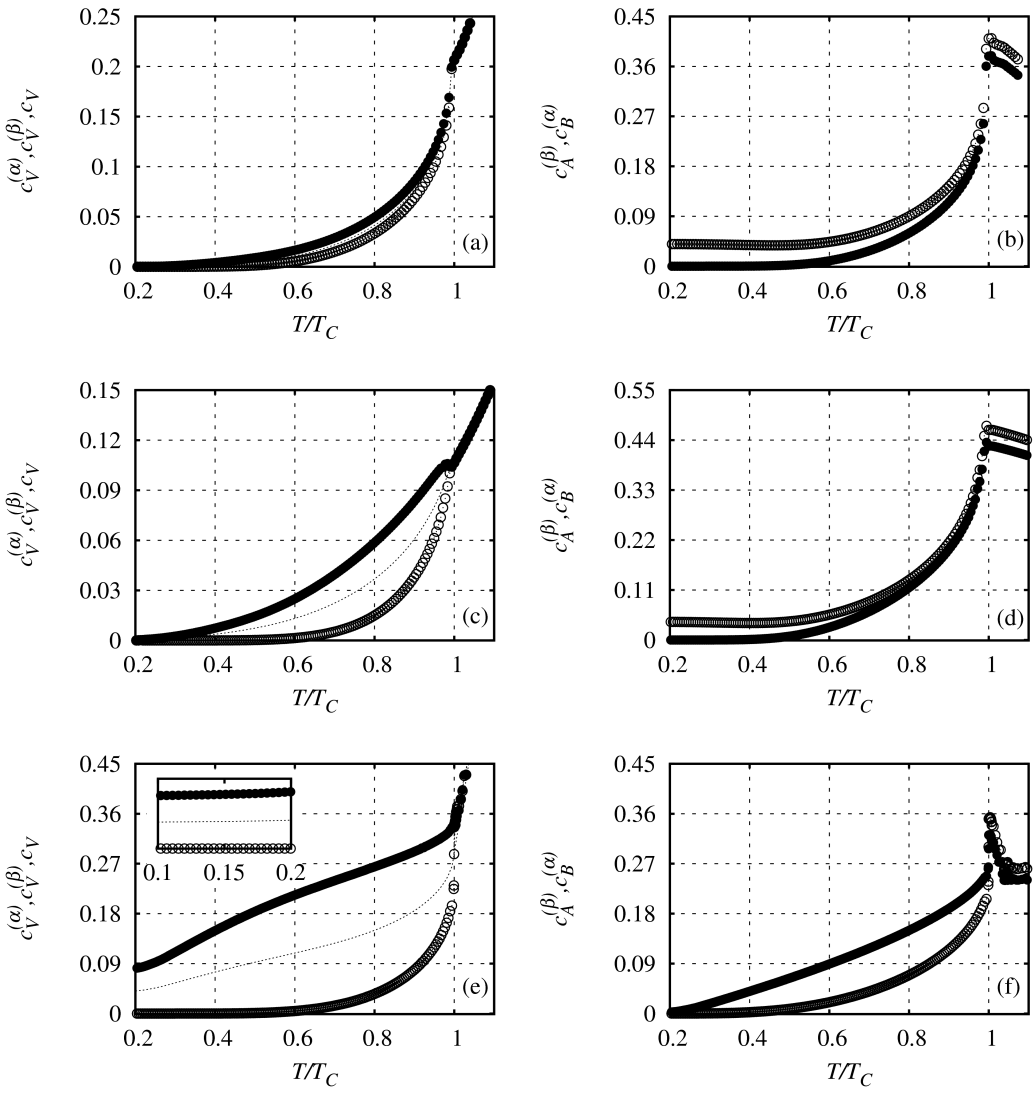

Figure 4.6: The results obtained for non-stoichiometric systems referring to $\delta = 0.52$: (a) and (b) - "A" energetics; (c) and (d) - "B" energetics, (e) and (f) - "C" energetics. Filled circles refer to $c_V^{(\alpha)}$ (a,c,e) and $c_A^{(\beta)}$ (b,d,f) while empty circles to $c_V^{(\beta)}$ (a,c,e) and $c_B^{(\alpha)}$ (b,d,f).

The results obtained allowed to conclude that "C" pair-wise energetics promotes the triple defect behaviour. However, to maintain the continuity of investigations A-atoms rich system referring to $\delta = 0.48$ was also examined assuming "C" pair interaction energetics (Fig.4.7).

It was found that definitely no structural vacancies existed and the deviation from stoichiometry was compensated in the system by A-atoms in their antistructural positions exhibited as not vanishing $c_A^{(\beta)}$ in $T \to 0$ limit extrap-

δ	$c_V(T \to 0)$	$c_A^{(\beta)}(T \to 0)$	c_V expected	$c_A^{(\beta)}$ expected
0.52	0.0383	0.0005	0.0384	0.0000
0.48	$<10^{-6}$	0.0400	0.0000	0.0400

Table 4.2: Concentrations of structural defects obtained for "C" pair-wise interactions. The expected values calculated by means of Eqs.4.11-12.

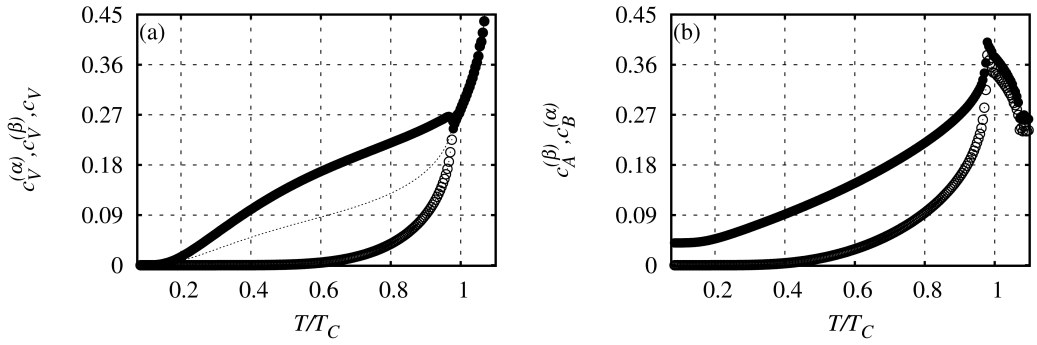

Figure 4.7: Results obtained for "C" energetics and stoichiometry parameter $\delta = 0.52$. Filled circles refer to $c_V^{(\alpha)}$ (a) and $c_A^{(\beta)}$ (b), empty ones to $c_V^{(\beta)}$ (a) and $c_B^{(\alpha)}$ (b).

olation. The important numbers obtained for both off-stoichiometric systems for "C" energetics are included in Tab.4.2.

The collected results are in nearly perfect agreement with values predicted by means of Eqs.4.11-4.12. Therefore, taking into account the analyzed data, it was concluded that pair interaction energies referring to "C" energetics, are representative ones for the modelled triple defect type system.

However, it was also interesting to investigate how constitutional defects influence the ratio between thermally activated antisites and vacancies. Therefore, two additional triple defect indicators were established, helpful in view of off-stoichiometric systems investigation.

$$TDI_{ACT} \equiv \frac{c_A^{(\alpha)} + c_B^{(\beta)} - c_A^{(\alpha)}(T \to 0) - c_B^{(\beta)}(T \to 0)}{c_V^{(\alpha)} + c_V^{(\beta)} - c_V^{(\alpha)}(T \to 0) - c_V^{(\beta)}(T \to 0)} \tag{4.13}$$

$$TDI_{ACT}^{(A)} \equiv \frac{c_A^{(\beta)} - c_A^{(\beta)}(T \to 0)}{c_V^{(\alpha)} - c_V^{(\alpha)}(T \to 0)} \tag{4.14}$$

The pure triple defect behaviour for off-stoichiometric systems might be considered as exhibiting the correlated formations of *thermally activated* defects limited only to $A^{(\beta)}$ and $V^{(\alpha)}$ (supposedly at lower temperatures). However, the triple defect indicators defined above were found still useful, though it had to be taken into account in further analysis that for off-stoichiometric systems, the values of $TDI's$ referring to purely triple defect behaviour are:

$$TDI_{ACT}\Big|_{T\to 0, c_B^{(\alpha)}\approx c_V^{(\beta)}\approx 0} = TDI_{ACT}^{(A)}\Big|_{T\to 0, c_B^{(\alpha)}\approx c_V^{(\beta)}\approx 0} = \delta \tag{4.15}$$

In Fig.4.8 the triple defect indicators are presented. It was found that if parameters defined in Eqs. 4.13-14 are considered, the triple defect type behaviour was still observed. Therefore, relatively small deviation from stoichiometry did not change the general tendencies observed in stoichiometric system ($\delta = 0.5$). Obviously, the "total" triple defect indicator (TDI) was tending to zero value with decreasing temperature for $\delta = 0.52$ since structural vacancies were found. Analogously, TDI value was rapidly increasing for $\delta = 0.48$ mutually with decreasing temperature caused by the existence of structural A-atom antisites. Both TDI_{ACT} and $TDI_{ACT}^{(A)}$ in lower temperature regime were close to the values predicted by means of Eq.4.15.

4.1.6 Comments on the applied procedure

The minimization of free energy functional followed by common tangent construction allowed to obtain the results presented above. However, as mentioned earlier (see sub-sec.4.1.1) the solution of model adopted approximation stating that decomposition into vacancy-poor and vacancy-rich phases, was studied along the equi-composition paths (both phases being in question had the same composition assumed). Such simplification was found valid taking into account the analysis of free energy surfaces $f(c_V, \delta)\Big|_T$. Mainly, "C" variant of energetics was analyzed in view of the desired properties exhibited (triple defect behaviour). The free energy surface obtained at $T/T_c = 0.43$ is presented in Fig.4.9. The shape of the surface indicated that only small "tilt" from stoichiometry for the vacancy-rich phase could occur (at temperatures equal or lower than $T/T_c = 0.43$) if non-constrained decomposition would be considered. The possible "tilt" was found not to be influencing equilibrium vacancy concentration in the atom-rich phase significantly. Such approximation was supposed to be especially valid at lower temperatures where vacancy-rich phase was found to be nearly pure vacancy lattice-gas. It must be mentioned in advance that the lattice-gas decomposition model solved in the framework of MC simulations (next section) with no constraint assuming equal ratio between A and B-atom number in vacancy-rich phase exhibited qualitative agreement with B-W solution.

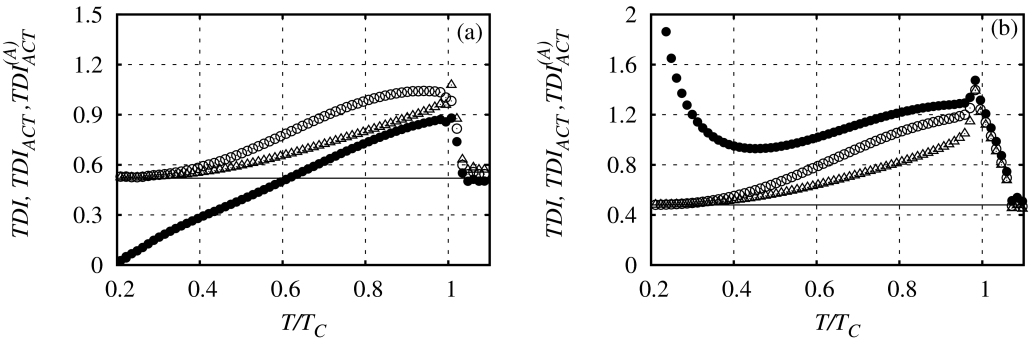

Figure 4.8: Triple defect indicators obtained for "C" energetics: (a) $\delta = 0.52$ (solid line); (b) $\delta = 0.48$ (solid line). Filled circles - TDI, empty circles - TDI_{ACT}, triangles - $TDI^{(A)}_{ACT}$.

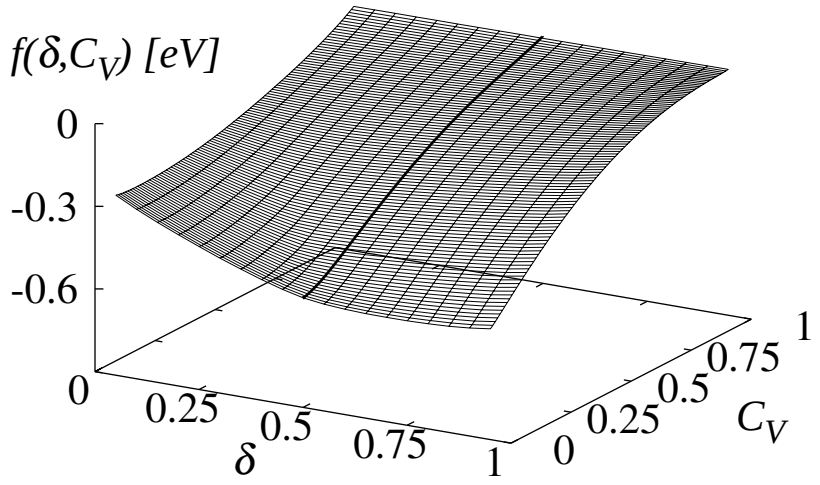

Figure 4.9: The free energy functional $f(\delta, c_V)\Big|_{T/T_c=0.43}$ obtained for pair-wise interactions referring to "C" energetics. Solid, bold black line refers to stoichiometry $\delta = 0.5$

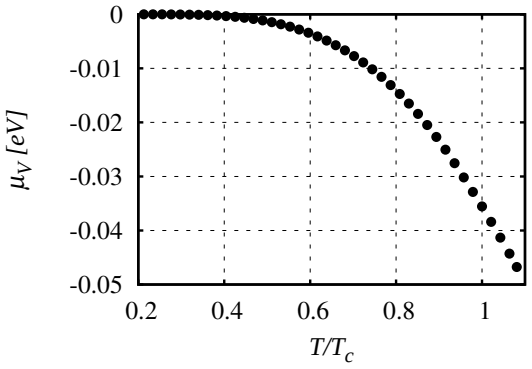

Figure 4.10: The equilibrium chemical potential of vacancies as a function of temperature obtained for "C" energetics.

The vacancy-rich phases in lower temperature range exhibited nearly zero concentrations of atomic species. Consistently, in that range of temperatures, the chemical potential of vacancy, in both phases being in equilibrium, was found nearly zero valued (Fig.4.10). Therefore, taking into account considerations from Chapter 2, where another "$\mu_V = 0$" model of vacancy thermodynamics was mentioned one finds that at lower temperatures both approaches (lattice-gas decomposition and "$\mu_V = 0$") should result in nearly the same solution. However, an increasing temperature resulted in monotonic decrease of chemical potential being always lower than "0" in agreement with consideration presented in Ref. [17].

The results presented above differ in some cases to those presented in Ref. [65]. It came from the fact that numerical procedure had been developed giving more accurate results (presented above). However, general conclusions presented in this work and those commented in Ref. [65] are similar. The discrepancies found, refer to pair-wise interactions promoting triple defect behaviour. The uncertainties were implied by the existence of locally shallow minima found after careful inspection of free energy planes at higher temperatures. At the lower temperatures, the gradients methods had to be excluded since the minima were located close to the limits induced by normalization boundaries of concentrations. Therefore, the "brute" algorithm of finding extrema was found the most reliable and effective.

4.2 SGCMC simulations

Despite the promising results, implementation of elaborated B-W vacancy thermodynamics in Kinetic Monte Carlo simulation of ordering kinetics would un-

doubtedly violate the consistency of the whole project. Therefore, the lattice-gas model with pair-wise interactions yielding the triple defect behaviour in B-W approach was solved by means of Semi Grand Canonical technique [69]. The methodology applied, results and comparison to B-W solution are presented in the following sub-sections.

4.2.1 Simulation procedure

The equilibrium composition and configuration of the ternary A-B-V lattice-gas at temperature T and the chemical potentials differences is determined by minimum of Semi Grand potential functional $\tilde{\Omega}$ (defined previously by Eq.3.15):

$$\Omega\left(\{\mu_p\}, T\right) = F\left(T\right) - \sum_{p=1}^{c} \mu_p N_p \tag{4.16}$$

Because of fixed number of lattice sites N, it is convenient to handle functions and parameters calculated per one particle $\omega\left(\{\triangle\mu_{pr}\}\, T\right)$. The chemical potential of vacancies was chosen as a reference value, therefore in the following considerations two independent parameters were applied:

$$\Delta\mu_{AV} = \mu_A - \mu_V \tag{4.17}$$

$$\Delta\mu_{BV} = \mu_B - \mu_V \tag{4.18}$$

The minima of the Semi Grand Potential were found by means of second variant of algorithm described in Chapter 3, sub-sec.3.2.2. A series of SGCMC runs applying Ising type Hamiltonian (defined by eq.2.6):

$$H = \sum_{p,q}^{c} N_{pq} V_{pq} \tag{4.19}$$

where N_{pq} denotes number of atomic pairs in a first co-ordination zone and V_{pq} is pairwise interaction, were carried out in the way that $\left(\triangle\mu_{AV}, \triangle\mu_{BV}\right)\Big|_T$ plane was scanned for fixed T. The procedure resulted in equilibrium $c_p\left(\triangle\mu_{AV}, \triangle\mu_{BV}\right)\Big|_T$ isotherms and configurations.

As discussed in sub-sec.3.3.1 possible decomposition of the lattice-gas into vacancy-poor and vacancy-rich phase inside a miscibility gap is equivalent to a discontinuous phase transition generated at temperature T by the field of $\triangle\mu_{AV}$ and $\triangle\mu_{BV}$ and occurring between configurations determined by two (or more) distinct minima ω. At the transition point $(\triangle\mu_{AV}^{eq}, \triangle\mu_{BV}^{eq})$ determining relative chemical potentials in co-existing phases, the minima become equal (Eq.3.26). According to Gibbs phase rule, at each temperature the transition points related to two phase equilibrium form a line on the surface $\left(\triangle\mu_{AV}, \triangle\mu_{BV}\right)\Big|_T$. Possible three-phase equilibria (never detected within the present study) would, of course, be represented at particular temperatures by single points on the $\left(\triangle\mu_{AV}, \triangle\mu_{BV}\right)\Big|_T$ surface.

The above discontinuous phase transitions showed up as characteristic "facets" on the respective $c_p\left(\triangle\mu_{AV}, \triangle\mu_{BV}\right)\Big|_T$ isotherms. In fact, however, the occurrence of metastable configurations resulted in a hysteresis of facet positions and

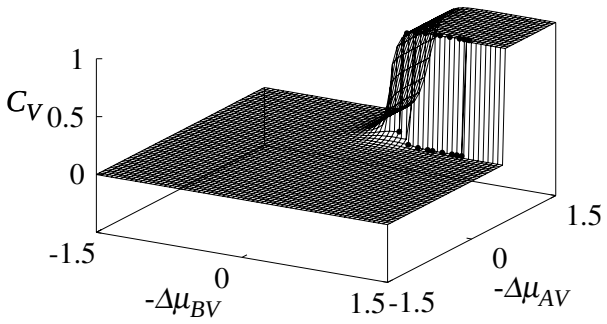

Figure 4.11: Typical $c_V\left(\triangle\mu_{AV},\triangle\mu_{BV}\right)\Big|_T$ isotherm with a facet showing the discontinuous phase transition.

accurate determination points of the $\left(\triangle\mu^{eq}_{AV},\triangle\mu^{eq}_{BV}\right)\Big|_T$ required specific techniques described in subsequent sections. In view of the particular interest of equilibrium vacancy concentration, analyzed were mainly $c_V\left(\triangle\mu_{AV},\triangle\mu_{BV}\right)\Big|_T$ isotherms as shown in Fig.4.11.

Out of the two solutions (pairs of black circles in Fig.4.11) observed in $\left\{c_V\left(\triangle\mu^{eq}_{AV},\triangle\mu^{eq}_{BV}\right)\right\}\Big|_T$ space the "lower" one ($c_V \ll 1$) is identified with the equilibrium vacancy concentration $c_V(T)$ in an A-B crystal with the stoichiometry δ determined by the point $\left\{c_V\left(\triangle\mu^{eq}_{AV},\triangle\mu^{eq}_{BV}\right)\right\}\Big|_T$.

The A-B-V lattice-gas was simulated by generating a B2 super-cell with periodic boundary conditions assumed. The super-cell was built of 15×15×15 bcc unit cells (i.e. with 6750 lattice sites). The study was pursued by repeating the following sequence of steps at a series of temperatures (Fig.4.12):

1. Determination of temperature T
2. Preliminary localization of $c_V\left(\triangle\mu_{AV},\triangle\mu_{BV}\right)\Big|_T$ facet by scanning a mesh of the entire $\{\triangle\mu_{AV},\triangle\mu_{BV}\}$ surface
3. Determination of $S^{(\delta)}_{\triangle\mu}$ lines on the $\left(\triangle\mu_{AV},\triangle\mu_{BV}\right)\Big|_T$ surface corresponding to fixed selected equilibrium ratios δ (Fig. 4.12a)
4. Accurate analysis of the facet by pursuing chains of "step-by-step" SGCMC simulations (see e.g. Ref. [70]) along particular lines $S^{(\delta)}_{\triangle\mu}$ crossing the facet $c_V\left(\triangle\mu_{AV},\triangle\mu_{BV}\right)\Big|_T$ (point A in Fig.4.12): each simulation starting from a configuration produced by the preceding one. The facets were

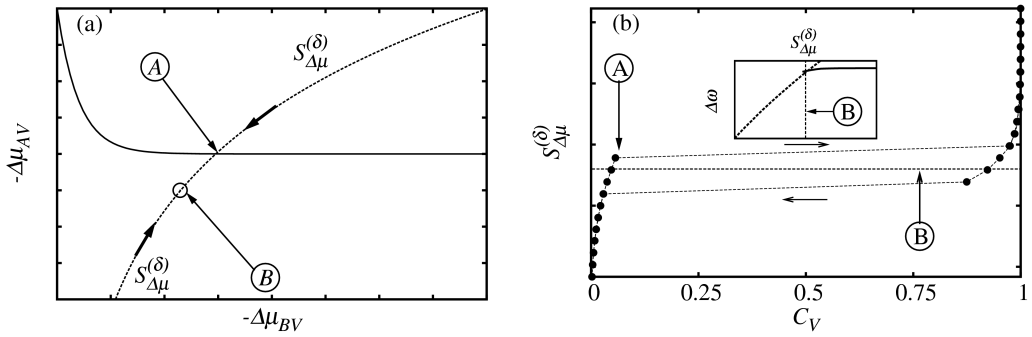

Figure 4.12: Scheme of the method for the evaluation of vacancy concentration: (a) Solid line represents the trace of $c_V\left(\triangle\mu_{AV},\triangle\mu_{BV}\right)\Big|_T$ facet, which is crossed $S^{(\delta)}_{\triangle\mu}$ path at the point A. Point B referring to equilibrium value of relative chemical potentials is determined by means of thermodynamic integration of SGC potential along $S^{(\delta)}_{\triangle\mu}$; (b) $S^{(\delta)}_{\triangle\mu}(c_V)$ hysteresis. The inset shows a typical result of thermodynamic integration.

crossed in both directions, which resulted in hysteresis (Fig.4.12b) mentioned in sec.3.3.1.

The points p.2 and p.3 in the procedure given above require additional comment. Since the two relative chemical potentials (at given temperature) described the system composition, the scan performed at p.2 allowed to determine fixed composition path $S^{(\delta)}_{\triangle\mu}$ for atom-rich solutions. However, to exclude the possible influence of initial configurations on the final compositions in the range of expected hysteresis, the set of initial configurations were examined (Tab.4.3). It was found that the position of the boundary between vacancy-poor and vacancy-rich solution (exhibited as an existence of the facet) varied, according to the initial configuration. However, the inspection of $\{\triangle\mu_{AV},\triangle\mu_{BV}\}$ surfaces indicated that depending on the initial configuration, the $S^{(\delta)}_{\triangle\mu}$ path in the atom-rich phase was only "elongated" or "shortened" according to the facet position. The analysis yielded, that initial configuration (a) (Tab.4.3) resulted in the "longest" $S^{(\delta)}_{\triangle\mu}$ path, which finally applied for the "step-by-step" simulations. The $S^{(\delta)}_{\triangle\mu}$ paths were found by means of interpolation of cubic-spline function performed for $\{\triangle\mu_{AV}(\delta)\}\Big|_{T,\triangle\mu_{BV}}$ isotherms in the range of atom-rich solutions. It was found that "step-by-step" simulations performed along selected path resulted in "jumps" into vacancy-rich phase for higher relative chemical potentials than those predicted by "facet" position ("before" facet position), conserving assumed composition in atom-rich phase. Therefore, the validity of procedure of finding $S^{(\delta)}_{\triangle\mu}$ paths was confirmed by final simulations ("step-by-step"). Since conserved composition of atomic species was not assumed in vacancy-rich solution starting from the point A (Fig.4.12a) the path $S^{(\delta)}_{\triangle\mu}$ was continued as a straight line. The scheme sampling of scans for different initial configurations and typical $S^{(\delta)}_{\triangle\mu}$ path obtained are presented in Fig.4.13.

	(a)	(b)	(c)	(d)	(e)
η_A, η_B	1	1	-	0	0
c_V	0	1/3	1	1/3	0

Table 4.3: Initial configurations in order to obtain $S^{(\delta)}_{\triangle\mu}$.

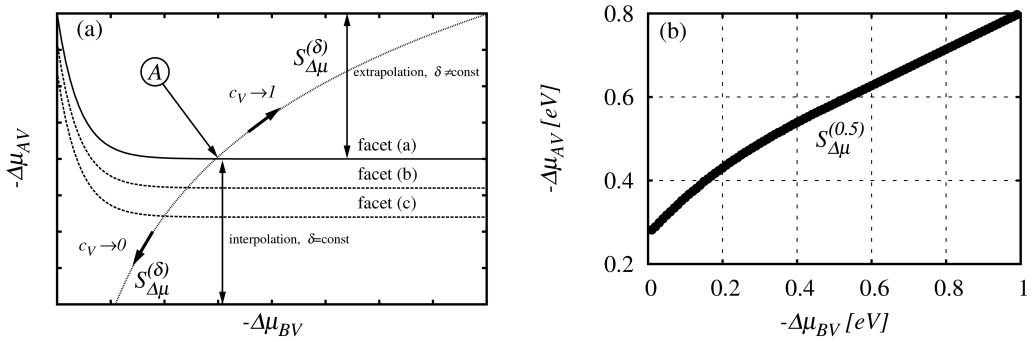

Figure 4.13: Scheme of the method for the evaluation of $S^{(\delta)}_{\triangle\mu}$ path (a) and the typical path obtained for the stoichiometric A-B-V system (b).

Each "step-by-step" simulation run was continued until a saturation of monitored parameters was observed for 60% of the total number of SGCMC steps and the equilibrium values of parameters were evaluated by taking arithmetic means from sets of randomly probed values appearing after the saturation of corresponding simulated MC-time dependence (the averaging was done with a special care so that possible correlations between the values were eliminated). The range of T was limited at the bottom by low rate of the SGCMC curve saturation and at the top by the critical temperature of the miscibility gap of A-B-V lattice-gas.

Two procedures were applied to determine accurate values of $(\triangle\mu^{eq}_{AV}, \triangle\mu^{eq}_{BV})\Big|_T$ (point B in Fig.4.12) corresponding to discontinuous phase transformation of the system and to equilibrium co-existence of vacancy-poor and vacancy-rich phases of the lattice-gas: at low T, where minima of $\omega(c_V)$ were localized at $c_V \ll 1$ and $c_V \approx 1$ the thermodynamic integration based on the scheme described in sec.3.3.2 was performed (Eqs.3.28-3.30) along the paths $S^{(\delta)}_{\triangle\mu}$ (see the inset in Fig.4.12b). Its reliability followed from the initial states (from which the integration starts) safely chosen as an A-B binary with no thermal vacancies and purely vacant bcc lattice-gas. The free energies of initial states referring to atom-rich solution, were found by means of integration technique based on Eq.3.31. Therefore, additional set of simulations were performed for the temperatures up to the one which was of interest, collecting configurational energy. Both integrations were realized by means of numerical methods including the cubic-spline interpolation techniques. The results showed, however, that with increasing T the hysteresis continuously shrunk and the values

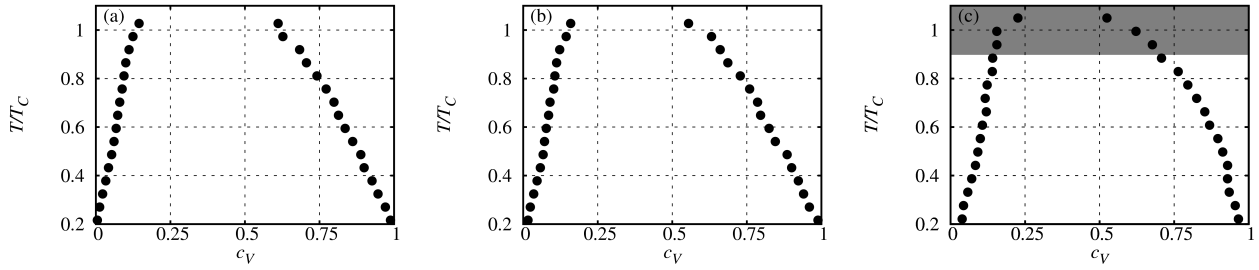

Figure 4.14: Sections of miscibility gap of A-B-V lattice-gas. Vacancy-poor borders of the sections correspond to: (a) $A_{0.52}B_{0.48}-V$; (b) $A_{0.5}B_{0.5}-V$; (c) $A_{0.48}B_{0.52}-V$.

of $\triangle\mu^{eq}_{AV}, \triangle\mu^{eq}_{BV}$ resulted close to the arithmetic means of its limits. Simultaneously, the accuracy of thermodynamic integration method deteriorated (since the initial atom-rich states contained thermal and the initial state of vacancy-rich solution contained atoms), therefore, the values of $\triangle\mu^{eq}_{AV}, \triangle\mu^{eq}_{BV}$ corresponding to $T/T_c > 0.47$ were estimated as arithmetic means of the hysteresis limits.

4.2.2 Pair-wise interactions

In consistency with the calculations performed for V_{pq} parameters yielding definite triple defect formation in B-W approximation (see Fig.4.4) two sets of pair interaction energies were applied in SGCMC simulations, basing on Ising type Hamiltonian (Eq.4.19):

- Set "C" defined in the previous section (B-W solution) - as the representative one for triple defect type system found by means of B-W solution. The results presented in the following sub-sections refer to that energetics
- Set "B" for the comparison purposes (mentioned in the final remarks)

4.2.3 Results - general overview

In qualitative consistency with the calculation performed in the framework of B-W approximation, detailed analysis was done for three systems: $A_{0.52}B_{0.48}(\delta = 0.48)$, $A_{0.5}B_{0.5}$ ($\delta = 0.5$) and $A_{0.48}B_{0.52}$ ($\delta = 0.52$). It was found out that while at low temperatures the co-existing vacancy-poor and vacancy-rich phases showed equal values of δ, this was not exactly the case at temperatures close to critical (consolute) point. Although the tilt of the tie-line orientation was quite slight, it was no longer strictly possible to identify particular $A_{1-\delta}B$ systems with vacancies as resulting from the decomposition of the same lattice-gas in the whole temperature range. Fig.4.14 shows three sections of miscibility gap of A-B-V lattice-gas as revealed by SGCMC simulations. Only the vacancy-poor borders of the sections correspond, however, in each case to strictly constant δ. The diagrams are scaled in a reduced temperature T/T_C.

As it additionally follows from Fig.4.14c, the critical point of the $A_{0.48}B_{0.52}-V$ section of miscibility gap appeared close to T_C which generated especially

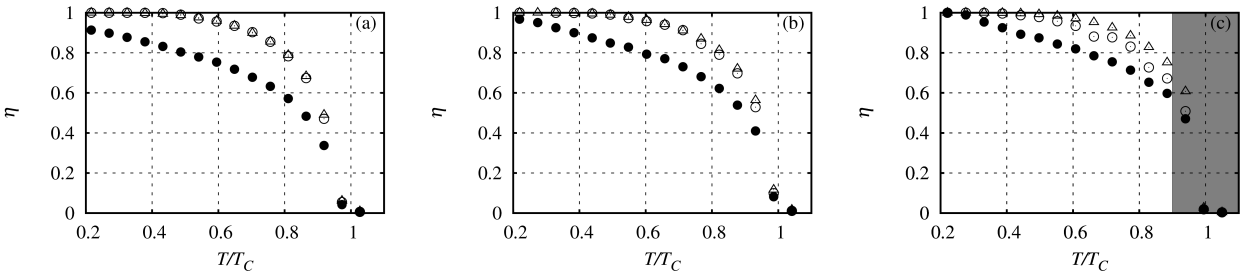

Figure 4.15: Temperature dependencies of LRO parameters in a) $A_{0.52}B_{0.48}$ ($\delta = 0.48$)); (b) $A_{0.5}B_{0.5}$ ($\delta = 0.5$); (c) $A_{0.48}B_{0.52}$ ($\delta = 0.52$); η_A - filled circles , η_V - empty circles , η_V - empty triangles

high uncertainty of related SGCMC results (gray area in already and further figures as well).

4.2.4 Degree of atomic long range order in B2 A-B binary systems

Continuous "order-disorder" transition was observed in all the three $A_{1-\delta}B_{\delta}$ binary systems examined. While all η_A, η_B and η_V LRO parameters reached zero value at the same temperatures T_C, their temperature dependencies differed one from another showing the definite preference for $A^{(\beta)}$ antisite formation at$T/T_C < 1$. The temperature dependencies of LRO parameters for all three compositions investigated are presented in Fig.4.15.

4.2.5 Correlated vacancy and antisite concentration and configuration in B2 A-B binary systems

As follows from the phase diagrams (Fig.4.14) the total vacancy concentration c_V increased with temperature showing the highest value in $A_{0.48}B_{0.52}$ ($\delta = 0.52$). Vacancies were generated predominantly on α sub-lattice, but the difference between $c_V^{(\alpha)}$ and $c_V^{(\beta)}$ obviously disappeared at "order-disorder" transition. The coincidence of the $c_V^{(\alpha)}(T/T_C)$ and $c_V^{(\beta)}(T/T_C)$ curves at $T/T_c = 1$ was proceeded by a decrease of $c_V^{(\alpha)}$ close to T_C (Fig.4.16c). The concentration $c_V^{(\alpha)}$ remaining in $A_{0.48}B_{0.52}$ at lowest temperatures (Fig.4.16c) was definitely higher than in case of $\delta = 0.48$ and $\delta = 0.5$ (Figs.4.16a and 4.16b). It is important that its value - being approximately 0.039 - is in a very good agreement with concentration of structural vacancies predicted and obtained previously (see Tab.4.2).

The asymmetric increase of $c_V^{(\alpha)}$ and $c_V^{(\beta)}$ with increasing temperature was accompanied by a similar behaviour of antisite concentrations $c_A^{(\beta)}$ and $c_B^{(\alpha)}$ (Fig.4.17) showing a markedly preferential formation of $A^{(\beta)}$ antisites. In case of the system $A_{0.52}B_{0.48}$ the concentration $c_A^{(\beta)}$ remaining down to the lowest temperature was definitely the highest (Fig.4.17), approximating 0.044, close to the value predicted and obtained in B-W solution (Tab.4.2).

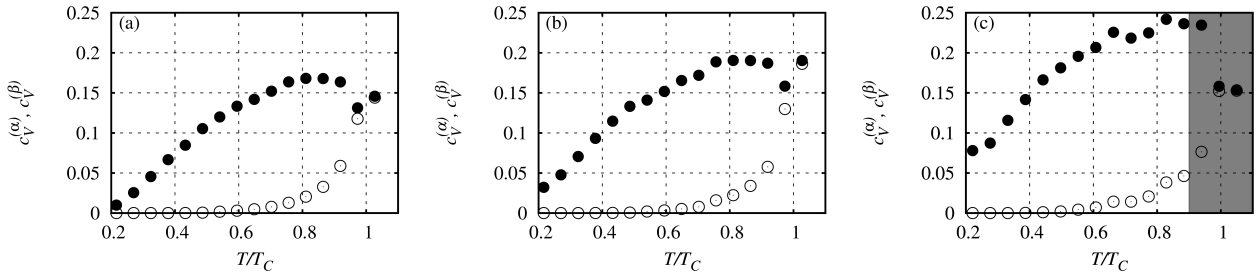

Figure 4.16: Temperature dependencies of vacancy concentrations on sublattices in a) $A_{0.52}B_{0.48}$; (b) $A_{0.5}B_{0.5}$; (c) $A_{0.48}B_{0.52}$; "α" sub-lattice - filled circles , "β" sub-lattice - empty circles.

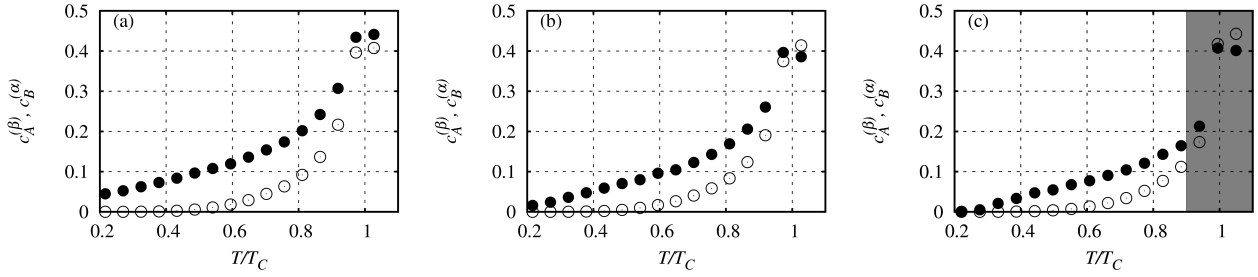

Figure 4.17: Temperature dependencies of antisite concentrations on sublattices in a) $A_{0.52}B_{0.48}$; (b) $A_{0.5}B_{0.5}$; (c) $A_{0.48}B_{0.52}$; $c_A^{(\beta)}$ - filled circles, $c_B^{(\alpha)}$ - empty circles.

4.2.6 Triple defect formation in B2 A-B binary systems

Following the idea of analysis performed for B-W solution, the simulation results were inspected for triple defect formation by investigating temperature dependencies of the ratio of antisite and vacancy concentrations (TDI). The results are shown in Fig. 4.18 for three variants of triple defect indicator (Eqs.4.9, 4.10, 4.11, 4.12).

Well-marked plateaux of $TDI_{ACT} = 1/2$ and $TDI_{ACT}^{(A)} = 1/2$ were observed for finite temperature ranges for all three examined systems (no plateaux were shown by TDI curves in case of $A_{0.52}B_{0.48}$ and $A_{0.48}B_{0.52}$). The result is in agreement with the previous obtained within the B-W approximation and indicates that the correlated triple-defect-like *thermal* generation of vacancies and antisite defects in the system takes place on both sides of the stoichiometric composition. An increasing temperature disturbs the correlation in this way that antisite generation becomes predominating. Comparison of TDI_{ACT} and $TDI_{ACT}^{(A)}$ curves (wider temperature range for $TDI_{ACT}^{(A)}$ plateau) additionally shows that plateau disturbance is triggered by activation of the energetically costly $V^{(\beta)}$ and $B^{(\alpha)}$ defects formation.

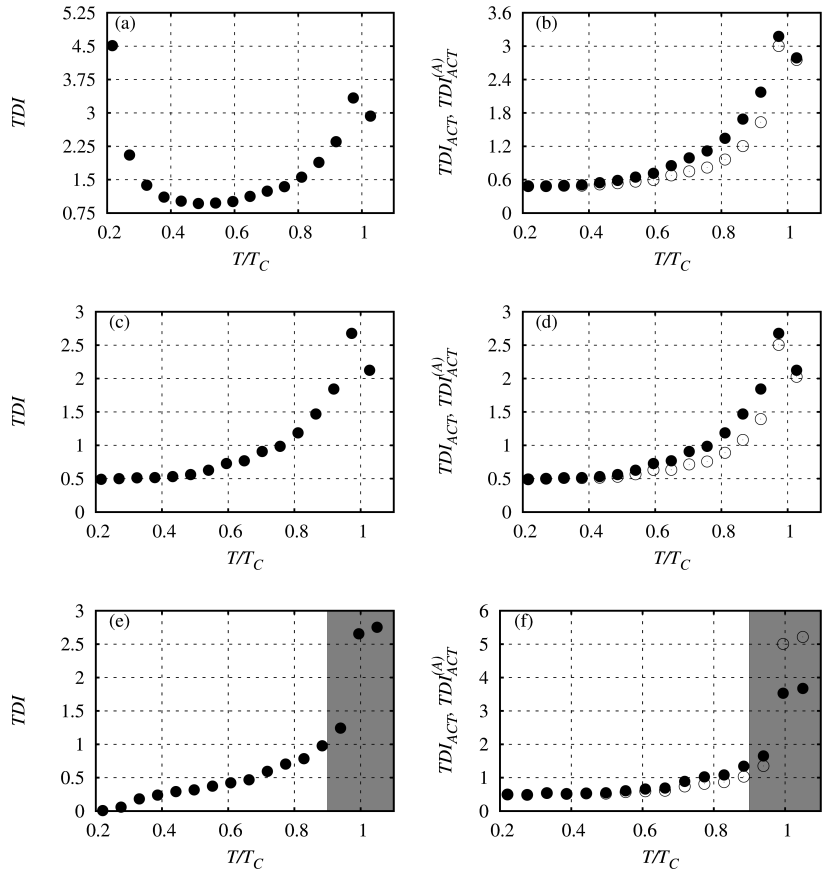

Figure 4.18: Reduced-temperature dependence of Triple Defect Indicators: $A_{0.52}B_{0.48}$ (a,b); $A_{0.5}B_{0.5}$(c,d); $A_{0.48}B_{0.52}$ (e,f). TDI,TDI_{ACT} filled circles, $TDI^{(A)}_{ACT}$ empty circles.

4.2.7 Statistical character of triple defects in stoichiometric B2 AB binary system

The *short range order* (SRO) parameters defined by following formulas were investigated:

$$\xi_{k:X^{(\nu)}-Y^{(\mu)}} \equiv \frac{N_{X^{(\nu)}-Y^{(\mu)}}}{\sum\limits_{Y} N_{X^{(\nu)}-Y^{(\mu)}}} \tag{4.20}$$

or in the variant[1]:

$$\xi_{k:X-Y} \equiv \frac{N_{X-Y}}{\sum\limits_{Y} N_{X-Y}} \tag{4.21}$$

where:

[1] Investigated in Chapter 5.

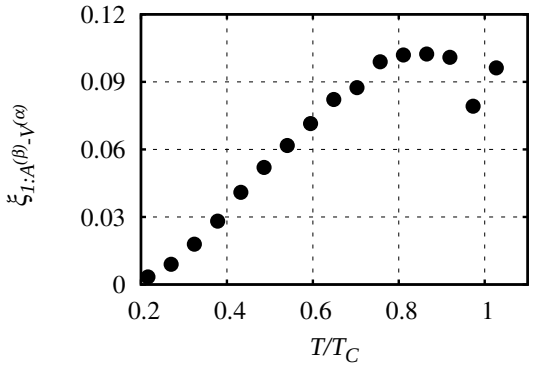

Figure 4.19: Temperature dependence of the SRO parameter $\xi_{1:A^{(\beta)}-V^{(\alpha)}}$.

- "k" is the number of the coordination zone
- $N_{X^{(\nu)}-Y^{(\mu)}}$ is the number of pairs of atoms of kind X and Y occupying μ and ν sub-lattice, respectively

The character of triple defects generated in $A_{0.5}B_{0.5}$ system was examined by analyzing the temperature dependence of SRO parameter $\xi_{1:A^{(\beta)}-V^{(\alpha)}}$. The "pure" triple defect configuration in view of strictly spatial correlation ($V^{(\alpha)}$ vacancy surrounded be exactly two A-atom antisites) would refer to value $\xi^{pure-TD}_{1:A^{(\beta)}-V^{(\alpha)}} \geq 0.25$. Despite the increase with increasing temperature, $\xi_{1:A^{(\beta)}-V^{(\alpha)}}$ was always much lower than 0.25, particularly in the temperature range of the TDI plateau (Figs.4.18c, 4.18d). This means that the triple defects were of purely statistical character – i.e. no nn complexes of two $V^{(\alpha)}$ vacancies and one $A^{(\beta)}$antisite were generated. This result, though being of natural consequence of $V_{AV} > 0$, is not trivial, which will be discussed in Chapter 6.

4.2.8 Size effect on the results: convergence study.

The size of the super-cells applied for the SGCMC simulations (15x15x15 cubic cells referring to 6750 lattice sites) was chosen in such a way that proper accuracy of equilibrium vacancy concentration might be obtained with reasonable length of CPU time. However, it was expected, that Kinetic Monte Carlo simulations (more expensive in view of CPU time), planned in the next stage of the project, would require bigger super-cells to ensure proper resolution of the relaxation curves. Therefore, SGCMC study of the finite-scale effect was performed for the single temperature, applying "C" energetics. The analysis was carried out focusing on equilibrium vacancy concentration in atom-rich phase.

dimensions of super-cell	10x10x10	15x15x15	20x20x20	25x25x25
number of lattice sites	2000	6750	16000	31250
$c_V^{(eq)}$in the atom-rich phase	0.072	0.071	0.071	0.071

Table 4.4: Vacancy concentrations, obtained for different size of super-cells. Results refer to "C" - triple defect promoting - energetics and $T/T_C = 0.53$.

It was found that the size of super-cell (15x15x15) assumed for the detailed thermal analysis was chosen properly, since the results obtained for the bigger super-cells exhibited no meaningful differences of equilibrium vacancy concentration in atom-rich solution (see Tab.4.4).

4.3 General remarks on the applied lattice-gas-decomposition model

The lattice-gas decomposition model for equilibrium vacancy concentration in B2-ordering binary systems was solved by means of B-W approximation [65, 66, 71] and SGCMC simulations [65, 69]. The presented results correspond to Ising gas with nn pair interaction parameters yielding the tendency for triple defect formation. The study should be regarded as modelling pure chemical ordering phenomena which in a real system occur together with processes controlled by other degrees of freedom. In case of the intermetallic compounds addressed to this study (first of all Ni-Al) the crystalline lattice appears less stable than B2 superstructure and the system shows almost perfect LRO up to the melting point. Consequently, the scale of ordering phenomena observed in the real systems is very fine and their simulation modelling is impossible by means of samples with sizes allowing the results to be obtained within realistic CPU time. The concept of modelling presented (aiming in elucidation of the correlated generation of vacancies and antisite defects) was to look at the processes through a specific "magnifying glass" which consisted of application of appropriately scaled system energetics. In contrary to B-W approach where particular quasi-binary A-B-V lattice-gases with fixed δ were considered separately, the SGCMC formalism was based on the analysis of entire ternary A-B-V system. This MC method based approach lead to a more general interpretation of the lattice-gas-decomposition model: A particular $A_{1-\delta}B_\delta$ crystal with equilibrium vacancy concentration should not be identified at each temperature with the vacancy-poor product of the decomposition of $A_{1-\delta}B_\delta - V$ lattice-gas, but should rather be considered as a vacancy-poor $A_{1-\delta}B_\delta - V$ lattice-gas phase being in equilibrium with a vacancy-rich $A_{1-\delta'}B_{\delta'} - V$ one with δ' not necessarily equal to δ. Non-negligible tilt of lattice-gas decomposition tie-lines from the $\delta = const$ orientation was, however, observed only at temperatures close to T_C and thus, the procedure applied in B-W solution may be regarded as an acceptable approximation.

4.3.1 Triple defect formation

The triple defect formation in $A_{1-\delta}B_{\delta}$ probed in by "1/2 plateaux" on $TDI(T/T_C)$, $TDI_{ACT}(T/T_C)$and $TDI^{(A)}_{ACT}(T/T_C)$ dependencies was the consequence of applied energetics in the framework of Ising type model, promoting the formation of $A^{(\beta)}$antisites and $V^{(\alpha)}$ vacancies. It is remarkable that TDI curves showed "1/2 plateuax" only after "reinforcing" the $V^{(\alpha)}$ formation preference with repulsive V_{AV} interaction. An increase of temperature activated long-range disordering showing preferential generation of $A^{(\beta)}$ antisites accompanied by almost exclusive formation of $V^{(\alpha)}$vacancies. Although the formation of $B^{(\alpha)}$ antisites and $V^{(\beta)}$ vacancies was delayed in the temperature scale, the system disordered at a particular temperature T_C, where all LRO parameters reached simultaneously their zero values. The "order-disorder" transition exhibited a continuous character, which, due to the preferential generation of $A^{(\beta)}$ antisites and vacancies on α sub-lattice, induced the characteristic shape of temperature dependencies $c_V^{(\alpha)}(T/T_{C)}$ and $c_V^{(\beta)}(T/T_C)$ of vacancy concentrations on α and β sub-lattices – in particular, a decrease of $c_V^{(\alpha)}$ in the vicinity of $T = T_c$ was observed. Lack of experimental evidence of the effect follows from the fact that most of real triple defect systems show almost perfect LRO up to the melting point. The vacancy concentration markedly depended on the system composition and gradually increased with increasing δ. Remarkably, the antisite concentration manifested an inverted δ-dependence. This result was directly related to the way the system compensated the departure from stoichiometric composition $\delta = 0.5$: while the deficit of A ($\delta > 0.5$) was predominantly compensated by $V^{(\alpha)}$, excess A-atoms ($\delta < 0.5$) predominantly occupied antisite positions on the β sub-lattice. The effect has been well known as the formation of constitutional point defects (vacancies or antisites) whose concentration does not vanish at $T \to 0$ K. The analysis of $TDI_{ACT}(T/T_C)$ curves indicated that, similarly to B-W solution, the concentrations of thermally activated antisites and vacancies determined by low temperature SGCMC simulations remained in a constant proportion 1/2 of finite low temperature intervals; the effect being observed both for $\delta < 0.5$ and $\delta > 0.5$. An increase of TDI_{ACT} at higher temperatures indicated that the equilibrium antisite concentration in the system was becoming higher than that resulting from triple defect formation and that "hybrid" defects (triple defects and single antisites) were activated. The comparison of TDI_{ACT} and $TDI^{(A)}_{ACT}$ curves additionally shows that the hybridization of defects was mainly due to the activation of $B^{(\alpha)}$ and $V^{()\beta}$ formation. The latter finding is of great importance for KMC modelling of "order-order" kinetics in the triple-defect B2 A-B binaries as due to high energetic cost, the process of $B^{(\alpha)}$ and $V^{(\beta)}$ formation is supposed to be highly sluggish.

4.3.2 SGCMC simulations and B-W approximation

Results of studies of phase equilibria carried out within B-W approximation and by means of SGCMC simulations have been compared and discussed in literature in diverse contexts (see e.g. Refs. [72]). The SGCMC results reported in the present study appear in a full qualitative agreement with the previous B-W ones (see also sub-sec.4.17). Figs. 4.20 show the SGCMC and B-W $c_V^{(\nu)}(T/T_C)$ and $TDI(T/T_C)$ curves obtained for the same Ising A-B-V lattice-

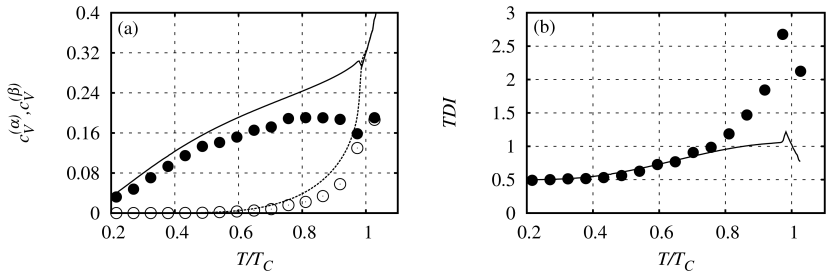

Figure 4.20: Fig. 12. Comparison of SGCMC and B-W solution of A-B-V Ising lattice-gas model ($A_{0.5}B_{0.5}$) applying pair-wise interaction parameters referring to set "C" (a) filled circles - $c_V^{(\alpha)}$SGCMC ; empty circles - $c_V^{(\beta)}$SGCMC, solid line - $c_V^{(\alpha)}$B-W;dashed line - $c_V^{(\beta)}$B-W; (b) filled circles - TDI SGCMC, solid line - TDI B-W.

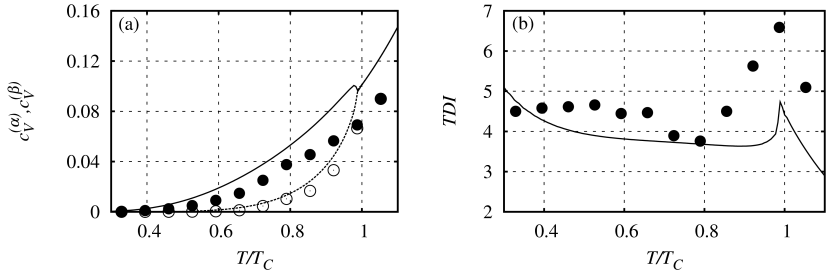

Figure 4.21: Fig. 12. Comparison of SGCMC and B-W solution of A-B-V Ising lattice-gas model ($A_{0.5}B_{0.5}$) applying pair-wise interaction parameters referring to set "B" (a) filled circles - $c_V^{(\alpha)}$SGCMC ; empty circles - $c_V^{(\beta)}$SGCMC, solid line - $c_V^{(\alpha)}$B-W;dashed line - $c_V^{(\beta)}$B-W; (b) filled circles - TDI SGCMC, solid line - TDI B-W.

gas with nn pair interaction parameters given by variant "C". Both solutions are given in a reduced temperature scale, however the normalization factors T_C differ for both cases. The B-W approximation resulted in absolute value of T_C approximately 20% higher than that obtained in the SGCMC formalism.

The similar qualitative behaviour was observed for both solutions for the whole range of temperatures investigated, though vacancy concentration found by means of B-W solution was generally higher. However, for $T/T_C \lesssim 0.75$ even good quantitative agreement was found.

It was interesting to compare the results obtained while applying energetics which had not reproduced triple defect behaviour in B-W approximation, to SGCMC solution. Therefore, an additional set of simulations was performed for "B" energetics (Fig.4.21) and qualitative agreement was observed. The differences between solutions exhibited similar relations as in case of energetics promoting triple defect behaviour. Therefore, it was concluded that triple-defect type behaviour of Ising-type B2 systems demands additional promotion

by means of introduction of non-zero antisymmetric interactions between atoms and vacancies.

The thermal dependence of vacancy concentration obtained by means of SGCMC formalism were applied into Kinetic Monte Carlo simulations, described in the following chapter.

Chapter 5

Kinetic Monte Carlo Simulations of "Order-order" Processes in B2 Triple Defect AB binary systems

Disordering kinetics in B2-ordered $A_{0.5}B_{0.5}$ system was studied by means of KMC techniques. The equilibrium vacancy concentrations obtained from SGCMC simulations were taken into account. Since system characterized by triple defect existence was mainly of interest, pair interaction energies referring to such behaviour in both B-W and SGCMC calculations were introduced (see Tab.5.1).

The values of corresponding saddle point energies of atomic jumps were determined basing on data obtained by means of Molecular Statics techniques applying EAM potential evaluated particularly for B2 NiAl intermetallic [73].

5.1 Simulation procedure

5.1.1 Vacancies and initial configuration

The MC simulations of "order-order" kinetics were performed in Canonical Ensemble, therefore temperature T and number of all atoms and vacancies were fixed. Simulations of disordering processes required to define the initial configuration of the sample which was chosen as nearly perfect ordered stoichiometric B2 super-lattice with a chemical order disturbed only by the equilibrium number of vacancies, initially randomly distributed over sub-lattices. The simulations of a system modelled with the Ising type Hamiltonian (assuming set of pair-wise interactions given in Tab.5.1) were performed for the lattice consisting of $25 \times 25 \times 25$ cubic cells (31250 lattice sites) assuming periodic boundary conditions, for the temperatures and vacancy concentrations listed in Tab.5.2.

5.1.2 Implementation of Residence Time Algorithm

The existence of many vacancies in the system, implies that the number of possible jumps in a single MC step equals:

$$n_T = N_V \times z \tag{5.1}$$

V_{ik}	V_{AB}	V_{AA}	V_{BB}	V_{AV}	V_{BV}
$[eV]$	-0.125	-0.12	-0.05	0.04	-0.04

Table 5.1: "C" set of pair interaction energies (see sub-sec.4.1.2) applied in KMC simulations.

$\frac{T_i}{T_C} \pm 0.01$	0.37	0.47	0.53	0.58	0.68	0.79	0.89	1.00
$c_V(T_i)$	0.047	0.067	0.071	0.078	0.090	0.106	0.122	0.190
$N_V(T_i, N)$	1476	2090	2230	2422	2806	3322	3822	5884

Table 5.2: Temperatures, vacancy concentrations and integer numbers of vacancy applied into KMC simulations.

where z is a nn co-ordination number. According to the rules described in sec.3.4 and Transition State Theory and its direct application to KMC, the acceptance probability per time unit for an atomic jump to nn vacancy was given by[1]:

$$w_{ij} = \frac{e^{-\beta(E_{ij}^{+} + \frac{1}{2}\Delta E_{ij})}}{R_{N_V \times z}^{(i)}} \tag{5.2}$$

with the cumulative function of possible transition probabilities $R_{N_{V\times z}}^{(i)}$:

$$R_{N_{V\times z}}^{(i)} = \sum_{k=1}^{k=N_V \times z} e^{-\beta(E_{ij}^{+} + \frac{1}{2}\Delta E_{ji})} \tag{5.3}$$

thus transition rate W_{ij} is expressed as:

$$W_{ij} = \tau^{-1} e^{-\beta(E_{ij}^{+} + \frac{1}{2}\Delta E_{ij})} \tag{5.4}$$

However, if many vacancies in the system exist, the configuration for which the vacancy-vacancy pair being the nearest neighbour, may occur. Therefore, the rate for the jump of vacancy into vacancy was fixed zero, giving no contribution to the value of cumulative function $R_{N_{V\times z}}^{(i)}$ and preventing the realization of such kind of the jumps.

5.2 Saddle point energies. Molecular Statics implemented with Embedded Atom Method potential.

The pair interaction energies applied in this work are model potentials found by means of methods dealing with equilibrium properties of lattice-gas imitating real B2 superstructure alloy. It was intended to relate the saddle-point energies E_{ij}^{+} to the pair interaction too. In order to find a proper criterion, an analysis of saddle-point energies resulting from *Embedded Atom Method* (EAM) potential devoted to B2 NiAl was performed.

[1] The time coefficient was fixed $\tau = 1$ [a.u.] in the performed KMC simulations.

5.2.1 EAM potential for B2 NiAl [73]

The potential applied in this study for the saddle point energy calculations was elaborated for B2 Ni-Al system by Mishin et al. [73] in the framework of EAM. The EAM formalism was originally proposed by Daw and Baskes[74] for the description of metallic systems. The total energy of a crystal in this model is given by a general formula:

$$E = \frac{1}{2}\sum_{l,m}^{N} \Phi_{pq}(r_{lm}) + \sum_{l}^{N} F_p(\bar{\rho}_l) \tag{5.5}$$

$$\bar{\rho}_l = \sum_{k \neq l}^{N} \rho(r_{kl}) \tag{5.6}$$

where:

- $\phi_{pq}(r_{lm})$ is a pair interaction energy between atoms of kind "p" and "q" in a distance given by r_{lm} where "l","m" label atomic positions
- $F_p(\bar{\rho}_l)$ is an embedding function of "host" atom "p" dependent on the total electronic density $\bar{\rho}_l$ at position "l". The total electronic density is a sum of values of density functions $\rho(r_{kl})$ contributed by all the atoms excluding the host atom. Therefore, the embedding function refers to the energy of placing the atom of kind "p" in the "electron cloud" characterized by density $\bar{\rho}_l$

The potential of interest, whose tabulated form is available, was obtained by means of a complex fitting procedure basing on the ab-initio and experimental data[73]. All necessary functions $\{\phi_{pq}, F_p, \rho\}$ were obtainable by means of the spline-function interpolations (relying on tabulated form of potential).

The range of the maximal distance between interacting atoms in the applied potential, so called "cut-off radius", includes atoms up to the distance referring to the $6th$ co-ordination zone ($r_{cut} \lessapprox 6.0\,\mathring{A}$).

All MS calculations were performed by means of modified VVA (see Chapter 6 sub-sec.3.4.1) - excluding basic calculations (see sub-sec.5.2.2). The modification relies on the fact, that MS simulations refer to temperature close to $T = 0^o\,K$. The kinetic energy of atoms in the context of classical system is an artefact of the initial configuration. Therefore, the total energy in such simulation is not assumed to be conserved - the velocity of a particular atom was reduced "by hand" if the atom had crossed the local minimum of energy during evolution governed by means of the set of Newtonian equations of motion. Additionally, the system was prevented from gaining the velocity of center of mass by fixing the positions of selected atoms. Such modifications ensured that after sufficiently long time of simulation the total kinetic energy converged to zero value (with assumed accuracy) and the minimum of the total energy was obtained.

In the context of saddle point energies calculations another modification was introduced - the detailed description may be found in sub-section 5.2.4.

	$a_0\ [\mathring{A}]$	$E_0\ [eV]$	$B\ [GPa]$
This work	2.859	-4.465	1.6
Mishin et. al[73]	2.859	-4.465	1.6
Experiment	2.88	-4.50	1.58

Table 5.3: Basic properties of EAM potential and available experimental data.

5.2.2 Tests of potential application. Basic calculations.

The following parameters were calculated for the comparison purposes:

- Lattice constant a_0
- Cohesive energy E_0
- Bulk modulus B

All the above parameters have been determined by means of calculation of the total energy curve versus the dimension "a" of the cubic cell $E(a)$.

- Lattice constant:
$$0 = \frac{\partial E(a)}{\partial a}\Big|_{a_0} \tag{5.7}$$
- Cohesive energy[2]:
$$E_0 = \frac{E(a_0)}{N} \tag{5.8}$$
- Bulk modulus (assuming harmonic approximation) at $T \to 0$:
$$B = -V\frac{\partial^2 E}{\partial V^2}\Big|_{a_0} \tag{5.9}$$
where V is volume of super-cell.

The obtained values compared to those referred in Ref. [73] and to available experimental data (also reported in Ref. [73]) are presented in Tab.5.3. Nearly perfect agreement between the results was found which confirmed validity of potential application into the code.

5.2.3 Formation energies of point defect complexes conserving overall system composition

The more sophisticated tests consisted of calculations of formation energies of point defects conserving the system composition related to the configurations important in view of disordering phenomena. The following, typical configurations were taken into account:

- Two antisites complex (ANTC): $Ni^{(\beta)} + Al^{(\alpha)}$

[2] In EAM formalism if $a_0 \to \infty$ then $E(a_0) \to 0$

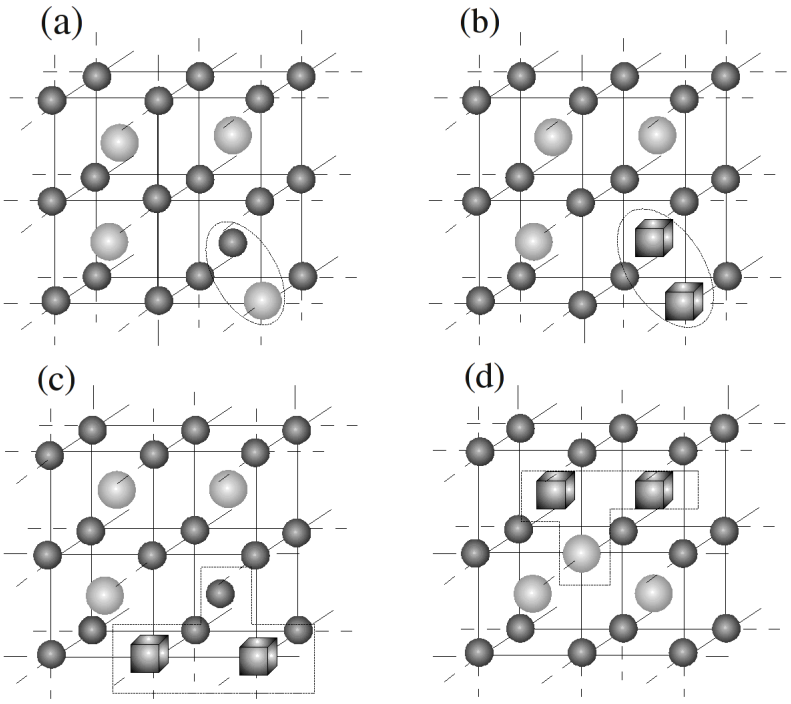

Figure 5.1: Spatially grouped defects investigated in MS calculations: (a) ANTC, (b) DV, (c) TD, (d) ATD.

- Divacancy complex (DV): $V^{(\alpha)} + V^{(\beta)}$
- Triple defect complex (TD): $2V^{(\alpha)} + Ni^{(\beta)}$
- "Anti" triple defect complex (ATD): $2V^{(\beta)} + Al^{(\alpha)}$

Two kinds of all listed complexes were considered:

- Spatially separated defects
- Spatially grouped defects - the total distance among defects was assumed to be minimal (Fig.5.1)

The complexes including vacancies correspond to a subtraction of two atoms from the system. Therefore, the formulas for related energies had to take that fact into account [73]:

$$E_{ANTS} = E(\sigma_{ANTS}) - N \times E_0 \tag{5.10}$$

	Grouped	Separated	Mishin et al.[73]
$E_{ANTS}\,[eV]$	2.23	2.766	2.765
$E_{DV}\,[eV]$	2.17	2.401	2.396
$E_{TD}\,[eV]$	1.85	2.285	2.281
$E_{ATD}\,[eV]$	-	5.279	5.276

Table 5.4: Formation energies of defect complexes.

$$E_{DV} = E(\sigma_{DV}) - N \times E_0 + 2 \times \frac{E_0}{N} \tag{5.11}$$

$$E_{TD} = E(\sigma_{TD}) - N \times E_0 + 2 \times \frac{E_0}{N} \tag{5.12}$$

$$E_{ATD} = E(\sigma_{ATD}) - N \times E_0 + 2 \times \frac{E_0}{N} \tag{5.13}$$

It must be emphasized that energies calculated by means of formulas 5.10-5.13 should not be understood as the energies of defect formation in thermally activated processes. Formation of defect in the kinetic process refers to forcing the saddle point energy, while Eqs.5.10-13 give information about energy differences between the defected and defect-free configurations, allowing to inspect defect formation tendencies by means of purely energetics considerations.

In all calculations performed, the super-cell consisting of $8\times8\times8$ cubic cells ($N = 1024$ lattice sites, periodic boundary conditions) was considered. Both, the local positions of all the atoms and the super-cell volume were allowed to relax during MS calculations. Good agreement between the obtained results and those reported by Mishin et al. was found. The differences of ca. 5×10^{-3} [eV] may originate from different kind of applied algorithms and different configurations since positions of defects in the lattice were not given explicitly in Ref. [73].

The analysis of the data listed in Tab.5.4 allowed to draw the following conclusions:

- The lowest formation energy of the composition conserving complexes were found for TD case in both spatially separated and spatially grouped defects
- Spatially grouped ATD defect was found unstable - aluminum atom relaxed into its "original" position (β sub-lattice)
- All kinds of stable spatially grouped defects (ANTS,TD,DV) show the notably lower formation energies than the corresponding spatially separated ones
- The defects including the aluminum atom in the antistructural position (ANTC, ATD) show higher formation energy than DV and TD complexes

5.2.4 Saddle point energy calculations

The saddle point energies were calculated for a range of local atomic configurations by means of artificial move of atom into the nearest neigbour vacancy applying VVA for super-cell consisting of 1024 lattice sites - sufficiently large to avoid periodical interaction of defects. The procedure was performed realizing steps listed below:

1. Generation of sample - initial configuration included two vacancies on both sub-lattices
2. Relaxation of atomic positions and volume with respect to potential energy
3. Selection of atom X at position $\vec{r}_X^{(init)}$ being the nn of vacancy at position $\vec{r}_V$
4. Displacement of chosen atom from the previous position $\vec{r}_i$ to the new one $\vec{r}_{i+1} = \vec{r}_i + \overrightarrow{\varepsilon}$ where $\vec{\varepsilon} \| \left(\vec{r}_V - \vec{r}_X^{(init)} \right)$
5. Relaxation of atomic positions and volume of the super-cell - the change of atom X position limited to directions perpendicular to vector $\vec{\varepsilon}$ to prevent the relaxation of atom X into its original position $\vec{r}_X^{(init)}$
6. Repetition of step (5) until total energy of the system relaxes to the constant value (deviation less than 10^{-4} [eV])
7. Repetition of procedure starting from step (4) until desired final position of atom X is achieved

It must be mentioned, that in practice it was impossible to create the complete catalogue of saddle point energies due to a huge number of configurations needed to be taken into account, since the CPU time of a single calculation of the particular displacement of jumping atom was about 5h. Therefore, only limited group of jump configurations were investigated to find some general relations between saddle point energies for both aluminum and nickel atoms.

Firstly, both aluminum and nickel atom jumps were calculated for the four different configurations which were representative from the disordering point of view (Figs. 5.2 and 5.3).

5.2.4.1 Nickel atom jump energy profiles

From the point of view of the results obtained for the formation energies of defect complexes the variants (c) and (d) of nickel jump were found useless. The aluminum atom in its antistructural position accompanied by vacancies in the nearest neighbourhood relaxed to its "original" position.

Both (a) and (b) variants exhibited deep minima in the vicinity of initial and final positions (vacancy) separated by distinctly marked maximum (Fig.5.4) $E^{(s)} - E_{fin} \approx 0.9\,[eV]$.

The results require an additional comment while in defect-free NiAl, both Ni and Al antisite positions mean an increase in configurational energy. This is not the case of a system containing vacancies. The results obtained are not surprising: (a) and (b) configurations refer to triple defect formation therefore

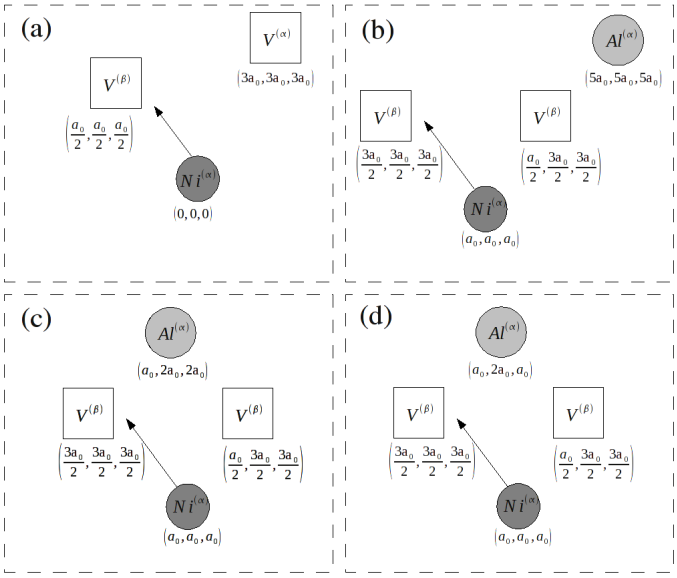

Figure 5.2: Initial configurations for energy profile calculations performed for the nickel atom jumps. Positions of atoms and vacancies given in Cartesian coordinates in the lattice constant units referring to the perfectly ordered system. The rest of atoms in sample (not marked) occupy their original positions. Variants (c) and (d) differ in positions of $Al^{(\alpha)}$ only.

final, stable states are characterized by lower energies than initial ones in both cases.

5.2.4.2 Aluminum atom jump energy profiles

The energy profiles for aluminum atom jumps into antistructural position were performed in the same manner as for the nickel atom. Taking into account the results obtained for nickel and calculation of ATD formation energy the lack of stability for aluminum antisite was expected. However, all four variants shown in (Fig.5.3a-5.3d) were investigated since it was important to check if "stable configuration" with $Al^{(\alpha)}$may exists when applying EAM energetics in the selected group of configurations.

It was found that one of the configurations (d) showed the stable position of aluminum antisite. However, it must be emphasized that the energy minimum accompanying the antistructural position was very shallow $E^{(s)} - E_{fin} \approx 0.1\,[eV]$ in comparison to those observed for the nickel atom jumps. Therefore the stability of aluminum antisite was found very "weak" . This "weakness" refers to an increase of total energy of the system and relatively low energy barrier for the reverse jump. It must be emphasized that instability of single aluminum antisite was reported by some authors in the last decade (see e.g. Ref. [75]). However, in the author's opinion further studies in this field

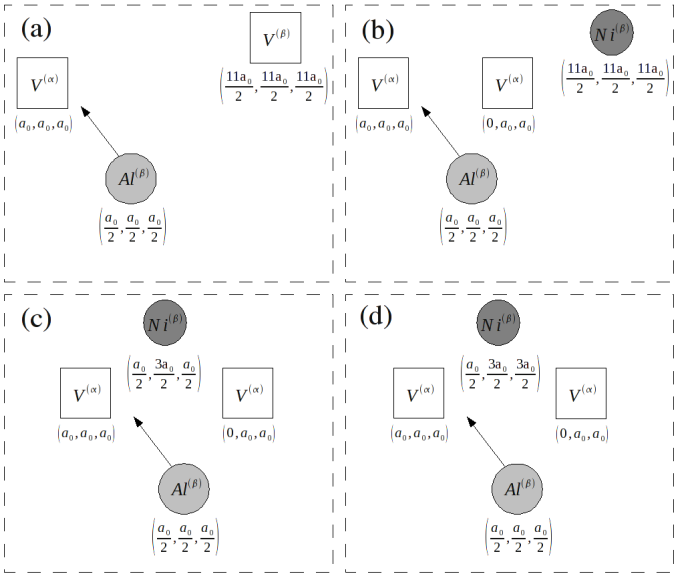

Figure 5.3: Initial configurations for energy profile calculations performed for the aluminum atom jumps. Symbols and units the same as on Fig 5.2

should be performed. It appeared that the calculations of energy profiles for hypothetical aluminum atom jump is a delicate field which needs to be studied deeper with the variety of methods. Mishin et al. investigated collective jump paths in view of self-diffusion mechanism [75]. It means that the jump of nickel and aluminum atoms occur simultaneously during the course of calculation, making the final position stable since the nickel atom is "following" the aluminum one. This mechanism is beyond the scope of present study but it must be mentioned that even single jump mechanism of aluminum is possible assuming the result obtained ((d) variant) and it is not an artifact of EAM potential applied. Probably ab-initio DFT calculations performed for the variety of configurations would help to answer this question.

5.2.4.3 The sequence of atomic jumps

The results of calculations performed by means of MS and presented above referred to single jumps of aluminum or nickel atom. In this section the sequence of jumps is considered as one of possible mechanisms of disordering.

Taking into account results obtained for energy profiles for both constituents, following sequence of configurations generated by atomic jumps has been considered:

$$V^{(\alpha)} + V^{(\beta)} \xrightarrow{(a)} Ni^{(\beta)} + 2V^{(\alpha)} \xrightarrow{(b)} Ni^{(\beta)} + Al^{(\alpha)} + V^{(\alpha)} + V^{(\beta)} \xrightarrow{(c)}$$
$$2Ni^{(\beta)} + Al^{(\alpha)} + 2V^{(\alpha)} \xrightarrow{(d)} Ni^{(\beta)} + Al^{(\alpha)} + V^{(\alpha)} + V^{(\beta)} \quad (5.14)$$

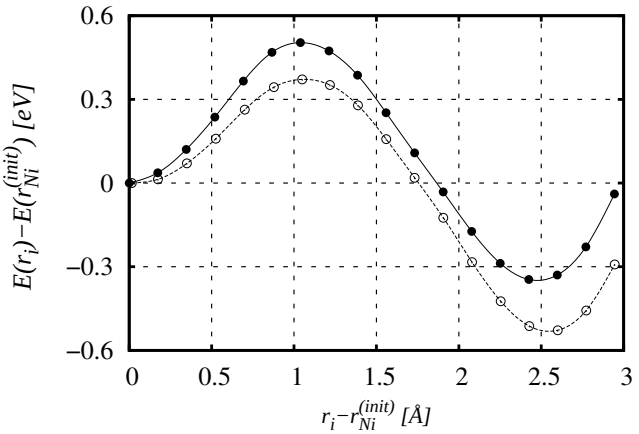

Figure 5.4: Energy profiles of Ni atom jumps into antistructural positions for two different configurations referred in Fig.5.2: (a) filled circles (b) empty circles. Lines are cubic splines which serve as a guide for the eye and for finding extrema.

The scheme of the sequence with the detailed description of configurations is shown on the Fig.5.6.

The results obtained for the sequence of jumps and for the single jumps of aluminum and nickel allowed to find the differences between the energies of the final and initial states $\triangle E_{ji}$ and related energy barriers E_{ij}^{+} (Tab.5.5). The (d) jump-configuration is the reversal jump of nickel atom jumping as the first one in the sequence (a). It was found that such reversal jump performed in the configuration formed previously as a consequence of steps (a),(b),(c) leads to the state characterized by higher energy than the initial one (final state of (c) variant). This behaviour may be interpreted as a strong tendency of the system to promote the triple defects.

The data collected during MS calculations resulted in the following main conclusions:

- The saddle point energies for nickel atom jumps are significantly lower than those for aluminum atom jumps regardless of configurations considered
- The stability of aluminum atom in its antistructural position depends on the configuration - e.g. formation of the aluminum antisite by means of single jump demanded the presence of a nickel antisite in its nearest neighbourhood

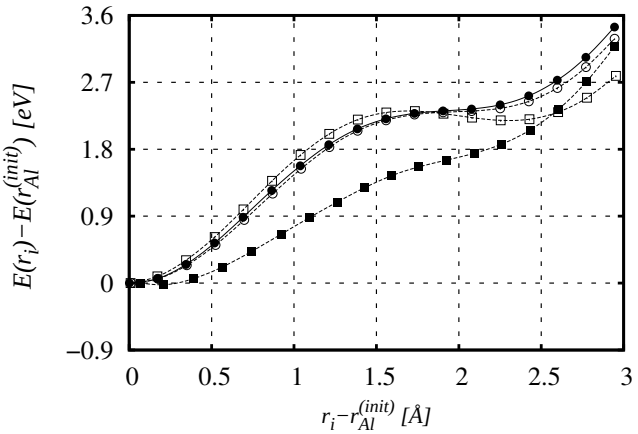

Figure 5.5: Energy profiles of Al atom jumps into antistructural positions for four different configurations referred in Fig.5.3: (a) filled circles (b) empty circles (c) filled squares (d) empty squares. Lines are cubic splines as a guide for an eye and for finding extrema purposes as well.

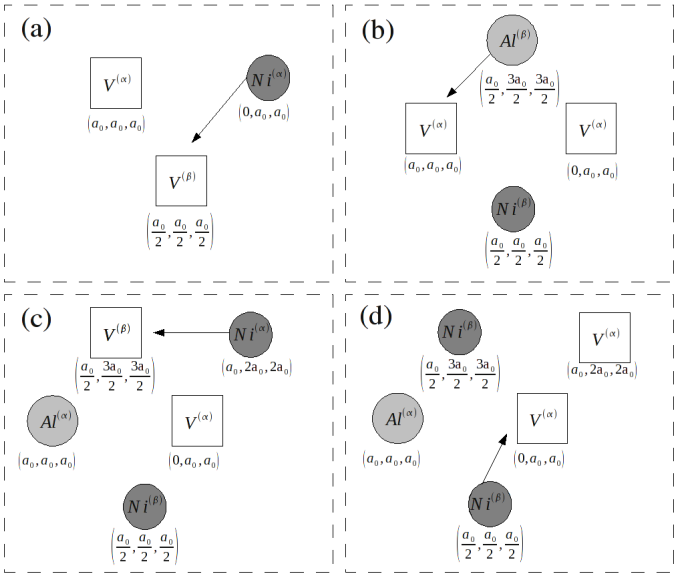

Figure 5.6: The sequence of jumps examined.

Variant	Ni single jump	Al single jump	The sequence examined
(a)	$\triangle E_{ij} = -0.35$ $E^+_{ij} = 0.675$	-	$\triangle E_{ij} = -0.32$ $E^+_{ij} = 0.79$
(b)	$\triangle E_{ij} = -0.53$ $E^+_{ij} = 0.635$	-	$\triangle E_{ij} = 2.19$ $E^+_{ij} = 1.225$
(c)	-	-	$\triangle E_{ij} = -0.31$ $E^+_{ij} = 0.435$
(d)	-	$\triangle E_{ij} = 2.18$ $E^+_{ij} = 1.22$	$\triangle E_{ij} = 0.31$ $E^+_{ij} = 0.735$

Table 5.5: The energy differences between final and initial states and effective saddle point energies. All the values given in [eV].

- More detailed analysis (MS calculations) should be performed to investigate the stability of aluminum antisites for the variety of configurations

The results of presented calculations involving EAM energetics for NiAl showed almost constant and configuration-independent ratio of the energetic barriers E^+ for $Ni-$ and $Al-$atom jumps:

$$\frac{E^+_{Ni}}{E^+_{Al}} \approx \frac{1}{2} \tag{5.15}$$

This justifies the approximation used in the KMC simulations of a model AB system, where the barriers were assumed constant for particular atoms and equal to:

$$A : E^+_{ij} \equiv E^+_A = 0.5\,[eV] \tag{5.16a}$$

$$B : E^+_{ij} \equiv E^+_B = 1.0\,[eV] \tag{5.16b}$$

The comparison between the energy profile of atomic jumps sequence obtained by means of EAM potential and by means of pair-wise interactions (Tab.5.1) and energetic barriers defined in Eqs.5.15-16 is shown in Fig.5.7.

As expected the absolute values of saddle point energies for corresponding configurations differed in both cases, but the similar, qualitative tendency was observed.

5.3 KMC simulation of "order-order" kinetics in B2 triple defect AB binary system

5.3.1 Averaging procedure

KMC simulations performed by means of the RTA allowed to obtain isothermal relaxation curves of parameters of interest. It must be mentioned, that in case of KMC simulations proper statistics had to be performed since the simulation

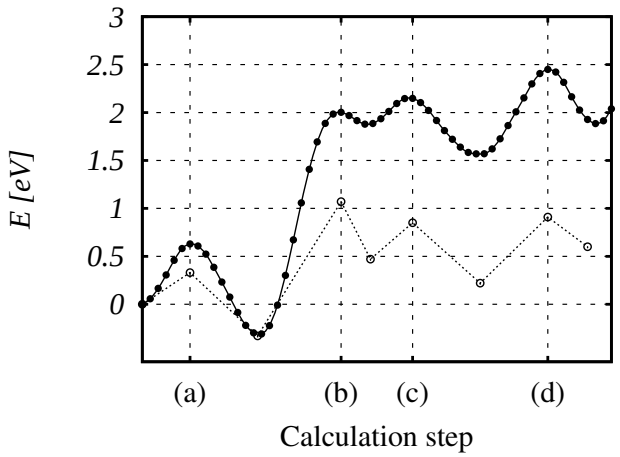

Figure 5.7: The comparison of energy profile for the sequence of the atomic jumps (Fig.5.6) obtained by means of MS calculations (filled circles and solid line as guide for the eye) and the jump energetics corresponding to the Ising type Hamiltonian (hollow circles and dotted line). The letters refer to the vicinity of configurations presented on the Fig.5.6.

is a stochastic experiment and the fluctuations of the relaxation curves are natural. Therefore, the simulations in the same conditions had to be repeated - which was not the case in SGCMC simulations were only equilibrium value was of interest and averaging was based on sampling of data in a single simulation after attaining equilibrium. The averaging of data obtained by means of RTA, however, requires a more sophisticated procedure than the one used in case of Metropolis type algorithms. This is because in every single RTA based simulation the MC time is a "product" of simulation (see e.g. Eq.5.3). The averaging procedure has to be performed carefully taking into account the fundamental idea of the algorithm. In the presented study, the following procedure was realized:

1. The total relaxation time t_{cm} was divided into arbitrary chosen time intervals $t_{cm} = \sum_k \triangle t_k$
2. The average value of parameter x_k^i (e.g. LRO parameter) in the time interval $\triangle t_k$ was evaluated for every simulation run "i":

$$< x_k^i >= \frac{1}{\triangle t_k} \int\limits_{\triangle t_k} x_k^i(t) dt \tag{5.17}$$

by means of numerical integration (simple trapezoidal algorithm)

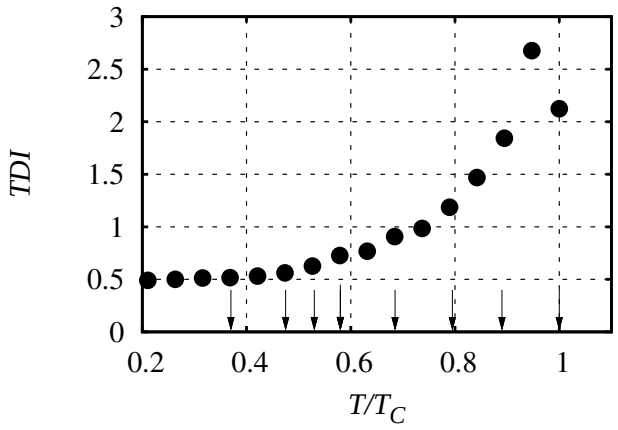

Figure 5.8: TDI as a function of temperature obtained in SGCMC simulations. Arrows denote temperatures considered in KMC simulations.

3. The average value of parameter $x(t_j)$ was calculated:

$$< x(t_j) >= \frac{1}{n} \sum_{i=1}^{n} < x_j^i > \tag{5.18}$$

All results presented in following sub-sections refer to the number of simulations $n = 5$ in a set.

5.3.2 Results

Temperatures at which "order-order" relaxations were simulated are presented in view of $TDI(T/T_C)$ behaviour obtained by means of SGCMC (Fig.5.8). Such selection of temperatures allowed to investigate the kinetic processes within and out of the "triple defect" temperature range.

The MC time evolution $\eta_A(t)$, $\eta_B(t)$ and $\eta_B(t)$ of the corresponding parameters (see Eqs.4.1, 4.2 and 4.4) obtained by means of KMC simulations in the range of temperatures considered is presented in Fig.5.9. As expected, relaxation times differed by orders of magnitude depending on assumed temperature. In the range of temperatures reproducing triple defect behaviour, complex (not monotonical) evolutions of LRO parameters were observed and relaxations were not attaining equilibrium despite long simulation runs. Therefore, the usual analysis based on the evolution of relaxation times, allowing to discuss activation energy of processes, was found questionable. Due to this fact, detailed description of evolution of various LRO and SRO parameters was performed instead, supported by analysis of atom jump statistics.

The study was focused on processes occurring at three, typical temperatures suggested by the shape of $TDI(T/T_C)$ (Fig.5.8):

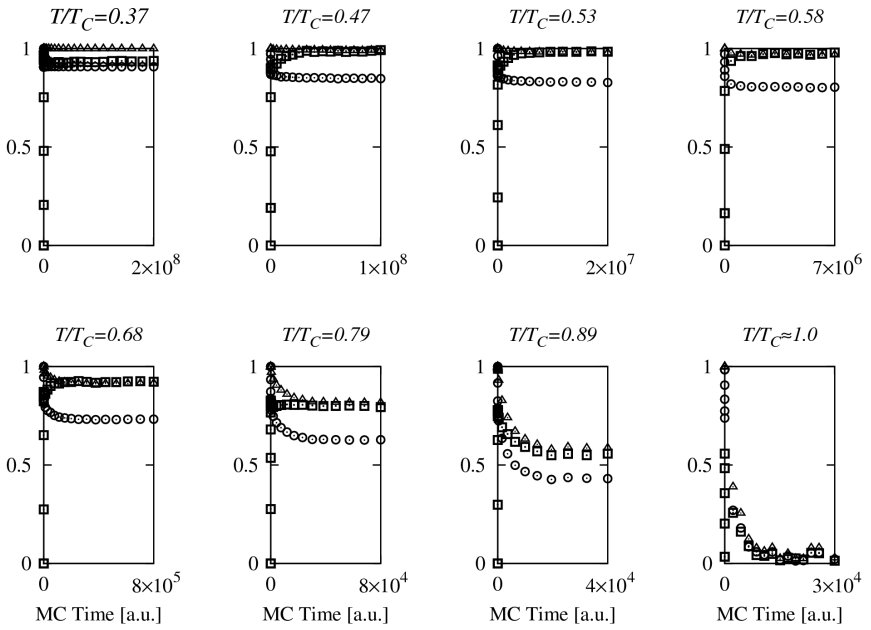

Figure 5.9: Evolutions of LRO parameters obtained at temperatures considered in KMC simulations:$\eta_A(t)$ - empty circles, $\eta_B(t)$ - empty triangles, $\eta_V(t)$ - empty squares.

- $T/T_C = 0.37$
  - Nearly pure triple defect range indicated by the plateau of $TDI(T/T_C)$, negligible formation of B-antisites
- $T/T_C = 0.53$
  - "Middle case" - the range of temperatures where the degree of atomic LRO referring to A-atoms is still relatively high ($\eta_A > 0.8$) but the concentration of B antisites becomes noticeable
- $T/T_C = 0.89$
  - Decay of the triple defect behavior

According to the considerations mentioned in the beginning of this chapter (see sec.5.1.1), the initial atomic configuration (in view of LRO parameters) of every single simulation run referred to:

- $\eta_A = 1$
- $\eta_B = 1$
- $\eta_V = 0$

5.3.2.1 MC time evolution of atomic long range order parameters

In this sub-section, the evolutions of degree of LRO and TDI parameters obtained by means of KMC simulations in the three representative temperatures are described. It must be noted, that"t" variable will be used interchangeably with "MC Time" to maintain the clarity of text.

LRO and TDI relaxations at $T/T_C = 0.37$

- $\eta_A(t)$

The LRO degree relating to A-atoms (Fig.5.10a) rapidly decreased in the very first stage of relaxation (see Fig.5.10d). Such behaviour was expected according to the tendency of triple defects formation. That high-rated process, characterized by significant amplitude, stopped at the level of $\eta_A \approx 0.905$ and was followed by an extremely slow one. The "stopping" occurred after a specific "over-shooting", reflected by a sequence of local minimum and maximum of η_A. The "overshooting" was followed by a slow decrease of η_A(see Tab.5.6).

- $\eta_B(t)$

The number of B-atom antistes was found negligible (more than 10 defects never detected at the temperature of interest) and the amplitude of η_B relaxation exhibited very low value ($\propto 10^{-4}$). Therefore, the quality of data obtained was found poor. However, qualitative analysis allowed to find out that $\eta_B(t)$ was monotonically decreasing (Fig.5.10b).

- $\eta_V(t)$

As expected after analysis of $\eta_A(t)$ and $\eta_B(t)$, an evolution of $\eta_V(t)$ was found strongly correlated with the formation of A-atom antisites. At a very first stage of process, initially disordered vacancies started to order very quickly (see Fig.5.10c). Similarly, as in the case of $\eta_A(t)$, the process was stopped showing an "over-shooting" effect. After these extraordinary effects observed, the increase of $\eta_V(t)$ was slowly continued.

- TDI_{ACT} and $TDI^{(A)}_{ACT}$

The evolution of triple defect indicators (ratio of thermally activated antistes and vacancies see Eqs.4.9 and 4.10) is presented in Fig.5.11. Initially, both parameters equaled zero (invisible in the figure) according to the lack of antisites in the system. After an initial, very rapid increase associated with migration of A-atoms into β sub-lattice, both factors decreased attaining local minima (localized at $MC\ Time \propto 10^3$) - related to the "over-shooting" of η_A and η_V and subsequently started to increase very slowly. Both TDI_{ACT} and $TDI^{(A)}_{ACT}$ were found below 1/2 value (dashed line in Fig.5.11) indicating, that the relaxation did not equilibrate despite long simulation run (more than 500h of CPU time for a single simulation).

The analysis performed for LRO and TDI parameters at temperature of interest, indicated complex character of the relaxation. It was found that the role of migration of B-atoms is negligible in comparison to A ones. The inital, fast process relating to fast formation of triple defects did not lead to equilibrium

MC Time interval [a.u.]	$\propto (0, 10^3)$	$\propto (10^3, 10^7)$	$>\propto 10^7$
$\triangle\eta_A$	$\sim (-0.095) \searrow$	$\sim (0.05) \nearrow$	$\searrow$ not converged
$\triangle\eta_B$	$\sim (-10^{-4}) \searrow$	$(-3 \times 10^{-4}) \searrow$	$\searrow$ not converged
$\triangle\eta_V$	$\sim (0.96) \nearrow$	$\sim (-0.035) \searrow$	$\nearrow$ not converged

Table 5.6: The general behavior of the LRO parameters in $T/T_C = 0.37$; $\triangle\eta_i = \eta_i(t_2) - \eta(t_1)$ and MC Time interval is (t_1, t_2). Arrows indicate general tendency of variation.

and significant number of vacancies remained on the α sub-lattice. The relaxation continued but its rate became noticeably lower than that referring to the initial stage of evolution, however the system still tended to form triple defects (Fig.5.11). Beside those global observations (the existence of very quick disordering process continued by a significantly slower one) another one, related to "over-shooting", was found. These extraordinary effects exhibited as "deviation" of monotonicity of $\eta_A(t)$ and $\eta_V(t)$ dependencies. However, the shape of both curves, and coincidence of anomalous behaviour (appearance of local extrema) suggest strong correlation between them, clearly following from the domination of triple defect behaviour. Taking into account the results obtained by means of procedure of saddle point energies evaluation (see sub-sec.5.2.4 and Fig.5.7), one may expect domination of A-atom jumps, at least at lower temperatures. Therefore, the following hypothesis was raised: the stop of initial process, and the existence of extrema on LRO parameter curves are effects of triggering reversal jumps of A-atoms implied by an increase of vacancy concentration on α sub-lattice and immobility of B-atoms. This idea was confirmed by means of analysis of SRO parameters (see next sub-sec.5.3.2.2).

LRO and TDI relaxations at $T/T_C = 0.53$

- $\eta_A(t)$

The evolution of η_A parameter is shown in Fig.5.12a, one finds that general shape of relaxation curve remained similar to that observed in $T/T_C = 0.37$. The tendency of immediate formation of triple defects is still manifested by rapid decrease of η_A in the initial stage of relaxation (see inset in Fig.5.12a). That high-rated process, characterized by the significant amplitude (see Tab.5.7) is subsequently followed by the substantially slower one. However, no local extrema on $\eta_A(t)$ curve i.e. no "over-shooting" were observed - the degree of LRO referring to A-atoms was decreasing monotonically.

- $\eta_B(t)$

The formation of $B^{(\alpha)}$ defects were find significantly higher than at $T/T_C = 0.37$, hence the quality of $\eta_B(t)$ curve (Fig.5.12b) is better. However, η_B remains still significantly higher than η_A and monotonously decreases during the whole simulation course.

- $\eta_V(t)$

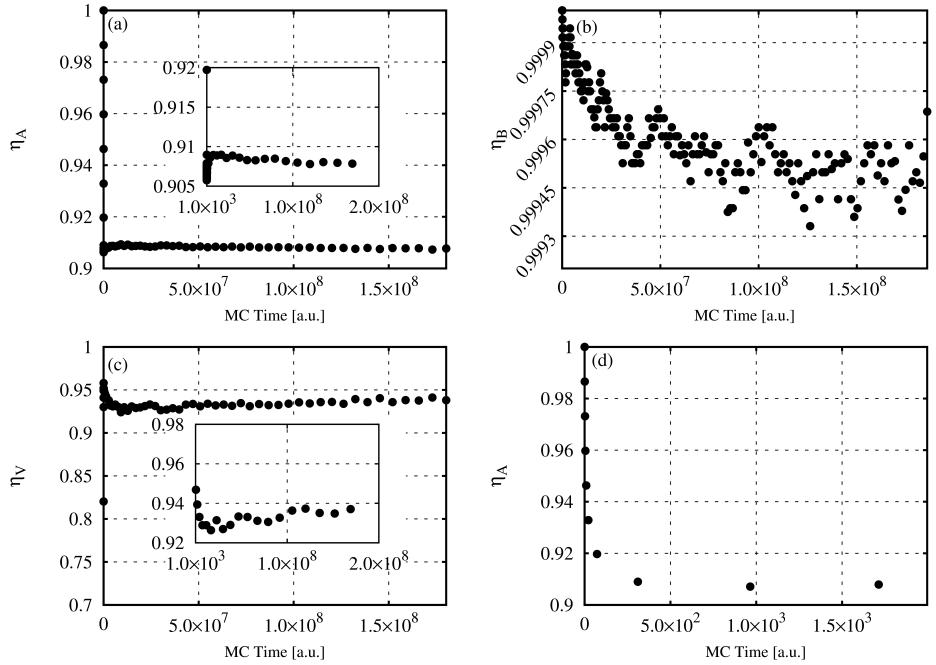

Figure 5.10: Long range order parameter relaxation curves obtained at $T/T_C = 0.37$.

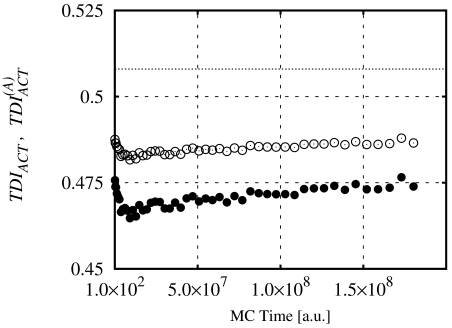

Figure 5.11: Triple defect indicator evolution curves in $T/T_C = 0.37$: filled circles refer to TDI_{ACT} and hollow circles $TDI^{(A)}_{ACT}$. Dotted line indicates SGCMC value of $TDI_{ACT} \approx TDI^{(A)}_{ACT}$.

In contrary to $\eta_A(t)$ and $\eta_B(t)$ curves, the $\eta_V(t)$ dependence did show an "over-shooting" effect (Fig.5.12c).

- TDI_{ACT} and $TDI^{(A)}_{ACT}$

The $TDI_{ACT}(t)$ and $TDI^{(A)}_{ACT}(t)$ exhibited no extraordinary features. Both indicators were mutually increasing during the system evolution. It should be noted, that finally system equilibrated since both parameters attained values predicted by means of SGCMC simulations (see Fig. 5.12d)

The analysis of the MC time evolution of atomic LRO parameters (see Figs.5.12a-d and Tab.5.7) allowed to recognize the nearly pure triple defect type behaviour ($TDI^{eq}_{ACT} \approx 0.6$) though slightly deviated by means of existence of $B^{(\alpha)}$ antisites ($\eta^{eq}_B \approx 0.98 > \eta^{eq}_A \approx 0.83$). In the first stage of evolution, the system exhibited existence of high-rated process associated with triple defect formations (migration of A-atoms to β sub-lattice), followed by a significantly slower one, leading the system to equilibrium. Although no anomalous features of $\eta_A(t)$ and $\eta_B(t)$ were observed, it was not the case of $\eta_V(t)$ curve, exhibiting well marked "over-shooting" effect. The origin of the "over-shooting" effect visible on $\eta_V(t)$ and invisible on $\eta_B(t)$ parameters, was investigated by means of an analysis of ratio $\eta_A(t)/\eta_B(t)$ and separately $\eta_A(t)$ and $\eta_B(t)$ in better resolution (see Figs.5.13a and 5.13b). It was found, that $\eta_A(t)/\eta_B(t)$ ratio exhibited well marked maximum at about $\propto 1.5 \times 10^5$ MC Time coinciding with the local minimum found for η_V. Analyzing Figs.5.13a and 5.13b, one finds that the formation of B antistes is locally more efficient than formation of $A^{(\beta)}$ ones slowed down supposedly by means of effect of the reversal jumps, this implies local decrease of η_V. The formations of $B^{(\alpha)}$ additionally stimulated A-atoms to form antistites since the jumps of B-atoms automatically generated $V^{(\beta)}$ and the process might continue. Although the extraordinary features of LRO parameter evolutions in the intial stage of simulations (at both described temperatures) were found intuitively understood and confirmed later by analysis of SRO parameters (see next sub-sec), the nature of second, low-rated process, being mainly of interest, remained unknown at this stage. Therefore, more sophisticated investigation, based on the analysis of correlations in the 1st coordination zone (SRO parameters) and direct inspection of local environment of the jumping atoms was performed (described in the next sub-sec.5.3.2.3).

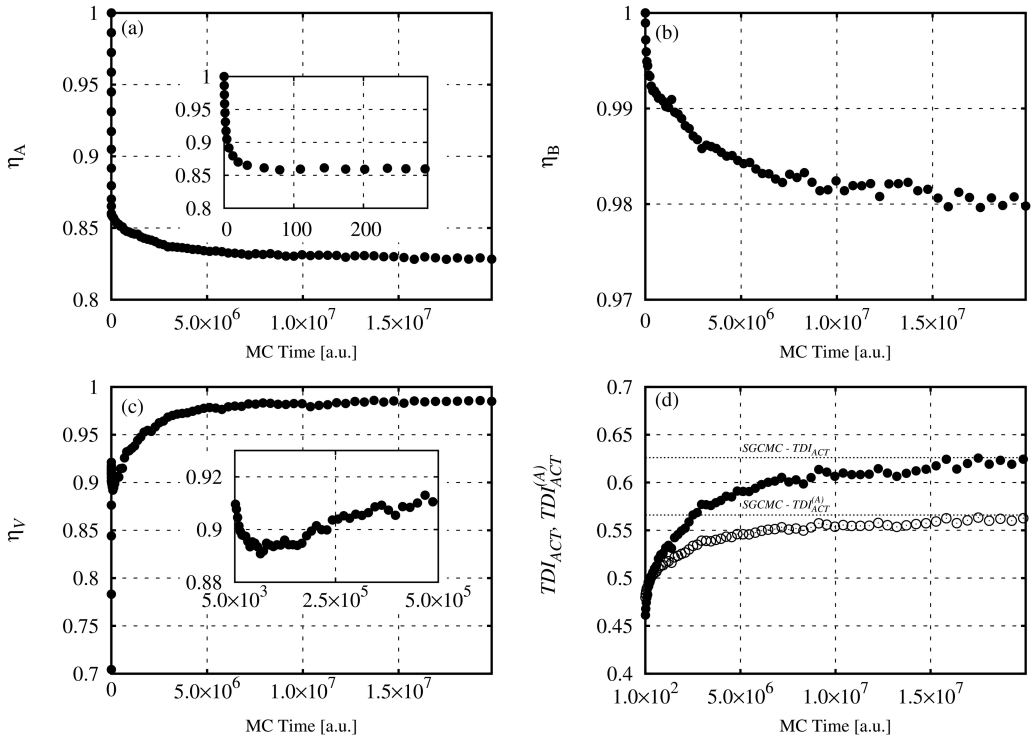

Figure 5.12: The LRO parameters (a,b,c) and triple defect indicators (d) at temperature $T/T_C = 0.53$. Dotted lines indicate equilibrium values obtained in SGCMC (d).

MC Time [a.u.]	$\propto (0, 1.5 \times 10^3)$	$\propto (1.5 \times 10^3, 10^5)$	$>\propto 10^5$
$\triangle\eta_A$	$\sim (-0.15) \searrow$	$\searrow$	$\searrow$ converged $\eta_A(\propto 2 \times 10^7) \approx 0.83$
$\triangle\eta_B$	$\sim (-0.008) \searrow$	$\searrow$	$\searrow$ converged $\eta_B(\propto 2 \times 10^7) \approx 0.98$
$\triangle\eta_V$	$\sim (0.92) \nearrow$	$\sim (-0.03) \searrow$	$\nearrow$ converged $\eta_V(\propto 2 \times 10^7) \approx 0.98$

Table 5.7: The general behavior of the LRO parameters in $T/T_C = 0.53$.

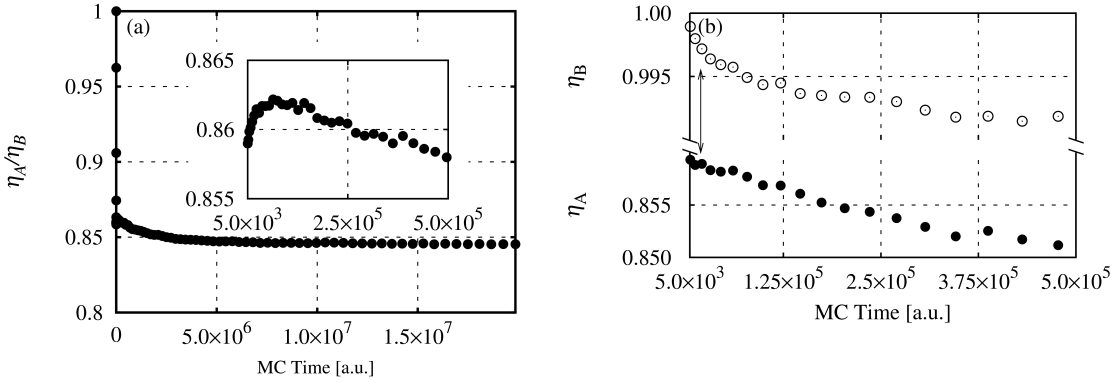

Figure 5.13: MC time dependence of the ratio between long range order parameters η_A and η_B at $T/T_C = 0.53$ (a), well marked local maximum (inset) coincides with local minimum of η_V; (b): comparison between η_A and η_B in better resolution - the arrow indicates the range of time where formation of B-atom antisites is more effective than formation of $A^{(\beta)}$antisites.

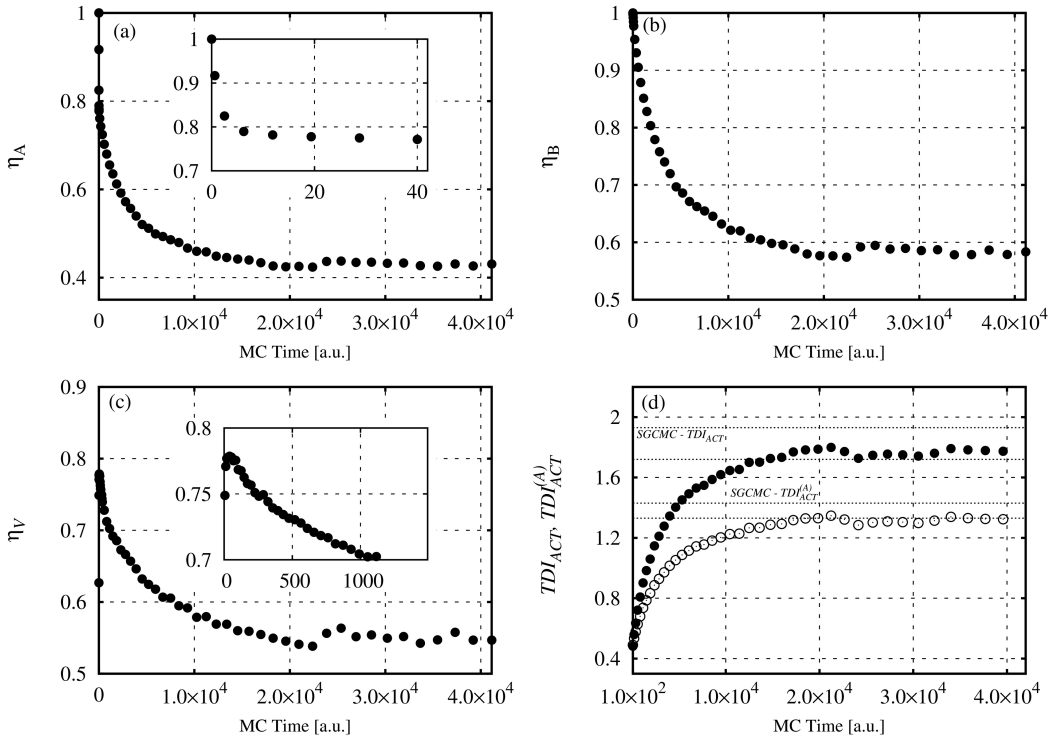

Figure 5.14: MC Time dependence of LRO parameters (a,b,c) and the relaxations of triple defect indicators (d) at $T/T_C = 0.89$. The pairs of dotted lines denote approximate values obtained in SGCMC simulations.

MC Time [a.u.]	$(0, 40)$	> 40
$\triangle\eta_A$	$\searrow$	$\searrow$ converged $\eta_A(\propto 2\times 10^5) \approx 0.42$
$\triangle\eta_B$	$\searrow$	$\searrow$converged $\eta_B(\propto 2\times 10^5) \approx 0.58$
$\triangle\eta_V$	$\sim (0.78) \nearrow$	$\searrow$converged $\eta_V(\propto 2\times 10^5) \approx 0.42$

Table 5.8: The general behaviour of the LRO parameters in the temperature$T/T_C = 0.89$.

LRO and TDI relaxations at $T/T_C = 0.89$

- General behaviour of $\eta_A(t)$, $\eta_B(t)$, $\eta_V(t)$ and triple defect indicators

Though the kinetic processes at higher temperatures referring to "vanishing" of the triple defect behaviour had been generally out of scope, the LRO parameters evolution at $T/T_C = 0.89$ is presented in Fig.5.14 and Tab.5.8 to maintain reviewable character of this sub-section. As expected, the first, very fast process referring to the triple defect formation was still observed.

The rapid increase of η_V during the first fast process, led to maximal value of η_V, however in the further relaxation it was monotonically decreasing contrary to ordering tendency observed at lower temperatures. According to the fact, that temperature ($T/T_C = 0.89$) of simulations in this case was close to the "order-disorder" transition point, the total amplitude of η_B was found substantial ($\Delta\eta_B \approx 0.6$) in comparison to those obtained at lower temperatures. The triple defect indicators relaxed to values close to those obtained in SGCMC simulations (Fig.5.14d) though the maximal error (significantly higher in the higher temperatures in a case of SGCMC simulations) was taken into account (the pairs of dotted lines in Fig. 5.14d).

5.3.2.2 MC time evolution of atomic short range order parameters

Evolution of selected SRO parameters at $T/T_C = 0.37$

The set of MC Time evolutions of selected SRO parameters defined by Eqs.4.20 and 4.21 in a sub-sec.4.27, important in view of further analysis were collected for the temperature $T/T_C = 0.37$ (Fig.5.15). Firstly, parameters $\xi_{1:A^{(\beta)}-A^{(\alpha)}}$ and $\xi_{1:A^{(\beta)}-V^{(\alpha)}}$ were analyzed. It was found that during very fast, initial disordering process, $\xi_{1:A^{(\beta)}-A^{(\alpha)}}$ decreased until attaining local minimum (Fig.5.15a), in contrary $\xi_{1:A^{(\beta)}-V^{(\alpha)}}$ increased until its local maximum (Fig.5.15b). Therefore, undoubtedly the very first, high-rated process led to an increase of $c_A^{(\beta)}$ and to an increase of the number of vacancies in their nearest neighbourhood. Although $A^{(\beta)}$ antisite is extremely stable in view of energetic considerations, increasing average number of nn $V^{(\alpha)}$ vacancies promoted reversal jumps of A-atoms to α sub-lattice (first local extrema in Fig.5.15a and 5.15b). Subsequently (after reaching the local extrema), $\xi_{1:A^{(\beta)}-A^{(\alpha)}}(t)$ curve exhibited an immediate increase related to the reversal jumps of A antisites. The shape of the $\xi_{1:A^{(\beta)}-V^{(\alpha)}}(t)$ relaxation curve was perfectly inverted with respect to the $\xi_{1:A^{(\beta)}-A^{(\alpha)}}(t)$ (compare Fig.5.15a and 5.15b) which stopped and even inverted, the process. The correlation between the "shapes" of $\xi_{1:A^{(\beta)}-V^{(\alpha)}}(t)$ and

$\xi_{1:A^{(\beta)}-A^{(\alpha)}}(t)$ curves, occurring with negligible concentration of $B^{(\alpha)}$, allowed to confirm the hypothesis of reversal A-atom jumps stopping the initial stage of evolution and to explain the origin of local extrema ("over-shooting") found for LRO parameter dependencies.

The second process referring to increase of $\xi_{1:A^{(\beta)}-A^{(\alpha)}}$ and decrease of $\xi_{1:A^{(\beta)}-V^{(\beta)}}$ was smoothly slowing down similarly to the relaxation of η_A. It is interesting, that $\xi_{2:V-V}$ SRO parameter (Fig.5.14d) in the first stage of the simulation dramatically increased and during the evolution of system the rate of its evolution became very low or even constant[3]. Such behaviour was recognized as exhibiting the slow continuation of process associated with the formation of triple defects.

It is worthy of note that although the role of B atoms migration was negligible $\left(c_B^{(\alpha)} \leq 10^{-4}, c_A^{(\beta)} \approx 10^{-2}\right)$ the value of $\xi_{1:B^{(\alpha)}-A^{(\beta)}}$ parameter during the low-rated, second process, remained approximately constant: $\xi_{1:B^{(\alpha)}-A^{(\beta)}} \approx 0.25 = 2/8$ (Fig.5.15c).

This effect strongly corresponds to the results obtained by means of MS calculations devoted to $B2\ NiAl$ system in a context of saddle-point energy calculations (energetic profiles - see sub-sec.5.2.4). It should be reminded that the energetical stability of $Al^{(\alpha)}$ ($B^{(\alpha)}$ in the presented model) antisite referred to the configurations with at least one nickel antisite in the nn of $Al^{(\alpha)}$, more over two nickel antisites in nn resulted in even deeper stability of $B^{(\alpha)}$ in terms of configurational energy (see Fig.5.7).

Evolution of selected SRO parameters at $T/T_C = 0.53$

A similar kind of inspection of selected SRO parameters was performed at a higher temperature $T/T_C = 0.53$ (Fig.5.16). The conclusions coming from the analysis of $\xi_{1:A^{(\beta)}-A^{(\alpha)}}$ and $\xi_{1:A^{(\beta)}-V^{(\alpha)}}$ relaxation curves (Figs.5.16a and 5.16b) are similar to those previously described. The first, fast process exhibited as an immediate increase of number of the $A^{(\alpha)} - V^{(\beta)}$ pairs. This high-rated evolution was followed by the notably slower one referring to increase of $\xi_{1:A^{(\beta)}-A(\alpha)}$ and decrease of $\xi_{1:A^{(\beta)}-V^{(\alpha)}}$. It should be noted that although initially $\xi_{1:A^{(\beta)}-V^{(\alpha)}}$ attained value close to that associated to the spatial character of triple defect complex (0.25) further evolution (referring to the significantly slower process) led to the separation of A-atom antisites and vacancies on α sub-lattice. The decrease of $\xi_{1:B^{(\alpha)}-A^{(\beta)}}(t)$ (Fig.5.16c) curve during low-rated relaxation process confirmed that disordering process did not rely on formation of anti-phase domains. Relatively low values of $\xi_{1:B^{(\alpha)}-V^{(\beta)}}$ (excluding the initial stage of evolution - see Fig.5.16d) reflect asymmetry of vacancy distribution over sub-lattices.

At the end of this sub-section the SRO parameters referring to of A-V and B-V nn pairs are presented (see Fig.5.17). As expected, at both temperatures after the completion of the first, fast process mainly B-atoms were nn neighbours of vacancies due to still high value of η_A and almost all vacancies residing on α sub-lattice. However, it should be noted that although $\xi_{1:A-V}(t)$ decreased and $\xi_{1:B-V}(t)$ increased initially very rapidly, subsequently the process was slowly continued and both curves (at both temperatures of interest)

[3]The quality of the data obtained did not allow to recognize if the process "stopped" .

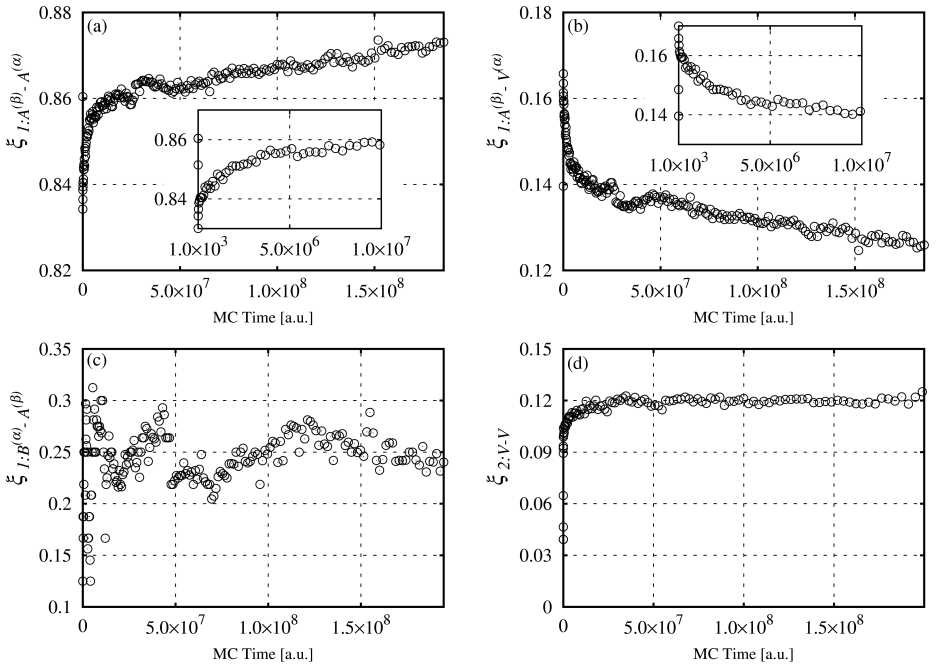

Figure 5.15: Correlation parameters relaxations obtained for the temperature $T/T_C = 0.37$.

were evolving as seen (although hardly) in the Fig.5.17. This fact plays an important role in a further considerations presented in next sub-section.

5.3.2.3 Statistics of atomic jumps: origin of the slow final stage of disordering despite high vacancy concentration in B2 triple defect AB binary system

The efficiency of atom jump events in view of disordering processes was investigated by means of analysis of frequencies of jumps defined as:

$$f_{X:\mu\rightarrow\nu}(t) \equiv \frac{\triangle J_{X:\mu\rightarrow\nu}(t)}{\triangle t}\,[\frac{1}{MC\ Time}] \tag{5.19}$$

where $\triangle J_{X:\mu\rightarrow\nu}(t)$ denotes the number of jumps performed by atom X from sub-lattice μ to sub-lattice ν within a MC time interval $\triangle t$. Additionally, it was convenient to define the following parameter useful in view of further analysis:

$$f_{X:\alpha\leftrightarrow\beta}(t) \equiv \frac{f_{X:\alpha\rightarrow\beta}(t)}{f_{X:\beta\rightarrow\alpha}(t)} \tag{5.20}$$

The parameter $f_{X:\alpha\leftrightarrow\beta}(t)$ describes the efficiency of atomic jumps in increasing the concentration of antisite defects. The evolutions of $f_{A:\mu\rightarrow\nu}(t)$ curves obtained for $T/T_C = 0.37$ are presented in Fig.5.18. The B-atom jumps were extremely rare, resulting in very low concentration of $B^{(\alpha)}$ and their marginal role in the relaxation process (see Fig. 5.10b).

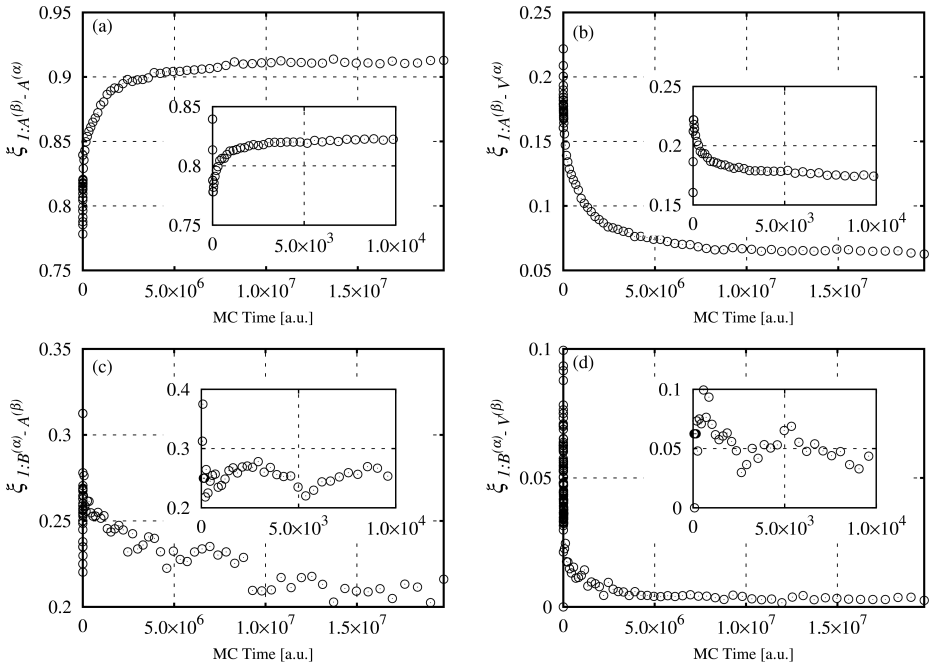

Figure 5.16: Correlation parameter relaxations obtained in KMC simulations performed for temperature $T/T_C = 0.53$.

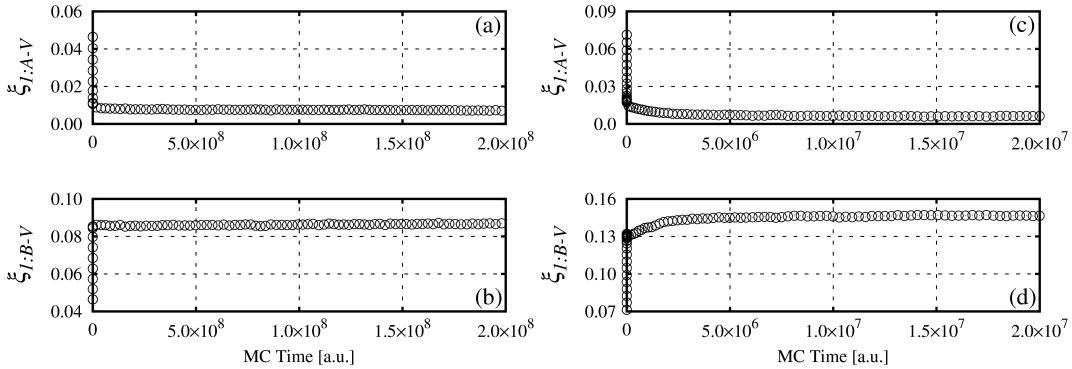

Figure 5.17: Correlation parameters relaxations obtained in KMC simulations at temperatures: (a) and (b) $T/T_C = 0.37$; (c) and (d) $T/T_C = 0.52$

The initial values of $f_{A:\alpha\to\beta}$ frequency are much higher than the $f_{A:\beta\to\alpha}$ ones, which stems from the energetic tendency - promoting the formation of triple defects (see Fig.5.7). Purely visible effect of the decrease of $f_{A:\alpha\to\beta}$ and $f_{A:\beta\to\alpha}$ parameters (Figs.5.18a and 5.18b) will be discussed and explained at the end of this sub-section. The values of $f_{A:\alpha\leftrightarrow\beta}$ (Fig.5.18c) were found initially higher than "1" referring to the rapid formation of the triple defects. Afterwards, $f_{A:\alpha\leftrightarrow\beta}$ fluctuated, being locally less than "1" - in the range of local extrema of LRO and SRO parameters and then, in the range of the slow

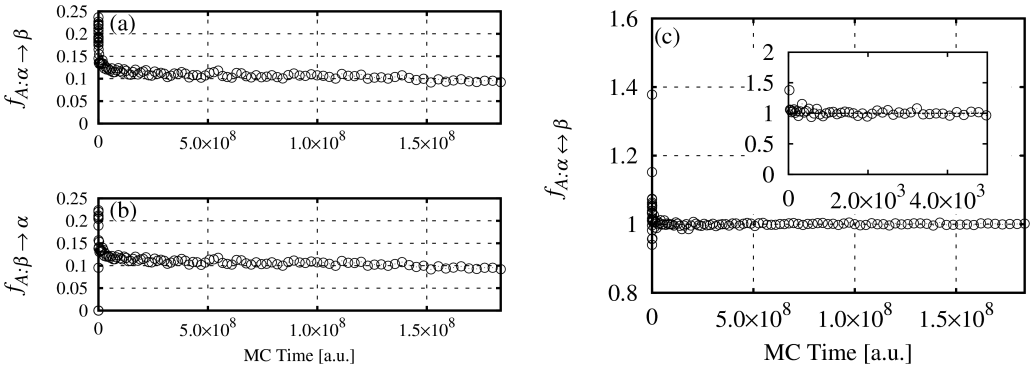

Figure 5.18: A-atom jump frequencies (a,b) and the ratio between them (c) in a function of MC time, collected for $T/T_c = 0.37$.

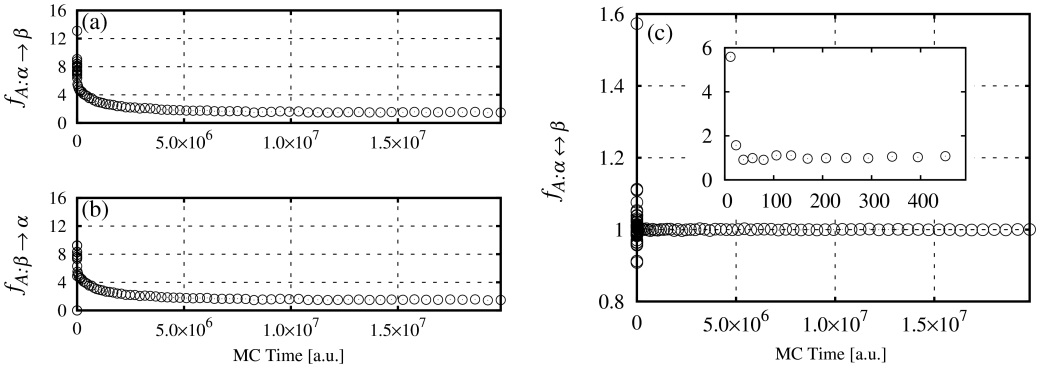

Figure 5.19: A-atom jump frequencies (a,b) and their ratio (c) in a function of MC time, collected for $T/T_c = 0.53$.

"order-order" relaxation fluctuated in the vicinity of "1". It was thus concluded that dramatic decrease of the *efficiency* of atomic jumps (studied by means of $f_{X:\mu\leftrightarrow\nu}$) accompanied by the general decrease of rate of jumps performed per time interval (observed for both kinds of atoms) were direct reasons of the low rate of disordering in the final stage of the process.

The similar analysis (including the frequencies of B-atoms) had been performed at a higher temperature referring to $T/T_C = 0.53$ (Figs. 5.19 and 5.20). The inefficiency of disordering jumps ($f_{A:\alpha\leftrightarrow\beta} \approx 1$) deduced from Fig.5.17c was again observed in the range of MC time referring to the slow decrease of η_A (see Fig. 5.12a).

As expected (from the energetic profile of the atomic jumps - Fig.5.7) the frequencies of B-atom jumps were found much lower than those referring to A-atoms ($\sim 10^2 \div 10^3$ times). Therefore, the lower quality of data for B-atoms came from the smaller amount of B atom jumps during simulations. However, the frequency curves obtained (Fig.5.20) exhibited the qualitatively similar behaviour to those referring to A-atoms. Hence, the formation of $B^{(\alpha)}$ was also found very inefficient.

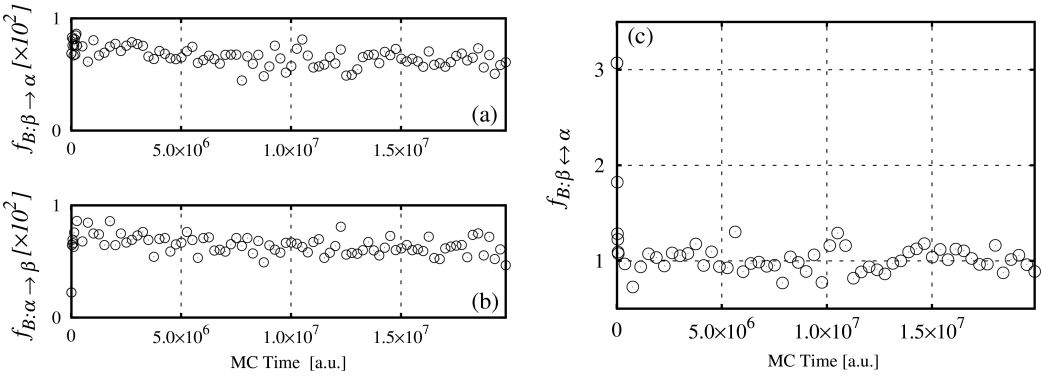

Figure 5.20: B-atom jump frequencies (a,b) and their ratio (c) in a function of MC time, collected for $T/T_c = 0.53$.

Although the inefficiencies of the formation of $A^{(\beta)}$ and $B^{(\alpha)}$ are correlated, the direct reasons of these effects remain different. The mechanism of inefficiencies was explained by means of the supporting analysis of average values of energy barriers *forced* effectively by atoms (see also Chapter 2 sec.2.4 Eq.2.24):

$$E^{+}_{X:\mu\to\nu} = E^{+}_{X} + \frac{1}{2} \times \triangle E_{\mu\nu} \tag{5.21}$$

and inspection of the local configuration of jumping atoms.

The average values (per time intervals) of effective saddle point energies obtained for A-atom jumps are shown in Fig.5.21a. The analysis of the values of $E^{+}_{X:\mu\to\nu}$ allowed to find out that during relaxation, the average values of $E^{+}_{A:\alpha\to\beta}$ referring to A-atom jumps responsible for formation of $A^{(\beta)}$ antisites decreased, contrary to values $E^{+}_{A:\beta\to\alpha}$ referring to the reversal jumps. That not intuitive result may be explained by means of auxiliary SRO parameters $\xi^{j}_{1:A:\mu\to\nu}$ where additional index "j" denotes that only jumping atoms are taken into account in eq. 4.21(Fig. 5.21b).

An average number of vacancies being the nn of $A^{(\alpha)}$ atoms *jumping* to the β sub-lattice was found significantly lower than for the $A^{(\beta)}$ atoms *jumping* to the α sub-lattice. The energetic tendency of $A^{(\beta)}$ formation was compensated by the configurational factor since most of the vacancies occupied α sub-lattice and thus the $A^{(\beta)}$atoms "possessed" more "possibilities" to perform reversal jumps. Therefore, competition between the effects of saddle-point energies and vacancy availability may be proposed as the atomistic reason for low-rated final stage of disordering process. That "competition" may be regarded as a sort of *reverse feedback*. The lower saddle-point energy promotes the $A^{(\beta)}$ formation but the side effect is the formation of $V^{(\alpha)}$, whose existence increase the probability for the reversal jumps $A:\beta\to\alpha$ ($A^{(\beta)}$ annihilation).

The general decrease of $f_{X:\mu\to\nu}$ (Figs.5.18, 5.19 and 5.20) in the first stage of the process was a result of an increase in the number of $V^{(\alpha)}$ vacancies located as nn of B-atoms and resulting in general increase of $[R_{N_V\times z}]^{-1}$(eq.5.3).

Although the role of B-atoms in the disordering process may be treated as marginal in view of the real B2 NiAl system, where the concentration of $B^{(\alpha)}$ is predicted negligible (e.g. see Ref.[76]), the "magnifying glass" of the model

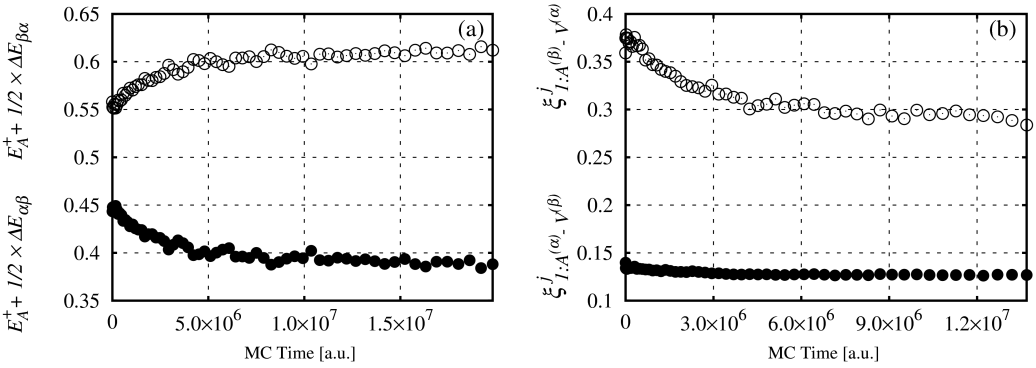

Figure 5.21: The energetic barriers (in [eV]) for an A-atom jumps (a) and $\xi^j_{A:\mu\to\nu}$ SRO parameters (b) for $T/T_C = 0.53$: filled circles - formation of antisite jump ($A:\alpha\to\beta$); empty circles - reversal jumps ($A:\beta\to\alpha$)

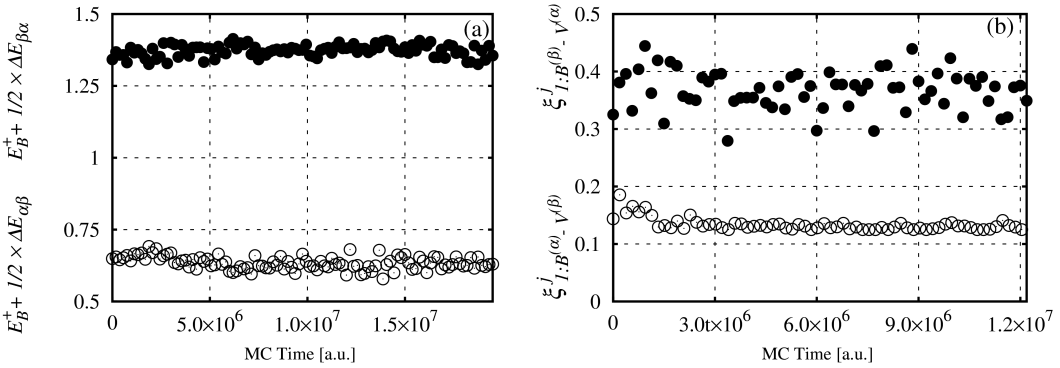

Figure 5.22: The energetic barriers (in [eV]) for an B-atom jumps (a) and $\xi^j_{B:\mu\to\nu}$ SRO parameters (b) for $T/T_C = 0.53$: filled circles - formation of antisite jump ($B:\beta\to\alpha$); empty circles - reversal jumps ($B:\alpha\to\beta$)

studied in this work allowed to investigate B-atom jumps mechanism (Fig.5.22) at $T/T_C = 0.53$ where an acceptable amount of B-atom jumps was observed. It is interesting that the feedback effect observed for the A-atoms was also found for the B-atom jumps but in a "reflected" form. The $E^+_{B:\beta\to\alpha}$ energies (Fig.5.22a) were found significantly higher than $E^+_{B:\alpha\to\beta}$ ones (as expected - see Fig.5.7). However, the average number of vacancies surrounding the B-atoms performing the jump into $V^{(\alpha)}$ was obviously found higher than for the reversal jumps (Fig.5.22b), since most of vacancies resided on the α sub-lattice (vacancy distribution). Therefore, although the formation of $B^{(\alpha)}$ in view of height of the barrier is energetically "expensive" for the system, the configuration factor (triple defect existence) increased the probability of such event.

At higher temperatures, entropy contribution "forces" the system to form the $B^{(\alpha)}$antisites (see 5.14b), however at $T/T_C = 0.53$ the energetic preferences for triple defect disordering seemed to be still very strong since the $\eta^{eq}_A < \eta^{eq}_B \approx 0.98$ and $TDI^{(eq)} \approx 0.6$. On the other hand, the existence of $B^{(\alpha)}$ antisites

"helps" A-atoms to perform the disordering jumps because of vacancy formation on β sub-lattice (see sub-section 5.3.1.1).

The above remarks indicate that the efficiency of A-atom jumps in creating $A^{(\beta)}$ antisite defects increases with temperature as stimulated by an increase of $B^{(\alpha)}$ antisite concentrations.

Chapter 6

Summary

The chemical ordering phenomena in B2 superstructure based alloys were investigated by means of the MC techniques supported by other computational methods. The study was focused on the atomic scale model of crystal exhibiting the triple defect behaviour. Therefore thermodynamical model of the thermal vacancy formation had to be established and solved to maintain the correctness of a whole treatment. The equilibrium vacancy concentration was studied in a framework of lattice-gas decomposition model, preliminary tested in B-W approximation and solved by means of SGCMC simulations of A-B-V ternary lattice-gas. Equilibrium concentration of thermal vacancies was applied in Kinetic Monte Carlo simulations performed by means of Residence Time Algorithm with energetic barriers (saddle point energies) evaluated with the help of the supporting Molecular Statics calculations. MC simulations were mainly based on the Ising type Hamiltonian with the model pair-wise interactions reproducing the triple defect type behaviour.

6.1 Vacancy Thermodynamics

According to the experimental motivation of this study, referring to the low-rated "order-order" kinetics in a nearly stoichiometric B2 NiAl intermetallics [8], systems exhibiting the triple defect type behaviour were of interest. The existence of the triple defect is associated with high thermal vacancy concentration correlated with degree of LRO, therefore, the vacancy thermodynamics model had to be elaborated firstly. The idea of modelling the equilibrium thermal vacancy concentrations originate from the concept proposed by Schapink[32]. The model considered the possibility of the decomposition of $A-B-V$ lattice-gas into vacancy poor and vacancy-rich phases being in equilibrium. Therefore, vacancies were treated as an additional component of the lattice-gas. Vacancy poor phase was interpreted as an $A_{1-\delta}B_{\delta}$ crystal with equilibrium vacancy concentration. Though different procedures for the determination of equilibrium vacancy concentration are known (e.g. "$\mu_V = 0$" approach, see the review of the methods in Ref.[17]) the lattice-gas decomposition model was found applicable into the MC simulation techniques effectively. That feature gave an opportunity to investigate the chemical ordering phenomena in triple defected systems in the framework of MC methods consistently.

The model was preliminary solved by means of Bragg-Williams approxi-

mation, assuming pair-wise interaction between nearest neighbours. Such limitation allowed to perform clear analysis of the model by scanning possibly wide space of pair-interaction parameters which resulted in selection of values referring to the triple defect behaviour. An extension of the model upon pair interactions in further co-ordination zones is possible but was supposed to bring no substantially new results in the field of interest. This fact has been remarked by Breuer et al. in Refs.[77, 18]. Breuer et al. considered B-W based approach to obtain equilibrium vacancy concentrations in B2 NiAl system. Assuming pair-wise interactions up to 2nd co-ordination zone. The pair-wise interactions were obtained by means of fitting the experimental data of enthalpy and activity. It was concluded that pair interaction energies referring to 2nd co-ordination zone may be neglected in the model considered. On the other hand, other authors showed[19] substantial discrepancies between the experimental data and the results of Monte Carlo simulations of atomic ordering in B2-ordering binary systems performed with nn and next-nearest neighbour (nnn) atomic pair interactions, but with a fixed (temperature-independent) number of vacancies. It seems, therefore, that the problems of model approaches stem rather from the negligence of vacancy thermodynamics than from the limited range of atomic interactions considered.

The analysis of defect distribution over the sub-lattices and temperature dependencies of triple defect indicator (TDI) allowed to select the model pair-wise interactions reproducing the triple defect behaviour. The identified triple defect type system exhibited the existence of constitutional vacancies in B-atom-rich non-stoichiometric system (consistently with the definition given by Wasilewski[11]), which was detected by means of $c_V(T \to 0)$ inspection.

The lattice-gas decomposition model yielded the chemical potential μ_V of vacancies tending to zero at low temperatures, which means that at $T \to 0\ K$ the approach converges to the standard formalism[25] based on simple minimization of the thermodynamic potential of a crystal with respect to the number of vacancies and on relating the equilibrium value of c_V to $\mu_V = 0$.

The pair-wise interactions promoting the triple defect existence were subsequently applied into SGCMC simulations. Simulations covered the inspection of sub-space of relative chemical potentials, "step-by-step" simulations allowing to detect the effect of the phase separation (hysteresis loop) and simulations supporting the thermodynamic integrations. It must be mentioned that the method proposed in a present work for obtaining equilibrium vacancy concentration by means of SGCMC technique, is to the author knowledge, a novel approach. The study resulted in the equilibrium vacancy concentrations in B2 AB binaries in the wide range of temperatures. The data obtained, allowed to perform the analysis of both LRO and SRO parameters. The good qualitative agreement of the results with B-W solution was found. The atom-rich phase, interpreted as $A_{1-\delta}B_{\delta}$ crystal with the equilibrium vacancy concentration exhibited the triple defect behaviour which was reflected by means the existence of "1/2 plateux" on $TDI(T/T_C)$ curves and by the presence of constitutional vacancies for $\delta > 0.5$.

Additionally, the simulations performed, gave an opportunity to investigate the character of the triple defects in particular of their spatial distribution correlations, by means of SRO parameter analysis. It was found, that $V^{(\alpha)}$ and $A^{(\beta)}$defects , did not occur in the form of spatially grouped triple defect complexes (see Fig.5.19). Such an effect might be expected since V_{AV} interaction

parameter had been assumed as the repulsive one.

Though, the treatment presented relates to the Ising type model, commonly used in the field of interest (see e.g. [77, 78]) the recent development of "ab initio" calculation methods gave rise to the elaboration of models enabling direct implementation of the "ab initio" result[26, 27, 28, 29]and [76]. Hybrid approaches consisting of "ab initio" evaluation of pair interactions have also been proposed [68, 67] and [79].

In the first case Cluster Variation (CVM) thermodynamics of a system regarded as a regular solid solution is developed. The pair-interaction energies are usually independent of temperature and defect concentration, but the effective defect formation energies, as following from particular configuration, show these dependencies. Although the Cluster Expansion (CE) method has been elaborated as a natural link between CVM and "ab initio"-calculated crystal energetics (see e.g. Ref.[80] for up-to-date description and references), rather few particular systems have been modelled in this way. For the time being, "ab initio"-calculated defect formation energies are most often implemented with Wagner–Schotky-type approaches (see e.g. Refs.[28] and [20]) with the system energy being linearly dependent of defect concentration. These energies, despite their firm physical background, most often correspond to $T \rightarrow 0\,K$ and are fixed parameters.

Though the direct application of ab-initio based energetics into MC simulations in the field of interest is still the challenging task, taking into account the computational power available, the many body quasi-phenomenological potentials (e.g. EAM) are applicable for this simulation purposes. The SGCMC simulations based on the EAM potential were carried out in diverse contexts[1] (see e.g. Refs.[81, 83]), particularly for B2 NiAl alloy[75].

Obviously, the lattice-gas decomposition (into vacancy-poor and vacancy-rich phases) model, assuming vacancy being an additional component, should not be interpreted strictly as a description of realistic decomposition but rather as computational method allowing to obtain the equilibrium vacancy concentration in a framework of rigid lattice treatments, directly applicable into MC simulation techniques. Though the use of realistic potentials, seems to be somehow artificial, the application of EAM potential into presented model, may be treated as an attempt of "small step into the reality[2].

The EAM potential elaborated for B2 NiAl[73], and applied in a MS calculations (see Chapter 5) were adopted into SGCMC simulations. Apart from simplification, associated with the rigid-lattice model where only configurational degrees of freedom are considered, relatively small simulation block consisting of 10x10x10 cubic cells was investigated with the lattice constant fixed at $a_0 = 2.859\,\mathring{A}$(see Tab.5.3). The SGCMC procedure was pursued for a single temperature $T = 1500\,K$. It was found, that $Ni - Al - V$ system exhibited tendency to decomposition into atom-rich and vacancy-rich phases (see Fig.6.1a), however, the vacancy-rich phase appeared to be practically pure vacancy lattice-gas (see the lower branch of hysteresis loop in Fig.6.1b). The equilibrium vacancy concentration in the $Ni_{0.5}Al_{0.5} - V$ phase, was found

[1] E.g. liquid-liquid phase co-existence, nano-particles etc.

[2] Negligence of "elastic" degrees of freedom e.g atomic position relaxations in vicinity of defects, total volume change associated with thermal expansion, may be found questionable since e.g. bulk modulus was taken into account in EAM potential elaboration.

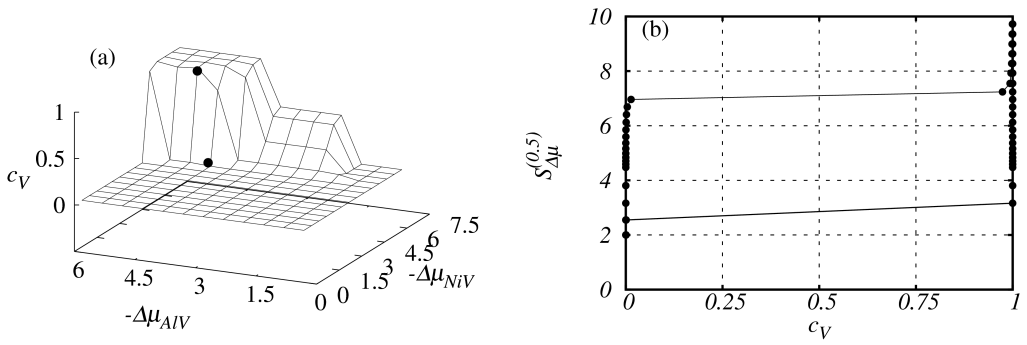

Figure 6.1: The "facet" inducing phase separation, found in EAM potential based SGCMC simulations in a space of vacancy concentration and relative chemical potentials (in eV) , empty circles refer approximately to $Ni_{0.5}Al_{0.5} - V$ phase (lower one) being in equilibrium with nearly pure vacancy-rich one (a). The hysteresis loop obtained in a "step-by-step" mode simulations for stoichiometric $B2\,NiAl$ (b).

close to the limit of available resolution: $c_V \sim 10^{-3}$, only few vacancies were observed in a sample in the vicinity of the phase separation observed as discontinuous transition in a $c_V\,\{\Delta\mu_{Ni-V}, \Delta\mu_{Al-V}\}$ space (inside the hysteresis loop during "step-by-step" simulation mode).

Schaefer et al. [9] reported vacancy concentration measured by means of the dilatometric experiment, at temperature $T \approx 955\,K$ - twice lower than the melting point one - as $c_V^{eq} \approx 7 \times 10^{-4}$. Breuer et al. [18] report the experimental data obtained by Zobel [84] in a wide range of temperatures from which the value $c_V^{eq}(\sim 1500K) \approx 5 \times 10^{-3}$ $T = 1500\,K$ may be deduced. This result is in a fine agreement with value obtained by means of model presented.[3]

It is remarkable that the fluctuating values of $c_V^{(\alpha)}$ and $c_A^{(\beta)}$ yielded a stable level of $TDI_{ACT}^{(A)} \approx 0.5$, but the low value of $\xi_{1:A^{(\beta)}-V^{(\alpha)}} \propto 10^{-2}$ again indicated the statistical character of triple defects. The result is non trivial because in contrary to the case of the Ising model where $V_{AV} > 0$ and spatially separated triple defects are promoted by configurational energy, the $T \to 0$ formation energy for nn triple defects in the EAM NiAl was significantly lower (see Tab.5.4) than the formation energy for the statistical (spatially separated) triple defects. Preliminary results of ab-initio calculations, predict the lower energy for spatially separated triple defects in stoichiomteric B2 NiAl[85], the similar effect found by means of MS calculations[86] was reported for $B2{-}FeAl$ intermetallic.

[3] An exact value obtained by means of integration procedure of Semi Grand Canonical potential was $c_V(1500\,K) = 7.5 \times 10^{-3}$. However, the estimated value of the relative error was high: $\pm 30\%$ therefore, only an agreement between orders of magnitude may be discussed.

6.2 "Order-order" kinetics and saddle point energies

The equilibrium thermal vacancy concentrations, obtained by means of SGCMC basing on pair-wise interactions promoting the triple defect behaviour were applied into KMC simulations in Canonical Ensemble performed by means of RTA. The initial configuration of the system was generated by introducing and randomly distributing an equilibrium amount of vacancies (in the temperature assumed) into the perfectly ordered $B2$ AB sample. Such simplification was justified by the equilibration of vacancy concentration being approximately two order of magnitude faster than "order-order" transformations[8, 10].

It has to be stressed that only disordering "order-order" relaxations were modelled within the presented study. Simulation of ordering processes - i.e. the elimination of antisites and vacancies following a decrease of temperature would definitely require that particular mechanism for vacancy annihilation (trapping) is assumed. This would be possible by considering e.g. B2 binary systems limited by free surfaces, which might play a role of vacancy sinks. Such studies are planned to be taken up in the future.

The KMC simulations of disordering demanded evaluation of saddle point energies. These energies, related to the kind of jumping atoms, were evaluated and fixed taking into account quantitative relations between values obtained by means of Molecular Statics study based on EAM potential devoted to B2 NiAl system[73]. It must be mentioned, that studies of atomic jumps in B2 NiAl, reported in the last decade (see e.g Refs.[75, 87]) referred mainly to the self-diffusion paths (sequence of jumps) maintaining the initial and final configurations identical in view of LRO parameters. In this work investigated configurations and considered paths of jumps did not conserve the degree of LRO conservation since disordering phenomena had been of interest. It was found problematic to study the saddle point energies for aluminum atom jumps due to difficulties of finding minimum of the potential energy corresponding to Al antisite (being nn of vacancy) position in B2 NiAl. That effect was pointed out in Ref.[75], Divinski and Herzig[88] also reported the lack of stability referring to some particular configurations in the MS calculations. However, in the present study, it was found that if aluminum atom jump is performed into $V^{(\alpha)}$ neighbouring with $Ni^{(\beta)}$ ("d" configuration in Fig.5.3) the shallow, local minimum on energy profile curve appears (Figs. 5.5, 5.7) and is attainable provided energetic barrier significantly higher than any one investigated for nickel atom jumps is forced. It leads to the conclusion, that small concentration of $Al^{(\alpha)}$ antisites, in a stoichiometric $B2 - Ni_{0.5}Al_{0.5}$ (probably at high temperatures) is possible if triple defects were generated firstly.

It must be emphasized, that though energies E_A^+ and E_B^+ were fixed, the effective saddle point energies $E^+_{X:\mu\rightarrow\nu}$ (see Eq.5.21) were evolving during relaxations since their values depended on energies referring to initial and final atom positions. Therefore, configurational factor influenced dynamically the evolution of system. The use of RTA allowed to prevent the inefficiency (low rate of accepted MC moves) expected in case of using Glauber algorithm, though the number of vacancies introduced into the system caused rather long CPU time of relaxation. As a consequence, relaxation curves at lower temperatures were not saturated. Detailed simulation studies concerned "order-order" kinetics in B2-ordered $A_{0.5}B_{0.5}$binaries at $T/T_C = 0.37$ referring to "purely" triple defect case and at $T/T_C = 0.53$.

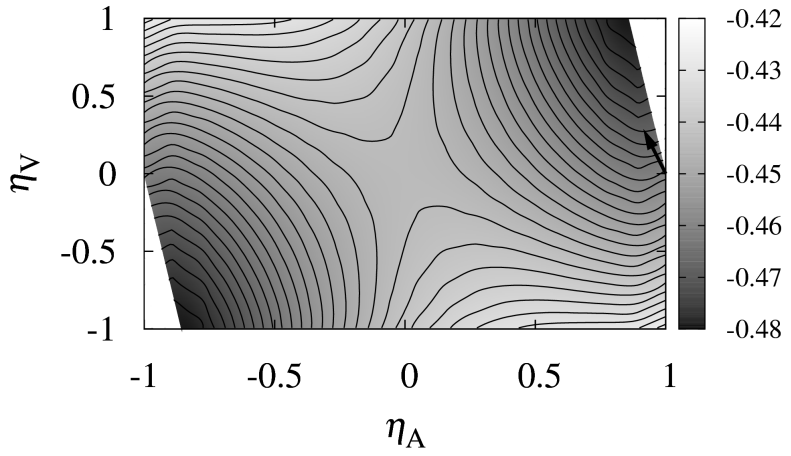

Figure 6.2: Free energy functional plane obtained by means of B-W approximation obtained at $T/T_c = 0.43$, $\delta = 0.5$, $c_V^{(eq)} = 0.067$. The arrow indicates the direction of driving-force in a $(\eta_A, \eta_V) = (1, 0)$ point referring to the initial configuration applied in KMC simulations. The iso-lines refer to the constant free energy functional values. The gray-scale refers to values of $f(\eta_A, \eta_V)$ given in [eV]. The white triangle spaces visible in vicinity of upper-right and bottom-left corners correspond to the concentration constraint limits.

The first, extremely fast stage of the evolution of the system with vacancies initially distributed at random in perfectly B2-ordered lattice consisted of the generation of triple defects, which resulted in a generation of $A^{(\beta)}$antisites and a shift of almost all vacancies to α sub-lattice. The high driving-force of this process resulted from the fact that while generation of any antisite defects increases the configurational energy of the pure $A_{0.5}B_{0.5}$ system without vacancies, the situation inverts at the presence of vacancies: the configuration with a triple defect shows lower energy than configuration with no antisites and two vacancies residing on counterpart sub-lattice.

The high contribution of driving-force in the initial stage of relaxation could be better understood by means of analysis of the free energy functional plane $f(\eta_A, \eta_V)\big|_{T,\delta,c_V}$ resulting from B-W approximation (Fig.6.2). The starting configuration implies that system evolution is initially dominated by process responsible for the vacancy ordering, until the configuration corresponding to the vicinity of pure triple defect is attained (the darkest areas in Fig.6.2).

That immediate process (triple defect formations) finds its continuation in a low-rated, consisting mainly of the formations of $A^{(\beta)}$ antisites, though in a $T/T_c = 0.53$ the creation of $B^{(\alpha)}$ antisites became noticeable. The analysis of LRO and SRO parameters and investigations of statistics of jumping atoms and related values of energetic barriers allowed to conclude that slow evolution of the system was caused by statistical inefficiency of jumps performed. Additionally it came out, that mentioned inefficiency had its origin

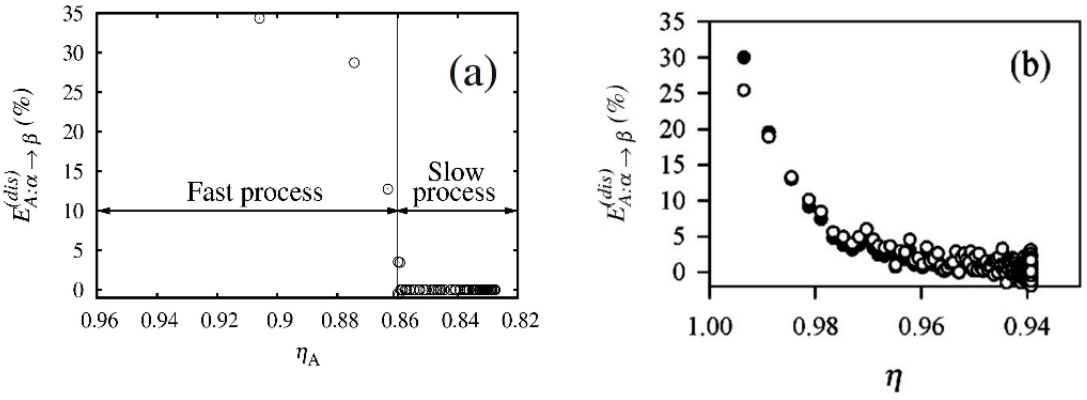

Figure 6.3: The disordering efficiency parameter as function of the degree of LRO parameter: (a) B2 AB system - present study, $T/T_C = 0.53$; (b) $L1_2\, A_3B$ system [38], filled circles refer to $E^{dis}_{Ni:\alpha\to\beta}$, $T_{init}/T_C \approx 0.52$, $T_{fin}/T_C \approx 0.78$.

in the "competition" between the energetic tendency promoting $A:\alpha\to\beta$ jumps and simultaneous formations of $V^{(\alpha)}$vacancies statistically stimulating the reversal jumps $A:\beta\to\alpha$.

Final remarks are focused on comparison to chemical ordering kinetics in $L1_2\ A_3B$ (the model of $L1_2\ Ni_3Al$ system) reported by Oramus et al. in Ref. [38]. It is interesting to consider the disordering efficiency parameter defined in Ref. [38]:

$$E^{dis}_{A:\alpha\to\beta}(\%) \equiv \frac{f_{A:\alpha\to\beta} - f_{A:\beta\to\alpha}}{f_{A:\alpha\to\beta}} \times 100\% \tag{6.1}$$

and to compare its evolution in $L1_2$ and B2 superstructures.

$E^{dis}_{A:\alpha\to\beta}$ parameter considered as a function of degree of long range order parameter η_A in $L1_2$ and $B2$ superstructures is presented in Fig 6.3.

It is clearly visible that while in case of $L1_2$ - ordered A_3B the parameter $E^{dis}_{A:\alpha\to\beta}$ showed a relaxation-like behaviour in parallel with LRO degree and tended asymptotically to "0" (Fig.6.3b), in case of the B2-ordered triple defect AB system after an abrupt decrease the value $E^{dis}_{A:\alpha\to\beta}$ was close to zero all over the slow stage of the "order-order" process (see Fig.6.3a). Although it should be remembered that the relaxation curves shown in Fig.6.3 were simulated by means of different algorithms, at different temperatures and with different energetics, this very rough comparative analysis of "order-order" kinetics in $L1_2$ and B2 superstructure suggests especially low efficiency of the atomic disordering in the latter case.

The final comment should refer to the principal goal of the study, which was the explanation of the experimentally observed low rate of "order-order" relaxation in $Ni_{0.505}Al_{0.495}$ intermetallic [8]. There are two reasons, for which

only the slow stage of the simulated relaxation may be related to the one measured in the experiment:

1. The first fast simulated stage originated from the inital random distribution of vacancies, which, due to fast equilibration of vacancy concentration [8, 10] could hardly occur in a real material.

2. The experiment was performed by means of "in situ" resistometry, where thermal inertia of the equipment would definitely made it impossible to detect initial fast relaxation.

It is, therefore, concluded the the atomistic reasons found for the low rate of the final stage of the simulated "order-order" relaxation in the B2 triple-defect binary system are applicable to explain the experimental result.

6.3 Final conclusions

Modelling of vacancy thermodynamics and chemical order kinetics in B2 triple defect AB binary system was pursued in the following stages:

- Elaboration of model of vacancy thermodynamics correlated with B2 chemical ordering in the framework of lattice-gas decomposition model, solved by means of:

  - Bragg-Williams approximation of statistical thermodynamics
  - Semi Grand Canonical Monte Carlo simulations

  Resulting in:

  - Temperature dependence of equilibrium vacancy concentration
  - Evidence of triple defect behaviour exhibited as specific correlation between vacancies and antistructural defects formation

- Simulation of "order-order" kinetic processes of relaxations in the system performed by means of:

  - Kinetic Monte Carlo simulations implemented with Residence Time Algorithm incorporating: modelled saddle point energies obtained by means of supporting Molecular Statics calculations and equilibrium vacancy concentrations

  Resulting in:

  - Evidence of multi-time-scale character of the isothermal evolution of degrees of long range order and short range order
  - Elucidation of the atomistic origin of the effects in terms of an interplay between driving-force for chemical disordering and configuration of vacancies in the system
  - Indication of possible factors determining the low rate of the experimentally observed "order-order" relaxation in B2 NiAl

Appendix - comment on software

The simulations and calculations performed in the presented study based on the computer codes written by author.

- Bragg-Williams approach was solved by means of application of the following, combined codes:
  - The minimization "engine" - written in **C++** programming language
  - Spline-function interpolation procedures interp.py written in **Python** programming language and supported by **numpy** (numerical python) and **scipy** (scientific python) libraries
  - Lowest-tangent construction sub-program written in Python - incorporating spline-function interpolations and minimization procedures
- Monte Carlo simulations were realized by means of multi-algorithm program **mc-simul** written in C++ language. The program gives an opportunity to perform simulations in the following modes:
  - Semi Grand Canonical Ensemble simulations with arbitrary assumed initial configuration of sample
  - Semi Grand Canonical Ensemble simulations in "step-by-step" mode
  - Kinetic Monte Carlo in Canonical Ensemble with Residence Time Algorithm
  - Kinetic Monte Carlo adopting Glauber formula based dynamics by means of Metropolis type scheme

  The analysis of results obtained by means of Monte Carlo simulations was supported by the group of sub-programs written in Python programming language, dedicated to the following tasks:
  - Spline-function interpolation
  - Numerical integration and derivative calculation (in case of thermodynamics integration procedures)
  - Data analysis and averaging procedures (Kinetic Monte Carlo simulations with Residence Time Algorithm)
- Molecular Statics calculations were performed applying C++ written program **mstatic**. The program allows to calculate the following quantities, basing on application of Velocity Verlet Algorithm:

- Energies of defect formations
- Saddle point energies (modified Velocity Verlet Algorithm)

Bibliography

[1] T. Duffar in *"Alloy Physics: A Comprehensive Reference"*, edited by W. Pfeiler, Wiley Verlag GmbH & Co. KGaA (2007) pp.63-118

[2] W. Püschl, H. Numakamura, W.Pfeiler in *"Alloy Physics: A Comprehensive Reference"*, edited by W. Pfeiler, Wiley Verlag GmbH & Co. KGaA (2007) pp. 173-280

[3] R. Kozubski, " 'Order-Order' Reactions in Ni_3Al-Based Intermetallic Compounds with $L1_2$-type superstructure", Jaggielonian University Press, Kraków (1996)

[4] R.D. Noebe, R.R. Bowman,M.V. Nathal,"Physical and mechanical properties of the B2 compound NiAl", Int. Mater. Rev. 38 (1993), p. 193.

[5] D.B. Miracle, "Overview No. 104 The physical and mechanical properties of NiAl " ,Acta Metal. Mater. 41 (1993), p. 649.

[6] Y. Wang, Z. -K. Liu and L. -Q. Chen, "Thermodynamic properties of Al, Ni, NiAl, and Ni3Al from first-principles calculations",Acta Mater. Vol. 52, Issue 9, (2004), pp. 2665-2671

[7] T.B. Massalski, in "Binary alloy phase diagrams." Metals Park, OH: ASME; 1987 p. 142.

[8] R. Kozubski, D. Kmieć, E. Partyka and M. Danielewski, "Order–order kinetics in $Ni_{50.5}Al_{49.5}$ single crystal", Intermetallics 11 (2003), p. 897

[9] H.-E. Schaefer, K. Frenner, R. Wurschum, "High-temperature atomic defect properties and diusion processes in intermetallic compounds",Intermetallics 7 (1999) pp.277-287

[10] H.-E. Schaefer, K. Frenner and R. Würschum, "Time-differential length measurements for thermal defect investigations: intermetallic B2-FeAl and B2-NiAl compounds, a case study", Phys. Rev. Lett. 82 (1999), p. 949.

[11] R.J. Wasilewski, "Structure defects in CsCl intermetallic compound", J. Phys. Chem. Solids 29 (1968), p. 39.

[12] K. Huang, "*Introduction to Statistical Physisc"*, CRC Press (2001), Polish Edition "*Podstawy fizyki statystycznej*", Wydawnictwo Naukowe PWN (2006)

[13] L. Onsager, "Crystal Statistics. I. Two-Dimensional Model with an Order-Disorder Transition", Phys. Rev. 65,117(194)

[14] D. de Fontaine, "Configurational Thermodynamics of Solid Solutions" in Solid State Physics Vol.34 (1979)

[15] T. Mohri in *"Alloy Physics: A Comprehensive Reference"*, edited by W. Pfeiler, Wiley Verlag GmbH & Co. KGaA (2007) pp. 525-588

[16] S. Müller, W. Wolf, R. Podloucky in *"Alloy Physics: A Comprehensive Reference"*, edited by W. Pfeiler, Wiley Verlag GmbH & Co. KGaA (2007) pp. 589-649

[17] S.H. Lim, G.E. Murch and W.A. Oates, Equilibrium vacancy concentrations in non-stoichiometric B2 compounds by Monte Carlo simulations, J Phys Chem Solids 53 (1992), p. 181

[18] J. Breuer, F. Sommer and E.J. Mittemeijer, "Thermodynamics of constitutional and thermal point defects in B2 $Ni_{1-x}Al_x$" Philos. Mag. A 82 (2002), p. 479.

[19] P. Oramus, M. Kozłowski, R. Kozubski, V. Pierron-Bohnes, M.C. Cadeville and W. Pfeiler, "Dynamics of atomic ordering in intermetallics", Mater. Sci. Eng. A 365 (2004), p. 165.

[20] M. Hagen and M.W. Finnis, "Point defects and chemical potentials in ordered alloys", Philos. Mag. A 77 (1998), p. 447

[21] F.W. Schapink, "Thermodynamics of vacancies in binary alloys", Philos. Mag. 12 (1965), p. 1055

[22] S.M. Kim, "Vacancy properties in β-NiGa and β-NiAl", Acta Metall. Mater. 40 (1992), p. 2793.

[23] M. Kogachi and T. Haraguchi, "Possibilities of random vacancy distribution and antisite atom recovering in the point defect mechanism in B2-type intermetallics", Intermetallics 7 (1999)

[24] X. Ren, K. Otsuka and M. Kogachi, "Do 'constitutional vacancies' in intermetallic compounds exist?", Scr. Mater. 41 (1999), p. 907

[25] Mats Hillert, *"Phase Equilibria, Phase Diagram and Phase Transformations - Their Thermodynamic Basis"* , Cambride University Press (2008), p. 78, p. 462

[26] C.L. Fu, Y.-Y. Ye, M.H. Yoo and K.M. Ho, "Equilibrium point defects in intermetallics with B2 structure: NiAl and FeAl", Phys. Rev. B 48 (1993), p. 6712

[27] J. Mayer and M. Fähnle, "On the meaning of effective formation energies, entropies and volumes for atomic defects in ordered compounds", Acta. Mater. 45 (1997), p. 2207

[28] M. Fähnle, J. Mayer and B. Meyer, Theory of atomic defects and diffusion in ordered compounds, and application to B2-FeAl, Intermetallics 7 (1999), p. 315

[29] B. Meyer and M. Fähnle, Atomic defects in the ordered compound B2-NiAl: a combination of ab initio electron theory and statistical mechanics, Phys. Rev. B 59 (1999), p. 6072

[30] L. Cannavacciuolo and D. P. Landau, Critical behavior of the three-dimensional compressible Ising antiferrmagnet at constant volume: A Monte Carlo study, Phys. Rev. B 71, 134104 (2005)

[31] K. Binder, J.L. Lebowitz, M.K. Phani, M. H. Kalos, "Monte Carlo study of the phase diagrams of binary alloys with face centered cubic lattice structure", Act. Metall. Vol. 29, pp. 1655-1665 (1981)

[32] F.W. Schapink, The distribution of vacancies in ordered alloys of CsCl-type, Scr Metal 3 (1969), p. 113.

[33] R. Kozubski, "Thermal vacancies in B2 and L12 ordering alloys", Acta Metall Mater 41 (1993), p. 2565

[34] B. Fultz, J.J. Hoyt in *"Alloy Physics: A Comprehensive Reference"*, edited by W. Pfeiler, Wiley Verlag GmbH & Co. KGaA (2007) p.347-422

[35] W. L. Bragg, E. J. Williams, "The effect of thermal agitation on atomic arrangement in alloys" Proc. Roy. Soc. London 145A (1934) 699730.

[36] W. L. Bragg, E. J. Williams, "The effect of thermal agitation on atomic arrangement in alloys - II", Proc. Roy. Soc. London 151A (1935) 540566.

[37] E. J. Williams, "The effect of thermal agitation on atomic arrangement in alloys", Proc. Roy. Soc. London 152A (1935) 231252.

[38] P. Oramus, R. Kozubski ,V. Pierron-Bohnes, M. C. Cadeville, W. Pfeiler, "Monte Carlo computer simulation of order-order kinetics in the $L1_2$ - ordered Ni_3Al binary system ", Phys. Rev. B 63, 174109 (2001)

[39] P.M. Oramus, PhD thesis, Jaggelonian University ,Cracow (2001)

[40] W. W. Wood and F. R. Parker, "Monte Carlo Equation of State of Molecules Interacting with the Lennard-Jones Potential. I. A Supercritical Isotherm at about Twice the Critical Temperature" , J. Chem. Phys. 27, 720 (1957).

[41] D. W. Heerman "Podstawy symulacji komputerowych w fizyce" , Wydawnictwa Naokowo-Techniczne,1997

[42] D.P. Landau, K. Binder "*A guide to Monte Carlo Simulations in Statystical Physics*", Cambridge University Press, Third Edition (2009)

[43] D. A. Kofke and E.D. Glandt, Monte Carlo simulation of multicomponent equilibria in a semigrand canonical ensemble, Molecular Physics, 1988, Vol. 64, No. 6, 1105-1131

[44] J.G. Briano and E.D. Glandt, Statistical thermodynamics of polydisperse fluids, J. Chem. Phys. 80 (7), 1 April 1984

[45] A. van de Walle, M. Asta, "Self-driven lattice-model Monte Carlo simulations of alloy thermodynamic properties and phase diagrams",Modelling Simul. Mater. Sci. Eng. 10 (2002) 521–538

[46] E. de Miguel, E. M. del Río and M. M. Telo da Gama, "Liquid–liquid phase equilibria of symmetrical mixtures by simulation in the semigrand canonical ensemble " J. Chem. Phys. 103 (1995)

[47] A. Mori, B. B. Laird, Y. Kangawa, T. Ito, A. Koukitu, "Semigrand Canonical Monte Carlo Simulation with Gibbs-Duhem Integration Technique for Alloy Phase Diagrams", Mater.Phys.Mech. 6 (2003) 49-57

[48] S. Kammerer, B. Dunweg, K. Binder, and M. d'Onorio de Meo, "Nearest-neighbor Ising antiferromagnet on the fcc lattice: Evidence for multicritical behavior", Phys. Rev. B. 53 (1996)

[49] E. de Miguel, E. M. del Rio, M. M. Telo da Gama, "Liquid-liquid phase equlibria of symmetrical mixtures by simulation in the semigrand canonical ensemble",J. Chem. Phys., Vol. 103, No. 14, (1995)

[50] T. Morita, K. Hiroike, „A New Approach to the Theory of Classical Fluids. III', Progress of Theoretical Physics, Vol. 25, No. 4, April 1961

[51] T.D. Lee and C.N. Yang, Statistical Theory of Equations of State and Phase Transitions. II. lattice-gas and Ising Model, Phys. Rev., Vol. 87, N. 3 (1952), p. 413

[52] F. Tavazza, D. P. Landau, and J. Adler, "Phase diagram and structural properties for a compressible Ising ferromagnet at constant volume ", Phys. Rev. B. 70, 184103 (2004)

[53] S.H. Lim, G.E. Murch and W.A. Oates, "Thermodynamic properties of ternary alloys from Monte Carlo simulations", J.Phys.Chem.Solids, 50 (1989) 1251-1259.

[54] W.A. Oates, S.H. Lim, G.E. Murch, "Direct calculation of incoherent phase diagrams by Monte Carlo simulation", Phil. Mag. Lett. Vol. 57, No. 1, 11-16 (1988)

[55] B. Widom, "Some Topics in the Theory of Fluids", J. Chem. Phys, 39, p. 2808 (1963)

[56] N. Metropolis, A. W. Rosenbluth, M. N. Rosenbluth, A. H. Teller and E. Teller, "Equation of State Calculations by Fast Computing Machines", J. Chem. Phys. 21, 1087 (1953).

[57] R. J. Glauber, J. Math. Phys. 4, 294 (1963)

[58] F. Heider, R. Kozubski and T.A. Abinandanan in *"Alloy Physics: A Comprehensive Reference",* edited by W. Pfeiler, Wiley Verlag GmbH & Co. KGaA (2007)

[59] A. B. Bortz, M. H. Kalos and J. L. Lebowitz,"A new algorithm for Monte Carlo simulation of Ising spin systems",J. Comp. Phys.17 (1975) 10

[60] M. Athenes, Thesis, Universite Paris (1997)

[61] W. Pfeiler, D. Vogtenhuber, J. Houserova, W. Wolf, R. Podloucky and W. Püschl, Mat. Res. Soc. Symp. Proc. 842, S5.28.1-6 (2005)

[62] C. Goyhenex, R. Montsouka, M. Kozlowski, V. Pierron-Bohnes, "Interdiffusion of two L10 phases without long-range order decrease: Experiments and molecular dynamics simulations", Solid State Phenomena 129 (2007) 5966.

[63] L. Verlet, Phys. Rev. 159, 98 (1967).

[64] R. Kozubski, A. Biborski, L. Zosiak, V. Pierron-Bohnes ,"Lattice-Gas-Decomposition Model for Vacancy Formation Correlated with B2 Atomic Ordering in Intermetallics", Mat. Res. Sc. Fall Meeting Boston (2008)

[65] A. Biborski, L. Zosiak, R. Kozubski, "Triple-Defect B2 Binary Intermetallics: Bragg-Williams Solution and Monte Carlo Simulations", Deffect and Diffusion Forum, vol. 289 - 292, 361-368 (2009)

[66] A. Biborski, L.Zosiak, R. Kozubski and V. Pierron-Bohnes, "Lattice-gas decomposition model for vacancy formation correlated with B2 atomic ordering in intermetallics", Intermetallics 17 (2009) 46-55.

[67] R. Krachler and H. Ipser, "Triple defect complexes in the B2 intermetallic compound NiAl", Phys Rev B 70 (2004), p. 054113

[68] Y.L. Hao, Y. Song, R. Yang, Y.Y. Cui, D. Li and M. Niinomi, "Concentration of point defects in binary NiAl" , Philos. Mag. Lett. 83 (2003), p. 375

[69] A. Biborski, L. Zosiak, R. Kozubski, R. Sot, V. Pierron-Bohnes, "Semi-Grand Canonical Monte Carlo simulation of ternary bcc lattice-gas decomposition: Vacancy formation correlated with B2 atomic ordering in A-B intermetallics.", to be published in Intermetallics

[70] C. Pareige, F. Soisson, G. Martin and D. Blavette, "Ordering and phase separation in Ni-Cr-Al: Monte Carlo simulations vs three-dimensional atom probe", Acta Mater. 47 (1999) 1889-1899.

[71] A. Biborski, R. Kozubski, "Triple defect and constitutional vacancies in B2 binaries. Direct Bragg - Williams thermodynamics." Proceedings of the Third International Conference on Multiscale Materials Modeling MMM2006, Freiburg, Germany, P. Gumbsch (ed.), Fraunhofer IRB Verlag 2006, p. 854. (ISBN-10: 3-8167-7206-4; ISBN-13: 978-3-8167-7206-4).

[72] G.L. Aranovich, J.S. Erickson and M.D. Donohue, "lattice-gas 2D/3D equilibria: Chemical potentials and adsorption isotherms with critical points", J.Chem.Phys. 120 (2004) 5208-5216.

[73] Y. Mishin, M. J. Mehl and D. A. Papaconstantopoulos, "Embedded-atom potential for B2-NiAl ",Phys. Rev. B 65 (2002)

[74] Daw, Murray S., Mike Baskes. "Embedded-atom method: Derivation and application to impurities, surfaces, and other defects in metals". Phys. Rev. B 29 (12): 6443–6453.

[75] A. Y. Lozovoi, Y. Mishin, "Point defects in NiAl: The effect of lattice vibrations", Phys. Rev. B 68, 184113 (2003)

[76] P.A. Korzhavyj, A.V. Ruban, A.Y. Lozovoi, Yu. Kh. Vekilov, I.A. Abrikosov and B. Johansson, "Constitutional and thermal point defects in B2 NiAl", Phys. Rev. B 61 (2000)

[77] J. Breuer, F. Sommer and E.J. Mittemeijer, "Thermodynamics of B2 intermetallic compounds with triple defects: a Bragg–Williams model for (Ni,Co)Al" , Metall Mater. Trans. A 32 (2001), p. 2157.

[78] M.P. Gururajan and T.A. Abinandanan, "Effect of interaction energies on the vacancy behaviour in B2 ordered intermetallics", Mater. Sci. Eng. A 329–331 (2002), p. 388

[79] P. Oramus, A. Biborski, R. Kozubski, K. Parliński and P.T. Jochym, "Superstructure stability and site preferences in β-NiAl doped with Fe, Co, and Cr Monte Carlo simulation", Arch Metall Mater 52 (2007), p. 33

[80] S. Müller, W. Wolf and R. Podloucky In: W. Pfeiler, Editor, "Alloy physics. A comprehensive reference", Wiley-VCH, Weinheim (2007), p. 612

[81] J. J. Hoyt , J. W. Garvin , E. B. Webb III and Mark Asta, "An embedded atom method interatomic potential for the Cu–Pb system", Modelling Simul. Mater. Sci. Eng. 11 (2003) 287–299

[83] Ivailo Atanasov, Marc Hou, "Equilibrium ordering properties of Au–Pd alloys and nanoalloys ", Surface Science 603 (2009) 2639–2651

[84] F. Zobel, PhD Thesis, Technical University Berlin, Berlin (1994)

[85] R. Sot ICM Warsaw, private communication

[86] R.N. Nogueira and C.G. Schön, "Embedded atom study of the interaction between point defect in iron aluminides: Triple Defects", Intermetallics 13 (2005) 1245-1254.

[87] K. A. Marino, E. A. Carter, "First-principles characterization of Ni diffusion kinetics in $\beta-$NiAl", Phys. Rev.B 78, 184105 (2008)

[88] S. Divinski , Chr. Herzig ,"On the six-jump cycle mechanism of self-diusion in NiAl", Intermetallics 8 (2000) 1357-1368